ALGORITHM THEORETICAL BASIS DOCUMENT (ATBD) (NADIR TOTAL COLUMN OZONE)

for the

Ozone Mapping and Profiler Suite (OMPS)
of the
National Polar-Orbiting Operational Environmental
Satellite System (NPOESS) Program

Contract Number: F04701-99-C-0044
CDRL A012

PREPARED FOR:
NPOESS Program Office

Prepared by
Ball Aerospace & Technologies Corp. (BATC)
Boulder, CO 80306

PREPARED BY
Colin Seftor

_____
OMPS Total Column Algorithm Lead

APPROVED:
Juan Rodriguez

_____
OMPS Systems Engineer

APPROVED:
Roger Scarlotti

_____
OMPS Program Manager

Project Release _____

Revision Record

Revision	Date	Reasons for Revision	Project Released Date
Draft	March 1, 1999	1st Draft Release	
CFI	April 6, 1999	Proposal Modifications	
RRR1	February 15, 2000	Update for RRR1	
Initial Release	July 24, 2000	Corrections	
RRR2	November 5, 2000	Corrections, update of SDR algorithm	
Rev A RRR3	Aug 16, 2001	Further corrections, update of SDR algorithm Removal of Section 8, Appendices A and B	

Table of Contents

1 INTRODUCTION 1
1.1 System Description 1
1.2 Objectives 2
1.3 Scope 2
1.4 Overview 3
1.5 Data Products 3
1.6 Applicable Documents 4
1.6.1 Controlling Documents 4
1.6.2 OMPS Reference Documents 4
1.7 Revision History 4
1.8 Contributing Authors 5

2 SCIENTIFIC BASIS 5
2.1 Physical Description 5
2.2 Sensor Description 6
2.3 Forward Model 7
2.3.1 Radiative Transfer Tables 8
2.3.2 Sensitivity Tables 13
2.3.3 Rotational-Raman Scattering 14
2.4 Retrieval 14
2.4.1 Overview 14
2.4.2 OMPS Reflectivity (Cloud Fraction) 16
2.4.3 Initial Estimate of Ozone 17
2.4.4 Linear Correction 17
2.4.5 Profile Selection 19
2.4.6 Correction for Tropospheric Aerosols and Sun Glint 20
2.4.7 Correction for Temperature and Ozone Profile Shape 20
2.4.8 Correction for Tropospheric Ozone 21
2.4.9 Multiple Triplet Formulation 25
2.4.10 OMPS Channel Selection 26
2.4.11 Volcanic SO_2 30
2.5 Error Sources 33

3. ALGORITHM DESCRIPTION 35
3.1 SDR Production 35
3.1.1 Earth View 38
3.1.2 Calibration 42
3.2 EDR Production 55
3.2.1 Retrieval Algorithm Description 61

4 ASSUMPTIONS 72

5 INPUT DATA REQUIREMENTS 72
5.1 Primary Sensor Requirements 72
5.2 Other OMPS Sensor Data Requirements 73
5.3 Other NPOESS Sensor Data Requirements 73

5.4 Climatology Data Requirements 74

6 OUTPUT DATA DESCRIPTION 74
6.1 EDRs 74
6.2 Additional Data Products 75
6.3 EDR Content 75

7. SYSTEM ACCURACY AND PRECISION 76
7.1 System Accuracy 76
7.1.1 Sensor Accuracy 77
7.1.2 Algorithm Accuracy Errors 84
7.2 Long Term Stability 88
7.3 System Precision 93
7.3.1 Sensor Precision Errors 93
7.3.2 Algorithm Precision Allocations 95
7.3.3 Global Distribution of Total Column Precision Errors 102
7.4 Mapping uncertainty 105

8 REFERENCES 106

1 Introduction

The Ozone Mapping and Profiler Suite (OMPS) is an important component of the National Polar-Orbiting Operational Environmental Satellite System (NPOESS). The OMPS mission is to provide the NPOESS users with data products that describe the vertical, horizontal, and temporal distribution of ozone in the Earth's atmosphere. These data (or Environmental Data Records—EDRs) are derived from the spaceborne ultraviolet, visible, and near infrared observations of a two-sensor system.

1.1 System Description

The nadir system has two focal planes: one operating from 300 to 380 nm for total column ozone observations, and the other operating at 250 to 310 nm for profile ozone observations. The limb system has one focal plane operating from 290 to 1000 nm for high vertical resolution profile ozone observations. These systems together with the interface and control electronics are the OMPS sensor suite. Calibrated and un-calibrated sensor data are also provided to the NPOESS users in the form of Sensor Data Records (SDRs) and Raw Data Records (RDRs), respectively. In addition, we use the SDRs from the NPOESS CrIS sensor to generate ozone total column data products for very high solar zenith angles (>80°).

The EDR requirements thresholds listed in Section 3.2.1.1.1 of the OMPS System Specification, Document Number 542798, shall be met when data from OMPS is processed using the scientific algorithms described in these ATBDs.

The OMPS algorithms include the following:

1 **The UV Nadir Total Column Ozone Algorithm** is adapted from the heritage TOMS version 7 algorithm. We have included modular enhancements to meet EDR requirements and to provide for graceful degradation.
2 **The UV Nadir Profile Ozone Algorithm** is adopted from the heritage SBUV/2 operational algorithm. The ozone profile from this algorithm not only provides an initialization for the UV/VIS Limb Profile Algorithm but also provides a link to the heritage twenty-year ozone profile data set.
3 **The UV/VIS Limb Profile Ozone Algorithm** is adapted from the heritage SOLSE/LORE algorithm. We have included modular enhancements to achieve EDR requirements and to provide graceful degradation.
4 **The IR Total Column Ozone Algorithm** is adapted from heritage algorithms used for TOVS, CIRRIS-1A, and EOS-TES data. In order to improve the performance of the ozone retrieval, auxiliary parameters such as temperature and moisture profiles, surface emissivity, and surface skin temperature are retrieved simultaneously with the ozone column amount. The IR ozone values are reported at locations that complement the UV nadir total ozone values (i.e., for SZA greater than 80 degrees).

Figure 1.1-1 maps the flow of the OMPS data from the sensors through the RDR, SDR, and EDR algorithms. For the SDR algorithm, the figure identifies the required inputs as the external EDRs, the climatological databases, and the calibration data. For the EDR algorithms, this figure

also identifies the connection between the algorithms. The IR total column ozone product is used to expand the geographical coverage of the nadir Total Column sensor.

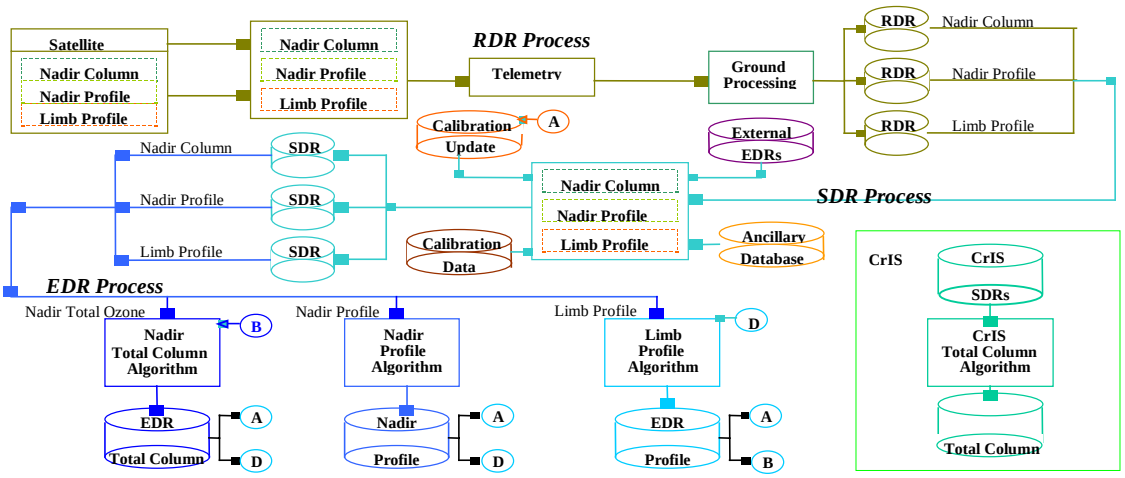

Figure 1.1-1. Overview of the data flow from the sensors through the RDR algorithms to the RDRs and then through the SDR algorithm to the SDRs. The final step takes the SDRs through the four EDR algorithms to the ozone EDRs. The letters indicate use of intermediate and final data products in the production of the SDRs and EDRs.

1.2 Objectives

This Algorithm Theoretical Basis Document (ATBD) describes the algorithm used to retrieve the OMPS Total Column Ozone Product. This product consists of the total ozone in a column of air from 0 to 60 km and observed for all solar zenith angle viewing conditions less than or equal to 80 degrees.

This document identifies the sources of input data that are required by the algorithm; provides the physical theory and mathematical background underlying the use of this information; describes practical considerations affecting the detailed algorithm development; lists any assumptions employed in the algorithm retrieval process, describes the EDR products and additional algorithm by-products; details expected sensor and algorithm errors (accuracy and precision); and discusses the use of calibration data sets.

1.3 Scope

An individual document has been developed for each of the four OMPS algorithms. These are summarized with their output products in **Table 1.3-1**.

Table 1.3-1. The OMPS Algorithms Take Advantage of Internally Generated Products While Minimizing Dependence on External Data

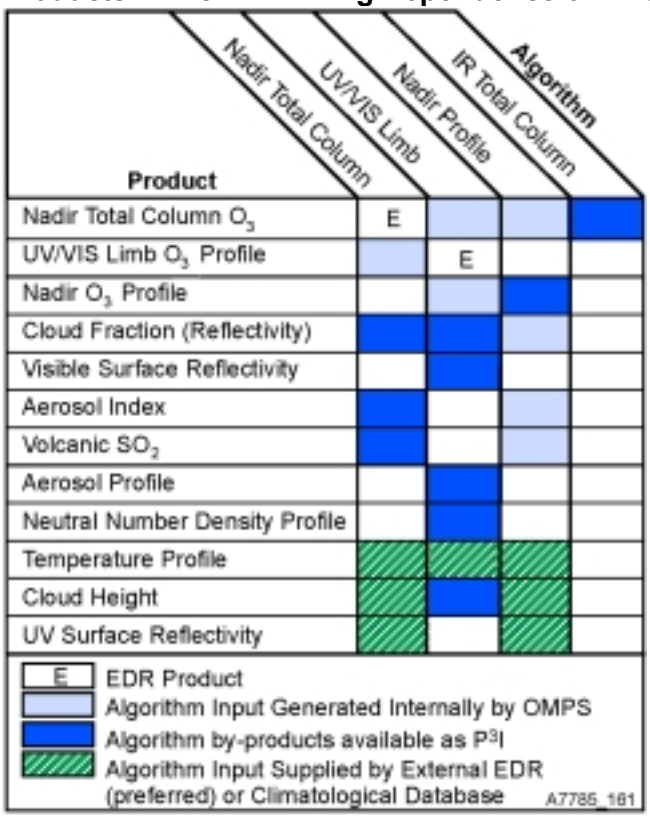

1.4 Overview

The Ball Team's Total Column Ozone Algorithm is adapted from the Total Ozone Mapping Spectrometer (TOMS) Version 7 Algorithm (McPeters et. al., 1996). The algorithm is based on the comparison of measured normalized radiance to calculated normalized radiance (using a standard UV radiative transfer model) for specific measurement geometry, viewing conditions, and surface conditions. The algorithm takes the IFOV information from the SDR, determines the viewing geometry, and characterizes the scene from either external EDR information or climatological data. It then constructs the normalized radiance as the ratio of measured radiance to irradiance. From a radiative transfer model the normalized radiances are calculated for the given viewing conditions. These are compared to the measured values and an ozone estimate is determined. This estimate is refined for effects from aerosols and other contaminants. After data quality flags are set the EDR output file is constructed.

1.5 Data Products

The main data product is the total column ozone amount in Dobson Units (DU), equivalent to milli-atm-cm of ozone, for solar zenith angles < 80°.

1.6 Applicable Documents

1.6.1 Controlling Documents

1. OMPS System Specification – Document Number 542798
2. OMPS Algorithm Development Specification – Document Number 542808

1.6.2 OMPS Reference Documents

1. OMPS Algorithm Theoretical Basis Document: Nadir Total Column Ozone Algorithm—Document Number IN0092-106.
2. OMPS Algorithm Theoretical Basis Document: UV/VIS Limb Profile Ozone Algorithm—Document Number IN0092A-107.
3. OMPS Algorithm Theoretical Basis Document: Nadir Profile Ozone Algorithm—Document Number IN0092A-108.
4. OMPS Algorithm Theoretical Basis Document: IR Total Column Ozone Algorithm—Document Number IN0092A-109.
5. OMPS Algorithm Test and Verification Plans and Procedures (ATVPP) – Document Number IN0092-124.

1.7 Revision History

The original version of this document was dated March 1, 1999. This is intended to be a working document that will not be finalized until just prior to the critical design review (CDR), although many of the sections may remain unchanged. Revisions to this document will be made as the nadir total column sensor design and algorithm mature, and as performance information is verified and validated. Significant changes to content or format for a given version of this document are given in Table 1.7.1.

Table 1.7-1. Revision History of This Document

Revision	Release Date	Section	Change Type
Draft	March 1, 1999		
CFI	April 6, 1999		
RRR1	February 15, 2000	Table of Contents	Update to reflect new Section 8
		2.3.2	Correct equation defining Q_2
		8	Revise section to reflect AVTPP
		9	Added missing reference
Initial Release	July 24, 2000	2.4.9	Correction to sensitivity derivation
		8.4.2	Correction to precision comparison
RRR2	November 5, 2000	3	Updated SDR earth view and calibration
		1.8	Updated contributing author list
		All	Corrected typographical and grammar
RRR3	July 23, 2001	3	Further updated SDR description, reviewed and corrected EDR description
		8	Deleted Section 8
		A	Deleted Appendix A (now described in Version Description Document)
		B	Deleted Appendix B
		All	Corrected typographical and grammar

1.8 Contributing Authors

Contributors to each of the four OMPS ATBDs include:

Lead:	Nadir Total Column Ozone Algorithm	Colin Seftor (Raytheon)
Lead:	Nadir Profile Ozone Algorithm	Charles Wellemeyer (Raytheon)
Lead:	UV/VIS Limb Profile Ozone Algorithm	Jack Larsen (Raytheon)
Lead:	IR Total Column Ozone Algorithm	Hilary Snell, John Pickle (AER)

Other contributors include:

Richard Buss	Raytheon
Brent Canova	Ball Aerospace & Technologies Corp.
Kelly Chance	Harvard-Smithsonian
David Flittner	University of Arizona
Jeffrey Hayes	Raytheon
Jennifer Hegarty	AER, Inc.
Benjamin Herman	University of Arizona
Glen Jaross	Raytheon
James Leitch	Ball Aerospace & Technologies Corp.
Jean-Luc Moncet	AER, Inc.
Hélène Rieu	AER, Inc.
Juan Rodriguez	Ball Aerospace & Technologies Corp.
James Russell	Hampton University
Richard Slonaker	Raytheon
Thomas Swissler	Consultant

2 Scientific Basis

2.1 Physical Description

To interpret the radiance measurements made by the OMPS nadir total column sensor requires an understanding of how the Earth's atmosphere scatters ultraviolet radiation as a function of solar zenith angle. Incoming solar radiation undergoes absorption and scattering in the atmosphere by atmospheric constituents such as ozone and aerosols, and radiation that reaches the ground is scattered by surfaces of widely varying reflectivity.

The backscattered radiance at a given wavelength depends, in principle, upon the entire ozone profile from the top of the atmosphere to the surface. For the ozone absorbing wavelengths in the OMPS sensor, the backscattered radiance consists primarily of solar radiation that penetrates the stratosphere and is reflected back by dense tropospheric air, clouds, aerosols, and the Earth's surface. The total optical depth above the scattering layer in the troposphere primarily determines the intensity. The amount of ozone below the scattering layer is small and can be estimated with sufficient accuracy to permit derivation of total column. Because most of the ozone is in the stratosphere, the principal effect of atmospheric ozone at these wavelengths is to attenuate both the solar flux going to the troposphere and the component reflected back to the satellite.

Derivation of atmospheric ozone content from measurements of the backscattered radiances requires a treatment of the reflection from the Earth's surface and of the scattering by clouds and

other aerosols. These processes are not isotropic; the amount of light scattered or reflected from a given scene to the satellite depends on both the solar zenith angle and view angle, the angle between the nadir and the scene as seen at the satellite.

Early versions of the algorithm used for Total Ozone Mapping Spectrometer (TOMS) sensors based their calculation of reflectivity on the treatment of Dave (1978). He represented the contribution of clouds and aerosols to the backscattered intensity by assuming that radiation is reflected from a particular pressure level called the "scene pressure," with a Lambert-equivalent "scene reflectivity," R. When this method was applied at the non-ozone-absorbing wavelengths the resulting reflectivity exhibited wavelength dependence correlated with partially clouded scenes.

To remove this wavelength dependence, the OMPS algorithm (as well as the latest version of the TOMS algorithm) uses a simple physical model that assumes the scene can be well characterized using two separate reflecting surfaces, one representing the ground and the other representing clouds. The fractional contribution of each to the reflectivity is obtained by comparing the measured radiances with the values calculated for pure ground and pure cloud origin.

2.2 Sensor Description

The NPOESS satellite will operate in a near circular, sun-synchronous orbit. The nominal orbit for the satellite is 833 km altitude, 98.7 degree inclination. The orbit will be a "precise" orbit (i.e., altitude maintained to ± 17 km, ± 0.05 degrees inclination, nodal crossing times maintained to 10 minutes throughout the mission lifetime) to minimize orbital drift (precession). The NPOESS platform will be capable of flying at any equatorial node crossing time. However, the nominal configuration will be a nodal crossing time of 1330.
The grating spectrometer and focal plane for total column measurements provide 0.45 nm spectral resolution across the wavelength range of 300 to 380 nm. The IFOV for the nadir cell of the total column measurement is 45.7 km cross track with an along-track reporting interval of 50 km. The total FOV cross track is 110 deg. to provide daily global coverage. A depolarizer in the telescope keeps the sensor linear polarization sensitivity ≤ 1%, well below the 5% allocation.

The signal-to-noise ratio (SNR) requirements for the 12 spectral channels used in the total column measurements were derived from a sensitivity analysis of the total column algorithm and are given in **Table 2.2-1**.

Table 2.2-1. SNR Requirements for the 12 Spectral Channels

Wavelength (nm)	Minimum Signal-to-Noise Ratio (SNR)	Min. Radiance ph/sec-cm^2-sr-nm	Max. Radiance ph/sec-cm^2-sr-nm
308.5	1000	7.87E11	1.14E13
312.5	1000	2.61E12	1.99E13
314	1000	1.51E12	5.30E12
318	1000	3.26E12	4.21E12
321	1000	6.34E12	3.49E13
322	1000	1.35E12	2.64E12
328	1000	3.06E12	6.56E12
331	1000	4.43E12	1.03E13
332	1000	4.43E12	1.03E13
336	1000	1.17E13	1.66E13
364	1000	5.01E12	6.49E13
377	1000	5.16E12	7.38E13

Sensor Calibration. On-orbit calibration is provided by weekly solar irradiance measurements with a reflective diffuser at the entrance aperture. The albedo calibration, defined as the ratio of radiance calibration to irradiance calibration at the same wavelength, will be determined to an accuracy greater than or equal to 2% at all wavelengths from 300-380 nm. Working and reference diffusers are used to monitor diffuser degradation. The reference diffuser comparisons should be able to measure working diffuser reflectance changes to provide good long-term stability of sensor measurements.

2.3 Forward Model

The intensity of radiation as it passes through a region where it is absorbed and scattered can be described using a simplified form of Beer's Law that assumes a pure Rayleigh scattering atmosphere with ozone absorption:

$$I = Fe^{-s(\alpha\Omega+\beta p)} \tag{1}$$

where

I	=	radiance (Watts / cm^3-steradian)
F	=	solar flux (Watts / cm^3)
Ω	=	total column ozone amount (atm-cm)
s	=	path length (unitless)
α	=	ozone absorption coefficient (1. / atm-cm)
β	=	Rayleigh scattering coefficient (1. / atm)
p	=	pressure (atm)

Taking the log of both sides:

$$N = -100\log_{10}\frac{I}{F} = c'\alpha s\Omega = C\Omega \tag{2}$$

The term I/F is known as the normalized radiance, NR. The N value provides a unit for NR that has a scaling comparable to the total column ozone; the factor of 100 is to produce a convenient numerical range.

The basic approach of the algorithm is to use the radiative transfer code TOMRAD to calculate the N values that should be measured for different ozone amounts given the location of the measurement, viewing conditions, and surface properties. The column ozone amount that yields calculated N values that match the measured N values is then determined.

In practical application, rather than calculate NRs (in the form of N values) separately for each scene, detailed calculations of N values are performed for a grid of total column ozone amounts, vertical distributions of ozone, solar and satellite zenith angles, and four choices of pressure at the reflecting surface. The calculated N value for a given scene is obtained by interpolation in this grid of calculated N values.

2.3.1 Radiative Transfer Tables

The calculation of NRs at each pressure level follows the formulation of Dave (1964), with the addition of a spherical correction for the incident beam and the incorporation of molecular anisotropy (Ahmad and Bhartia, 1995).

Consider an atmosphere bounded below by a Lambertian reflecting surface of reflectivity R. The backscattered radiance emerging from the top of the atmosphere as seen by a UV sensor, I_m, is the sum of purely atmospheric backscatter I_a, and reflection of the incident radiation from the reflecting surface I_s,

$$I_m(\lambda,\theta,\theta_0,\Omega,P_0,R) = I_a(\lambda,\theta,\theta_0,\phi,\Omega,P_0) + I_s(\lambda,\theta,\theta_0,\Omega,P_0,R) \quad (3)$$

where

λ	=	wavelength (nm)
θ	=	satellite zenith angle, as seen from the ground (degrees)
θ_0	=	solar zenith angle (degrees)
φ	=	azimuth angle (degrees)
Ω	=	column ozone amount (DU or atm-cm)
P_0	=	pressure at the reflecting surface (atm)
R	=	effective reflectivity at the reflecting surface (unitless)

The intensity due to atmospheric scattering can be expressed as a harmonic series in azimuth as:

$$I_a(\lambda,\theta_0,\theta,\phi,\Omega,P,R) = \sum_{m=0}^{N} I_m(\lambda,\theta_0,\theta,\phi,\Omega,P,R)\cos(m\phi) \quad (4)$$

N=2 for Rayleigh scattering, yielding two azimuthally dependent terms and one azimuthally independent term:

$$I_a = I_0 + I_1 \cos\phi + I_2 \cos 2\phi \tag{5}$$

The surface reflection term, I_s, can be expressed as:

$$I_s(\lambda, \theta_0, \theta, \Omega, P_0) = \frac{RT(\lambda, \theta_0, \theta, \Omega, P_0)}{1 - RS_b(\lambda, \Omega, P_0)} \tag{6}$$

$$T(\lambda, \theta, \theta_0, \Omega, P_0) = I_d(\lambda, \theta, \theta_0, \Omega, P_0)\, f(\lambda, \theta, \Omega, P_0) \tag{7}$$

where

S_b = fraction of radiation reflected from surface that atmosphere reflects back to surface
I_d = total amount of direct and diffuse radiation reaching surface at P_0
f = fraction of radiation reflected toward satellite in direction θ that reaches the satellite.

The denominator accounts for multiple reflections between the ground and atmosphere, where S_b is the fraction of the reflected radiation scattered back to the surface by the atmosphere.

The total intensity seen by the satellite (I_m or I_t) can now be written as:

$$I_t = I_0 + I_1 \cos\phi + I_2 \cos 2\phi + \frac{RT}{1 - RS_b} \tag{8}$$

Part of the angular dependence of I_1 and I_2 can be factored out as:

$$I_1 = Q_1(\theta_0, \theta) \cdot Z_1 \text{ and}$$

$$I_2 = Q_2(\theta_0, \theta) \cdot Z_2 \text{ ,}$$

where

$$Q_1(\theta_0, \theta) = -\frac{3}{8} \cos\theta_0 \sin\theta_0 \sin\theta \text{ , and}$$

$$Q_2(\theta_0, \theta) = \frac{3}{32} \frac{\sin^2\theta_0 \sin^2\theta}{\cos\theta}$$

Z_1 and Z_2 are better-behaved angular functions and are therefore used in table interpolations instead of I_1 and I_2.

(Note: the actual angular interpolations are performed on the quantities $\log(I_0)$, Z_1/I_0, Z_2/I_0, T/I_0. The interpolated values are converted to I_0, I_1, I_2, T and, along with S_b, are used to calculate I.)

A "master table" containing I_0, Z_1, Z_2, T, and S_b was generated using TOMRAD for the conditions shown in **Table 2.3-1**.

Table 2.3-1. Table Node Points

Quantity	Number	Values
Wavelength	3047	From 248 to 401 nm in steps of ~0.05 nm
Solar Zenith Angle	10	0, 30, 45, 60, 70, 77, 81, 84, 86, 88°
Satellite Zenith Angle	6	0, 15, 30, 45, 60, 70°
Pressure	4	1.0, 0.7, 0.4, 0.1 atm
Ozone Profiles	26	6 low, 10 mid, and 10 high latitude

For each wavelength, TOMRAD requires as input an ozone and temperature profile, Rayleigh scattering coefficient, the molecular anisotropy factor, and the ozone absorption coefficient at 0 °C. The temperature profile is used, along with the absorption coefficient at 0 °C (α_0), to determine the absorption coefficient at each of the 11 ozone and profile layers. If T_{layer} is the temperature for the atmospheric layer, then

$$\alpha_{layer} = \alpha_0 + c_1 T_{layer} + c_2 T_{layer}^2$$

The coefficients c_1 and c_2 are also provided for each wavelength.

The 6 low-latitude profiles range from 225 to 475 Dobson Units (DU) in steps of 50 DU. The 10 mid- and 10 high-latitude profiles range from 125 to 575 DU in steps of 50 DU. These standard ozone and temperature profiles were determined from an Empirical Orthogonal Function (EOF) analysis of the entire SAGE II data set.

2.3.1.1 Standard Ozone and Temperature Profile Determination

The OMPS total column algorithm's table is based on a set of climatological ozone profiles that account for the dependence of the measured radiances on the total amount of ozone and its vertical distribution (Klenk et al., 1982). To develop this set of standard profiles, empirical orthogonal functions (EOF) were derived for an external data set comprising SAGE II profiles over the period from launch in October 1984 through June 1991 (when the eruption of Mt. Pinatubo began to impact the SAGE II ozone retrieval). This problem is bounded by using only the first two EOFs to define a two-dimensional space that explains most of the variability in the ozone profile. To provide statistically consistent lower layers for SAGE II profiles, a set of balloonsonde profiles in the period from November 1978 through 1987 for 20 ground sites distributed about the globe were used in conjunction with the SAGE II profiles. The derived climatology spans the ensemble of possible profiles. For details of the analysis, see Wellemeyer et al. (1997). The standard OMPS profiles are defined in Umkehr layers (**Table 2.3-2**), so the SAGE II profiles are converted to pressure coordinates using the NMC temperature profiles provided with the SAGE II data and integrated into Umkehr layers. The resulting standard ozone and temperature profiles are given in **Tables 2.3-3** and **2.3-4**.

Table 2.3-2. Umkehr Layers Used for Ozone Profiles

Umkehr Layer No.	Layer Pressure (mb)	Pressure at Altitude of Midpoint (mb)	Layer Midpoint (km)
12	0.000 – 0.247	–	–
11	0.247 – 0.495	0.350	56.5
10	0.495 – 0.990	0.700	51.0
9	0.990 – 1.980	1.40	45.5
8	1.980 – 3.960	2.80	40.2
7	3.960 – 7.920	5.60	35.2
6	7.920 – 15.80	11.2	30.4
5	15.80 – 31.70	22.4	25.8
4	31.70 – 63.30	44.8	21.3
3	63.30 – 127.0	89.6	17.0
2	127.0 – 253.0	179.0	12.5
0 and 1	253.0 – 1013	507.0	5.5

Table 2.3-3. OMPS Standard Ozone Profiles

Prof	Umkehr Layer Number										
	0	1	2	3	4	5	6	7	8	9	> 9
225L	15.0	9.0	5.0	7.0	25.0	62.2	57.0	29.4	10.9	3.2	1.3
275L	15.0	9.0	6.0	12.0	52.0	79.2	57.0	29.4	10.9	3.2	1.3
325L	15.0	9.0	10.0	31.0	71.0	87.2	57.0	29.4	10.9	3.2	1.3
375L	15.0	9.0	21.0	53.0	88.0	87.2	57.0	29.4	10.9	3.2	1.3
425L	15.0	9.0	37.0	81.0	94.0	87.2	57.0	29.4	10.9	3.2	1.3
475L	15.0	9.0	54.0	108.0	100.0	87.2	57.0	29.4	10.9	3.2	1.3
125M	6.0	5.0	4.0	6.0	8.0	31.8	28.0	20.0	11.1	3.7	1.4
175M	8.0	7.0	8.0	12.0	26.0	41.9	33.6	22.3	11.1	3.7	1.4
225M	10.0	9.0	12.0	18.0	44.0	52.1	39.2	24.5	11.1	3.7	1.4
275M	16.0	12.0	15.0	29.0	58.0	63.7	40.6	24.5	11.1	3.7	1.4
325M	16.0	14.0	26.0	45.0	74.7	66.9	41.7	24.5	11.1	3.7	1.4
375M	16.0	16.0	39.0	64.0	85.7	71.1	42.5	24.5	11.1	3.7	1.4
425M	16.0	18.0	54.0	84.0	97.7	71.7	42.9	24.5	11.1	3.7	1.4
475M	16.0	22.0	72.0	107.7	101.0	72.6	43.0	24.5	11.1	3.7	1.4
525M	16.0	26.0	91.0	127.7	108.0	72.6	43.0	24.5	11.1	3.7	1.4
575M	16.0	30.0	110.0	147.7	115.0	72.6	43.0	24.5	11.1	3.7	1.4
125H	9.5	7.0	18.3	7.6	8.2	28.6	22.0	12.4	7.7	2.5	1.2
175H	9.5	8.0	22.8	22.0	26.9	32.3	26.8	15.0	8.0	2.5	1.2
225H	10.0	9.0	27.6	45.7	41.0	35.0	28.8	15.4	8.3	2.9	1.3
275H	14.0	12.0	34.0	66.9	54.2	36.0	28.8	15.4	8.9	3.4	1.4
325H	14.0	15.0	46.8	82.6	65.2	41.7	28.8	17.2	8.9	3.4	1.4
375H	14.0	20.0	61.2	93.8	75.2	45.9	32.5	18.7	8.9	3.4	1.4
425H	14.0	25.0	76.2	104.9	84.2	51.4	35.6	20.0	8.9	3.4	1.4
475H	14.0	32.0	91.0	117.1	93.0	55.8	37.5	20.9	8.9	3.4	1.4
525H	14.0	41.0	107.1	128.1	101.0	60.2	38.2	21.7	8.9	3.4	1.4
575H	14.0	49.0	123.2	142.2	111.0	60.6	38.8	22.5	8.9	3.4	1.4

Table 2.3-4. OMPS Standard Temperature

	Umkehr Layer Number										
Prof	**0**	**1**	**2**	**3**	**4**	**5**	**6**	**7**	**8**	**9**	**> 9**
225L	283.0	251.0	215.6	200.7	210.7	221.6	231.1	245.3	258.7	267.4	265.4
275L	283.0	251.0	215.9	203.5	211.9	222.5	231.1	245.3	258.7	267.4	265.4
325L	283.0	251.0	216.5	207.0	213.6	223.0	231.1	245.3	258.7	267.4	265.4
375L	283.0	251.0	216.0	210.0	216.0	224.0	231.1	245.3	258.7	267.4	265.4
425L	283.0	251.0	216.0	213.0	217.0	224.5	231.1	245.3	258.7	267.4	265.4
475L	283.0	251.0	216.0	216.0	219.0	225.0	231.1	245.3	258.7	267.4	265.4
125M	237.0	218.0	196.0	191.0	193.0	210.0	227.6	239.4	253.6	263.9	262.6
175M	260.0	228.0	201.7	198.0	202.1	214.3	227.6	239.4	253.6	263.9	262.6
225M	273.0	239.0	213.3	207.5	211.7	219.1	227.6	239.4	253.6	263.9	262.6
275M	273.0	239.0	217.1	212.2	214.9	220.4	227.6	239.4	253.6	263.9	262.6
325M	273.0	239.0	219.1	216.6	217.0	220.8	227.6	239.4	253.6	263.9	262.6
375M	273.0	239.0	220.2	219.0	219.0	221.9	227.6	239.4	253.6	263.9	262.6
425M	273.0	239.0	220.9	220.7	221.0	223.7	227.6	239.4	253.6	263.9	262.6
475M	273.0	239.0	221.5	222.5	222.7	224.4	227.6	239.4	253.6	263.9	262.6
525M	273.0	239.0	222.3	224.8	225.5	225.8	227.6	239.4	253.6	263.9	262.6
575M	273.0	239.0	225.0	227.0	227.0	227.0	227.6	239.4	253.5	263.9	262.6
125H	237.0	218.0	196.0	191.0	193.0	210.0	223.3	237.1	251.6	262.4	265.6
175H	260.0	228.0	201.7	198.0	202.1	214.3	223.3	237.1	251.6	262.4	265.6
225H	260.0	228.0	209.7	208.5	212.5	222.0	228.0	237.1	251.6	262.4	265.6
275H	260.0	228.0	222.6	223.4	223.8	226.5	231.6	237.1	251.6	262.4	265.6
325H	260.0	228.0	222.6	223.4	223.8	226.5	231.6	237.1	251.5	262.4	265.6
375H	260.0	228.0	222.6	223.4	223.8	226.5	231.6	237.1	251.5	262.4	265.6
425H	260.0	228.0	222.6	223.4	223.8	226.5	231.6	237.1	251.5	262.4	265.6
475H	260.0	228.0	222.6	223.4	223.8	226.5	231.6	237.1	251.5	262.4	265.6
525H	260.0	228.0	222.6	223.4	223.8	226.5	231.6	237.1	251.5	262.4	265.6
575H	260.0	228.0	222.6	223.4	223.8	226.5	231.6	237.1	251.5	262.4	265.6

2.3.1.2 Sensor Table Generation

The OMPS nadir total column sensor measures UV radiances in the range from 300 to 380 nm. The total column algorithm uses 22 wavelengths from this range (details of the wavelength selection are given in Section 2.4.10).

The OMPS sensor cannot actually measure monochromatic radiance, I(λ), because of its finite bandwidth. Therefore, in generating look-up tables for the algorithm, slit-averaged values were computed from the master table for the central value of the 22 wavelengths using slit functions from the OMPS sensor. Mathematically, the slit-average radiance is written as:

$$\bar{I}(\lambda_0) = \frac{I(\lambda)S(\lambda)d\lambda}{S(\lambda)d\lambda}\text{ , or} \qquad (9)$$

$$\bar{I} = \frac{NR(\lambda)F(\lambda)S(\lambda)d\lambda}{S(\lambda)d\lambda}, \tag{10}$$

where λ_0 is the central slit wavelength, S(λ) is the response function (slit function), and F(λ) is the extraterrestrial solar flux. Similarly, the measured average solar flux F may be expressed as

$$\bar{F}(\lambda_0) = \frac{F(\lambda)S(\lambda)d\lambda}{S(\lambda)d\lambda} \tag{11}$$

Consequently, the measured NR can be expressed as

$$\bar{NR}(\lambda_0) = \frac{NR(\lambda)F(\lambda)S(\lambda)d\lambda}{F(\lambda)S(\lambda)d\lambda} \tag{12}$$

Thus, the NR utilized in establishing the ozone look-up tables should be computed following Equation (12). In this equation, NR(λ) now represents the theoretical NR obtained from TOMRAD using a given ozone profile and at a given pressure, solar zenith angle, and satellite zenith angle, and employing the ozone absorption coefficient, $\alpha_{BP}(\lambda)$, provided by Bass and Paur as a parameter at given wavelength λ_{BP} (Bass and Paur, 1984). In the OMPS table, the exact NRs were derived using Equation (12) and values from the master table. In addition, the high-resolution solar flux measurements from the SOLSTICE instrument were included in the calculation (Woods et al., 1996).

2.3.2 Sensitivity Tables

As described above, the sensor table is based on a standard set of ozone and temperature profiles. To correct for deviations between the actual ozone and temperature profiles and the standard ones, the OMPS algorithm uses two sensitivity tables, one to calculate the change in N with layer temperature, dN/dt, and one to calculate the change in N with layer ozone amount, dN/dx.

dN/dx Table. As in the generation of the master table, TOMRAD was used to generate values of $\log(I_0)$, Z_1/I_0, Z_2/I_0, T/I_0, and S_b for each wavelength, angle, and pressure node point shown in Table 2.3-1. However, TOMRAD was run 12 times for each standard ozone and temperature profile, once unperturbed and 11 times with perturbations about the standard profile. On the first run, the standard ozone profile was used. On the second run, the standard ozone profile was perturbed by increasing ozone in the first layer by 10%. On the third run, the standard profile was perturbed by increasing ozone in the second layer by 10%. This process continued for the 11 layer ozone amounts. A table was generated containing values for the 26 standard profiles as well as all 11 perturbations of each standard profile.

By combining calculated N values for ozone profiles perturbed in different layers with calculated N values for the standard profile, dN/dx values for each of the layers can be generated and used by the algorithm.

A sensor table is generated from the sensitivity "master table" using the same procedure described in Section 2.3.1.2.

dN/dt Table. The dN/dt table was generated in a similar manner to the dN/dx table. On the first run, a standard temperature profile was used. On the second run, a standard temperature profile was perturbed by increasing the temperature in the first layer by 10°. On the third run, a standard profile was perturbed by increasing the temperature in the second layer by 10°. This process continued for the 11 layer ozone amounts. A table was then generated containing values for the 26 standard profiles as well as all 11 perturbations of each standard profile.

As with the dN/dx table, by combining calculated N values for temperature profiles perturbed in different layers with calculated N values for the standard profile, dN/dt values for each of the layers can be generated and used by the algorithm.

Again, a sensor table is then generated using the same procedure described in Section 2.3.1.2.

2.3.3 Rotational-Raman Scattering

In the algorithm, a correction to the computed table radiances is applied in order to account for the effects of rotational-Raman scattering (RRS), which is also known as the Ring effect. The RRS effect on backscattered ultraviolet (BUV) radiances, which has been modeled and described in detail elsewhere (Joiner et al., 1995) is complex and varies as a function of solar zenith angle, satellite zenith angle, reflectivity, and surface pressure as well as wavelength. The correction is applied to the table radiances after each lookup is performed.

In order to simplify the RRS correction, the dependencies on solar and satellite zenith angle, which are small under most conditions, are ignored. For example, at low reflectivities, the RRS correction varies with solar and satellite zenith angle by less than ± 0.2% at all wavelengths.

The RRS effect is approximately linear with surface pressure. Therefore, a single correction is applied at each wavelength to the 1.0, 0.7, 0.4, and 0.1 atmospheric pressure tables. These are computed at the surface and cloud reflectivities, respectively, and are chosen consistent with assumptions made in the partial cloud algorithm. All correction factors were computed at a solar zenith angle of 45° and a satellite zenith angle of 0°.

2.4 Retrieval

2.4.1 Overview

As stated previously, the retrieval of ozone is based on a comparison between the measured normalized radiances (NRs) and NRs derived by radiative transfer calculations for different ozone amounts and the conditions of the measurement. It is implemented by using the tables of backscattered NRs described in Section 2.3. Given the computed radiances for the particular observing conditions, the total ozone value can be derived by interpolation of NR as a function of ozone. It is also possible to reverse this process and use the tables to obtain the NRs that would be expected for a given column ozone and conditions of the measurement. The logarithm

of the ratio of the measured NR to this calculated NR (or the difference between measured and calculated N values) is the residue.

The retrieval starts out by calculating an effective cloud fraction. The reflecting surface is assumed to consist of two components, a surface component of lower reflectivity and a cloud component of higher reflectivity. By comparing the measured radiance at an ozone-insensitive wavelength with one calculated for cloud and for ground reflection alone, the effective cloud fraction and the contribution from each level can be derived.

Using this effective cloud fraction and the NRs measured at a pair of wavelengths (one strongly sensitive to ozone, one weakly sensitive or insensitive to ozone), an initial ozone estimate is derived by matching the measured N value to N values interpolated from the table using the viewing conditions of the measurement.

This ozone estimate is used to calculate residues for the pair of wavelengths. A linear correction to the initial ozone estimate is then derived from the residues at these two wavelengths. This linear correction accounts for differences between the Rayleigh scattering atmosphere model assumed in constructing the tables and the actual atmosphere measured by the sensor.

Although the linear correction accounts for most differences between the model Rayleigh and actual atmospheres, it overcorrects the amount of total ozone in the presence of tropospheric aerosols or for cases of sun glint. A second adjustment to the ozone value is therefore applied. This adjustment, which is determined by assuming that there must be a linear dependence in reflectivity with wavelength, effectively corrects for these effects.

Since the calculated N values are derived from tables based on a set of standard ozone and temperature profiles, deviations of the actual ozone and temperature profiles from the standard ones produce errors in the ozone retrieval. External data is used to determine the layer deviations between actual and standard profiles. Corrections for these profile differences are calculated by multiplying each layer deviation with sensitivities determined by table interpolation. These corrections are applied to the retrieved ozone.

Finally, the backscattered radiances at 1 nm resolution are not 100% sensitive to ozone in the troposphere. This inefficiency also produces errors in the retrieved ozone value. The algorithm uses climatological values for the amount of tropospheric ozone (depending on location and time of year) along with layer ozone sensitivities calculated from the dN/dx table to determine tropospheric efficiency. This efficiency factor is used to correct the tropospheric ozone amount and, in turn, the total column ozone amount.

In order to minimize errors due to sensor noise, the above procedure is performed on multiple sets of triplets using 4 different ozone-insensitive wavelengths to determine reflectivity. For each measurement, 12 different wavelength triplets are used (3 different wavelength pairs matched to the 4 different reflectivity wavelengths). The choice of triplets is based upon the optical path length of the measurement.

The ozone retrieval is checked for volcanic SO_2 contamination. If it is contaminated, the retrieval is flagged for post processing. The retrieval is also checked for the occurrence of a solar eclipse and, if affected, it is flagged.

Algorithms for the derivation of other parameters besides ozone have been developed. These include an estimate of UVB flux at the surface and estimates of aerosol loading due to the presence of atmospheric aerosols.

2.4.2 OMPS Reflectivity (Cloud Fraction)

The OMPS algorithm accounts for the presence of clouds using a simple physical model that assumes a scene can be represented by two separate reflecting surfaces, one for the ground and one for clouds. The fractional contribution of each to the reflectivity is obtained by comparing the measured NR with NR values calculated for pure ground and pure cloud scenes.

For a given measurement at a given non-ozone-absorbing wavelength, the NR tables are used along with Equation (12) to determine an NR value corresponding to reflection off of the ground and an NR value corresponding to reflection off of a cloud. The total NR is computed simply as the area weighted average of the terrain and cloud NRs.

In the calculation of the terrain NR, external terrain pressure information from CrIS is used. If not available, a data set compiled from the TUG87 geophysical model (Weiser, 1987) is used. This data set contains a 1° latitude by 1.25° longitude grid of pressure values.

The surface reflectivity is determined from a database of minimum UV surface reflectivity developed using the 15-year Nimbus-7/TOMS data set (Herman and Celarier, 1997). This data set contains a 1° latitude by 1.25° longitude grid of minimum UV surface reflectivity for each month.

In the calculation of cloud radiance, external cloud pressure information from VIIRS is used. If not available, a data-set compiled from the International Satellite Cloud Climatology Project (ISCCP) will be used to determine the cloud-top pressure. This data set, similar to the one described above, contains a 1° latitude by 1.25° longitude grid for each month. A cloud reflectivity of 80 percent is assumed.

The fractional cloud cover, f, is estimated as:

$$f = \frac{I_{measured} - I_{terrain}}{I_{cloud} - I_{terrain}} \tag{13}$$

where $I_{terrain}$ and I_{cloud} are the terrain and cloud-top NRs, respectively, from the tables, and $I_{measured}$ is the measured NR. An effective reflectivity, R, is calculated as:

$$R = R_{surface} + (0.8 - R_{surface}) * f \tag{14}$$

In cases where the reflectivity is less than $R_{surface}$ or greater than 80%, the effective reflectivity is calculated by inverting Equation (12).

External data from VIIRS is used to determine if snow or ice is on the ground. If there is no snow or ice, then the cloud fraction (determined from the nadir sensor) and the cloud top pressure (VIIRS EDR) and surface pressure (CrIS EDR) are used to determine the effective reflectivity and the pressure of the reflecting surface. If there is snow or ice, then the retrieval algorithm will calculate R assuming a clear scene (Ahmad, 2000).

If the external EDRs are unavailable, a snow/ice database is used. As above, it is determined from the database that snow or ice conditions are present, the OMPS algorithm will calculate R assuming a clear scene.

2.4.3 Initial Estimate of Ozone

The OMPS nadir algorithm uses the cloud fraction (or reflectivity) determined from an ozone-insensitive wavelength and the measured N value difference between a pair of closely spaced shorter wavelengths (one strongly ozone absorbing and one ozone insensitive or weakly ozone absorbing) to determine an initial estimate of ozone. The use of a pair difference provides an estimate insensitive to wavelength-independent errors, in particular, calibration errors. The ozone estimate is the ozone value at which, for the derived reflectivity and measurement geometry, the calculated N value difference for the pair of wavelengths best matches the measured N value difference. The pair chosen for this initial estimate is 318/336 nm.

For each measurement, NRs are calculated for a given standard ozone profile at each pressure level using the given viewing conditions. The ozone profile used for the calculation depends on the latitude of the measurement and the total ozone value corresponds to the closest table node point below the ozone amount from the previous measurement. For the ground situation, the surface reflectivity is assumed and terrain pressure is used to interpolate the 0.1, 0.4, 0.7, and 1.0 atm NRs in order to determine a calculated NR for this ozone profile. For the cloud situation, NRs for each ozone value are determined assuming a cloud reflectivity of 80% with the cloud pressure used for the interpolation. An NR is determined for the entire scene as an area-weighted average of the ground and cloud NRs using the fractional cloud cover, f. The NRs are converted into pair N values, and the calculated pair N value is compared to the measured pair N value.

If the calculated N value is lower, another pair N value is calculated (using the procedure just described) for the next higher ozone node point. If it is higher, another pair N value is calculated for the next lower ozone node point. In this way, two calculated pair N values that bracket the measured pair N value are found. An ozone estimate is determined using the measured pair N value to linearly interpolate between calculated N values to find the corresponding ozone amount.

2.4.4 Linear Correction

In the absence of other geophysical phenomena or calibration errors, N values calculated for each of the pair of wavelengths (using the ozone estimate and the reflectivity determined from the reflectivity wavelength) are equal to the measured N values for those wavelengths. Consequently, non-zero values of the difference between measured and calculated N value, or

residue, for a given wavelength signifies that either calibration errors or geophysical phenomena are not yet taken into account.

The OMPS algorithm corrects for this error by assuming that the residue dependence in the wavelength triplet is linear. If, for a given OMPS wavelength the measured N value is denoted by N_m, then, using a first order Taylor series expansion:

$$N_m = N_0 + (\Omega - \Omega_0)\frac{dN}{d\Omega} \tag{15}$$

where Ω_0 is an initial estimate of ozone obtained using the pair of wavelengths. N_0 is the N value calculated by using the long wavelength, cloud fraction, and Ω_0 in conjunction with the tables. Ω is the corrected ozone value. By assuming a linear wavelength dependence the above equation becomes:

$$r = N_m - N_0 = (\Omega - \Omega_0)\frac{dN}{d\Omega} + a + b\lambda \tag{16}$$

where r is the residue. Since the long or reflectivity wavelength is insensitive to ozone, $dN/d\Omega = 0$ and

$$r = a + b\lambda = a + b\lambda_R \tag{17}$$

Since the long wavelength is used to determine the cloud fraction (and, therefore, reflectivity), the calculated and measured N values are equal:

$$r_R = 0 \Rightarrow a = -\lambda_R b$$

For ozone-sensitive wavelengths:

$$r_\lambda = (\Omega - \Omega_0)\frac{dN}{d\Omega} + b(\lambda - \lambda_R) \tag{18}$$

Since there are 2 unknowns in Equation (18) - Ω and b, the pair of wavelengths in the triplet are used to solve for Ω:

$$\Omega = \Omega_0 + \frac{r_1(\lambda_2 - \lambda_R) - r_2(\lambda_1 - \lambda_R)}{(\frac{dN}{d\Omega})_1(\lambda_2 - \lambda_R) - (\frac{dN}{d\Omega})_2(\lambda_1 - \lambda_R)} \tag{19}$$

where 1 and 2 represent the two different wavelengths.

The triplets used to solve Equation (19) depend on the optical path length of the measurement, which is defined as the path length times ozone amount divided by 1000:

$$somega = \Omega_0 \cdot (\sec\theta_0 + \sec\theta)/1000. \tag{20}$$

This choice of triplets is discussed in Sections 2.4.9 and 2.4.10.

2.4.5 Profile Selection

The radiative transfer tables include ozone and temperature profiles for three broad latitude bands; low, middle, and high. For latitudes ≤ 15°, the retrieval is performed using only the low-latitude profiles. For 15° < latitudes ≤ 45°, retrievals are performed using low- and mid-latitude profiles. For 45° < latitudes < 75°, retrievals are calculated using mid- and high-latitude profiles. And, for latitude ≥ 75°, retrievals are performed for high-latitude profiles. Values of dN/dΩ are calculated, as well.

For retrievals at latitudes where two profiles are used, an ozone value appropriate to the latitude of the measurement is derived from the ozone values for the two profiles, using an equation of the form:

$$\Omega = (1 - f_{prof}) \cdot \Omega_{lower} + f_{prof}\,\Omega_{higher} \tag{21}$$

where

Ω	=	ozone,
Ω_{lower}	=	ozone retrieved using lower latitude profile,
Ω_{higher}	=	ozone retrieved using higher latitude profile, and
f_{prof}	=	weight given to higher latitude profile.

Thus, f_{prof} will be 0 if only the lower latitude profile is selected, 1 if only the higher latitude profile is selected, and in between for a combination of the two profiles.

For *somega* less than 1.5, a value of f_{prof} obtained by simple linear interpolation in latitude,

$$f_{prof} = \frac{|latitude| - |latitude|_{lower}}{|latitude|_{higher} - |latitude|_{lower}} \tag{22}$$

is used for latitudes between 15 and 75 degrees using the two profiles appropriate for the latitude. The low-latitude profile alone is used from the equator to 15 degrees, and the high-latitude profile alone is used from 75 degrees to the pole.

For longer path lengths, a profile mixing scheme is used to determine the profile mixing factor, f_{prof}. The basic principle is to calculate the residue of a fourth, shorter wavelength that is sensitive to ozone profile shape information. By defining a linear combination of the standard profiles that best explains the radiances at all four wavelengths, the algorithm calculates the profile mixing factor:

$$f_m = \frac{r'(lower)}{r'(lower) - r'(higher)} \tag{23}$$

where lower and higher refer to latitudes of the two profiles used and r′ refers to the residue for the shortest channel among four wavelength channels. In most cases, the appropriate profile will be between the higher and lower latitude profiles, and the residues will be of opposite sign; thus the denominator represents a distance between the residues (or sensitivity to profile shape) and the numerator a fraction of this distance. When the low- and mid-latitude profiles are used, and when the derived value of f_{prof} is greater than 1, the process is repeated using the mid- and high-latitude profiles. Similarly, if f_{prof} is less than zero using mid- and high-latitude profiles, then the process is repeated using the low- and mid-latitude profiles.

The value of Ω as obtained from Equation (21) represents the heritage Version 7 algorithm total ozone and will be reported as a separate data product, Ω_{V7}.

2.4.6 Correction for Tropospheric Aerosols and Sun Glint

Radiative transfer studies performed at NASA/GSFC and Raytheon indicate that in the presence of tropospheric aerosols, the linear assumption does not adequately account for tropospheric aerosols or sun glint. These studies further indicate that the retrieved ozone value can be corrected by assuming that the reflectivity dependence across the wavelength triplet λ_1, λ_2, and λ_R, is linear:

$$r_{\lambda_2} = (\Omega_{aercor} - \Omega_{V7})(\frac{dN}{d\Omega})_{\lambda_2} + (R_{\lambda_2} - R_{\lambda_R})(\frac{dN}{dR})_{\lambda_2}, \tag{24}$$

$$r_{\lambda_1} = (\Omega_{aercor} - \Omega_{V7})(\frac{dN}{d\Omega})_{\lambda_1} + (R_{\lambda_2} - R_{\lambda_R})(\frac{\Delta\lambda_1}{\Delta\lambda_2})(\frac{dN}{dR})_{\lambda_1} \tag{25}$$

Ω_{V7}	=	uncorrected ozone value
Ω_{aercor}	=	corrected ozone value
$R_{\lambda i}$	=	reflectivity determined from wavelength i
$r_{\lambda i}$	=	residue for wavelength i
$\Delta\lambda_i$	=	$\lambda_i - \lambda_R$
$(dN/d\Omega)_{\lambda i}$	=	ozone sensitivity for wavelength i
$(dN/dR)_{\lambda i}$	=	reflectivity sensitivity for wavelength i

2.4.7 Correction for Temperature and Ozone Profile Shape

Since the ozone absorption coefficient depends on temperature, differences between the standard temperature profiles and the actual atmospheric temperature profile lead to errors in retrieved ozone. The same is true for differences between the standard ozone profile shape and the actual ozone profile shape, particularly for large path length or large ozone amount.

To correct for these temperature and profile shape errors, two terms are added to the Taylor series expansion given in Equation 16. Expanding around Ω_{aercor}:

$$r = N_m - N_{aercor} = (\Omega - \Omega_{aercor})\frac{dN}{d\Omega} + \sum_{layer}(t_{layer} - t^0_{layer})\frac{dN}{dt_{layer}} + \sum_{layer}(x_{layer} - x^0_{layer})\frac{dN}{dx_{layer}} + a + b\lambda \qquad (26)$$

where:

t_{layer} = layer temperature obtained from the CrIS sensor,
t^0_{layer} = layer temperature used in the standard profile,
x_{layer} = layer ozone amount obtained from the OMPS limb sensor, and
x^0_{layer} = layer ozone amount used in the standard profile.

The layer temperature sensitivity, dN/dt_{layer}, and layer ozone sensitivity, dN/dx_{layer}, are determined from the radiative transfer tables described in Section 2.3.2.

The CrIS temperature profile information is matched to the 11 layers used in the tables through a spline fitting procedure. A similar procedure is used to match the OMPS limb retrieval.

Since the limb retrieval does not retrieve ozone amounts down to the surface, the ozone profile correction is only applied down to the level at which the limb retrieval contains ozone profile information.

The ozone solution becomes:

$$\Omega_{tpcor} = \Omega_{aercor} + \frac{r_1(\lambda_2 - \lambda_R) - r_2(\lambda_1 - \lambda_R)}{(\frac{dN}{d\Omega})_1(\lambda_2 - \lambda_R) - (\frac{dN}{d\Omega})_2(\lambda_1 - \lambda_R)} \qquad (27)$$

2.4.8 Correction for Tropospheric Ozone

The OMPS limb retrieval is used to correct profile shape errors and to correct for errors due to the insensitivity of the BUV solar radiation (at 1 nm spectral resolution) to tropospheric ozone.

The amount of tropospheric ozone that is measured strongly depends on the amount of tropospheric ozone contained in the standard profile, X^0_{trop}. We can write the amount of tropospheric ozone retrieved as:

$$X_{retr} = \Omega_{tpcor} - \sum_{strat} x_{limb} \qquad (28)$$

where $\sum_{strat} x_{limb}$ is the sum of the limb ozone profile down to the tropopause. If the technique were 100% efficient in measuring ozone in the troposphere, the difference between X_{retr} and X^0_{trop} would be an accurate measure of the difference between the retrieved amount and the amount in the standard profile. Since the technique is less efficient, we need to divide the difference by the measurement efficiency to determine the actual change:

$$\Delta X = \frac{X_{retr} - X^{0}_{trop}}{\xi_{trop}} \tag{29}$$

We can now write

$$X_{trop} = \frac{X_{retr} - X^{0}_{trop}}{\xi_{trop}} + X^{0}_{trop} \tag{30}$$

where X_{trop} is the actual amount of ozone in the troposphere. The tropospheric efficiency is:

$$\xi_{trop} = \frac{\sum_{trop} \xi_{layer} x_{layer}}{\sum_{trop} x_{layer}} \tag{31}$$

where ξ_{layer} represents the measurement efficiencies in each atmospheric layer in the troposphere and x_{layer} is the amount of ozone in each of those layers. The individual layer efficiencies are determined from

$$\xi_{layer} = \frac{dN_{triplet} / dx}{dN_{triplet} / d\Omega} \tag{32}$$

The layer sensitivities in the numerator are obtained from the sensitivity tables, and the total column ozone sensitivity is calculated when making the linear correction. The layer ozone amounts are obtained from a tropospheric ozone database.

Once the layer sensitivities and ozone amounts have been determined, Equation (30) can be used to determine the actual tropospheric ozone amount, which is used to correct **Ω**:

$$\Omega = \Omega_{tpcor} - X_{retr} + X_{trop} \tag{33}$$

The climatology used for the tropospheric ozone database is based on tropopause height and latitude data using the same 20-year ozone balloon-sonde data set as used in developing the WPTB test data sets. Separate regressions were done in five latitude zones from 90 - 60 S, 60 - 30 S, 30 S - 30 N, 30 - 60 N, and 60 - 90 N. A sample regression is shown in **Figure 2.4-1** for mid-southern latitudes. The layer ozone amounts are calculated using fractional amounts of the total tropospheric column. These layer fractions are derived from the sonde climatology and they are also regressed as functions of the tropopause height. This is a good way to provide a simplicity of implementation and reduction in variance. A sample regression of the layer 0 fractions is shown in **Figure 2.4-2**, also for mid-southern latitudes. With this implementation and

given the tropopause height for a retrieval at a particular latitude, the climatological tropospheric ozone amounts in the lowest three Umkehr layers are specified.

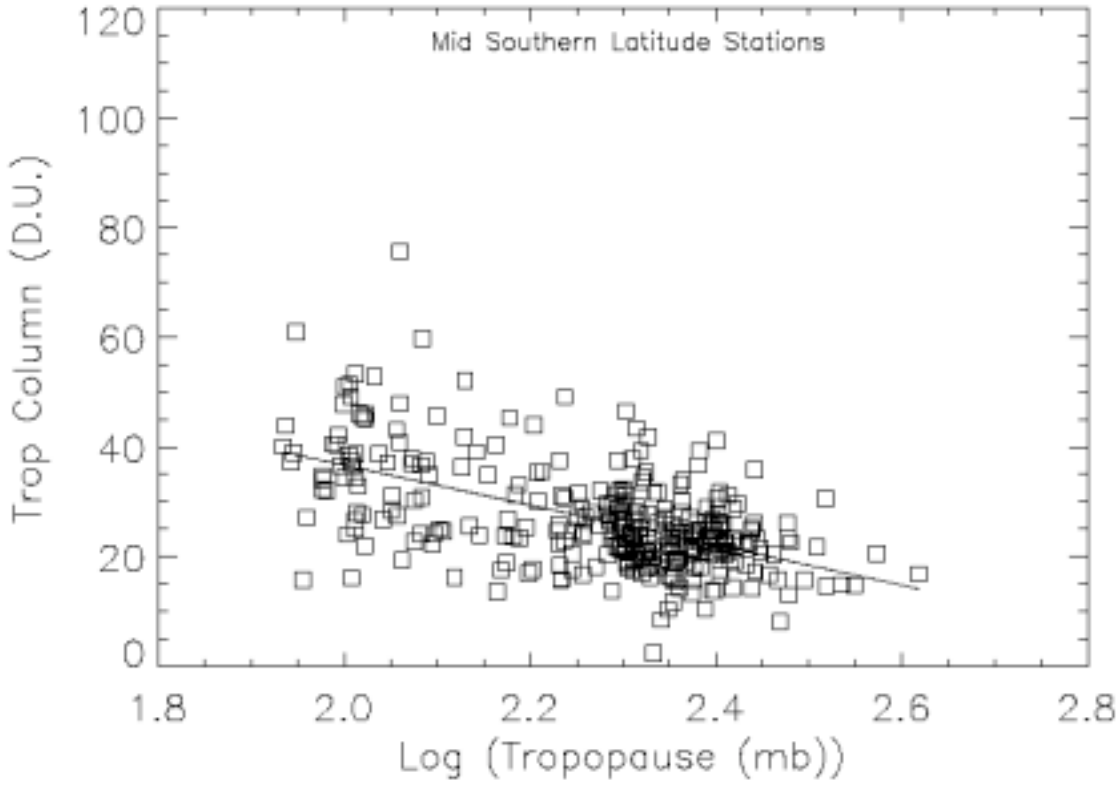

Figure 2.4-1. Regression of tropospheric column ozone vs. tropopause height for mid-southern latitude balloon-sondes

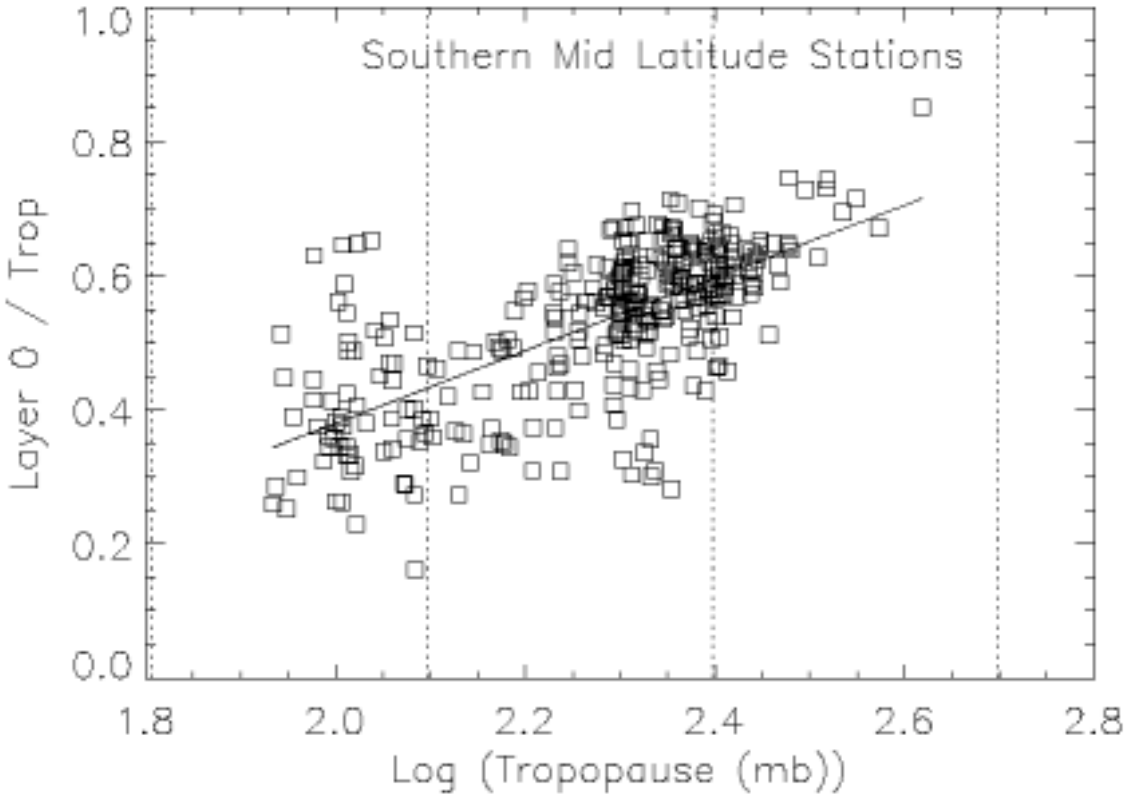

Figure 2.4-2. Regression of Layer 0 Tropospheric Ozone Fraction vs. Tropopause Height

The final form of the tropospheric ozone database design will consist of a grid of latitude by longitude by time for the lowest three Umkehr layers. The procedures to develop and populate this database are not finalized. It will start as a 5 degree latitude by 10 degree longitude by 12 month grid. As the database is updated with tropospheric ozone information from TOMS, SBUV/2, SAGE III, GOME, SCIAMACHY, balloon-sondes, lidar measurements, and OMPS, the grid resolution will be refined. The modular construction of the database permits flexibility to study different procedures in an effort to produce optimal results.

Determinations of tropospheric ozone amount and individual layer amounts obtained by the stratospheric residual (described above) or by the cloud slicing technique (described below) are used to populate this database. The layer ozone values used in the Equation (31) are the average of all database values for each grid point.

The cloud slicing technique (Ziemke et al., 1998) is similar to the stratospheric residual technique described above, except that the determination of stratospheric ozone is actually a determination of the ozone column above the cloud and is obtained using the nadir sensor itself. Retrievals over totally cloudy scenes can be differenced from the ozone column above cloud-free scenes to provide an estimate of the tropospheric ozone in the clear scene that is in the layer below the altitude of the cloud surface in the clouded scene. This technique has the potential of

improving knowledge of the tropospheric ozone distribution, because cloud surfaces well below the tropopause height may provide estimates of tropospheric ozone in shallow layers close to the Earth surface. Such determinations can be used to improve the efficiency estimate for the given clear scene retrieval.

In cases of totally clouded scenes, the tropospheric climatology will be used to estimate the amount of ozone below the cloud. Some residual error will remain since the tropospheric ozone amount is dependent on the amount of sunlight and the local circulation, and the climatology is determined using estimates derived from clear sunlit scenes. Estimates of this residual tropospheric ozone error will be provided prior to CDR.

2.4.9 Multiple Triplet Formulation

To reduce the effects of sensor noise, the above retrieval process is performed for each sensor measurement using 12 different sets of triplets.

The cloud fraction is determined using 4 different ozone-insensitive wavelengths (364, 367, 372, and 377 nm). Then, each of these reflectivity wavelengths is matched to 3 different pairs of wavelengths that form the wavelength triplets used to determine ozone. The choice of triplets depends on their ability to accurately measure ozone for the viewing conditions of the measurement or, in other words, their ozone sensitivity.

From Beer's Law we know that:

$$A = \frac{I}{F} = e^{-s(\alpha\Omega+\beta p)}; \tag{34}$$

$$\Delta A_\lambda = -\alpha s e^{-s\alpha_\lambda \Omega}\Delta\Omega; \tag{35}$$

$$\frac{\Delta A_\lambda}{A} = -\alpha s \Delta\Omega \cdot \tag{36}$$

The wavelength sensitivity (percent change in albedo per percent change in ozone) is therefore

$$\frac{\Delta A_\lambda / A_\lambda}{\Delta\Omega / \Omega} = -\alpha s \Omega \tag{37}$$

For a pair of wavelengths

$$\frac{\Delta A_p / A_p}{\Delta\Omega / \Omega} = -\Delta\alpha s \Omega \tag{38}$$

where p represents the wavelength pair. The quantity $\Delta\alpha s\Omega$ can therefore be used to assess the sensitivity of each ozone triplet.

Table 2.4-1 shows $\Delta\alpha s\Omega$ as a function of the path length $s\Omega$ between the wavelengths for each of the wavelength pairs that will be matched to the 4 reflectivity channels (the difference is presented since the algorithm uses a pair of wavelengths matched to the reflectivity wavelengths):

Table 2.4-1. Selection of the Multiple Triplets Available to OMPS

SΩ / λ Pairs	0.75	1.00	1.25	1.50	1.75	2.00	2.50	3.00	3.50	4.00	5.00	6.00
308.5 – 321.0	1.96	2.61	3.26	3.92	4.57	5.22	6.53	7.83	9.14	10.44	13.05	15.66
310.5 – 321.0	1.39	1.85	2.32	2.78	3.24	3.71	4.63	5.56	6.48	7.41	9.26	11.12
312.0 – 321.0	1.06	1.41	1.77	2.12	2.48	2.83	3.54	4	Too Sensitive		7.07	8.49
312.5 – 321.0	0.92	1.23	1.54	1.85	2.16	2.46	3.08	3			6.16	7.39
314.0 – 321.0	0.79	1.05	1.31	1.57	1.83	2.09	2.62	3.14	3.66	4.19	5.23	6.28
318.0 – 336.0	0.62	0.83	1.04	1.24	1.45	1.66	2.07	2.49	2.90	3.32	4.15	4.97
315.0 – 321.0	0.54	0.72	0.90	1.09	1.27	1.45	1.81	2.17	2.53	2.90	3.62	4.34
320.0 – 329.0	0.44	0.59	0.73	0.88	1.03	1.17	1.47	1.76	2.05	2.35	2.93	3.52
322.5 – 332.0	Too Insensitive			0.65	0.76	0.87	1.09	1.30	1.52	1.74	2.17	2.61
325.0 – 336.0				0.54	0.63	0.72	0.90	1.08	1.25	1.43	1.79	2.15
328.0 – 336.0	0.19	0.25	0.32	0.38	0.45	0.51	0.64	0.76	0.89	1.02	1.27	1.53
331.0 – 336.0	0.11	0.14	0.18	0.21	0.25	0.28	0.35	0.42	0.49	0.56	0.70	0.84
316.0 – 329.0	0.73	0.98	1.22	1.47	1.71	1.96	2.45	2.94	3.43	3.92	4.90	5.88
317.0 – 321.0	0.35	0.47	0.59	0.71	0.82	0.94	1.18	1.41	1.64	1.88	2.35	2.82

The clear area in the table indicates which wavelength pairs have ozone sensitivity needed to accurately determine ozone for each atmospheric condition. The path lengths across the top are the maximums for the corresponding bins.

2.4.10 OMPS Channel Selection

The OMPS channels are selected primarily to minimize temperature dependence in the triplet retrieval. The Huggins bands in the near UV display the periodic temperature dependence shown in **Figure 2.4-3**. By choosing short wavelengths at relative minimum in temperature dependence and mid-wavelengths at relative maximum in temperature dependence, the impact of changes in local temperature on triplet ozone are reduced. The lines in the figure indicate the possible values of short wavelength temperature dependence that provide zero triplet dependence for a given mid- and long-wavelength selection. (These channels were selected from an arbitrary scale of 0.5 nm steps at even 0.5 nm. They will be reselected at a particular sensor's absolute wavelength scale and reporting interval.) **Figure 2.4-4** shows the resulting sensitivity of the various triplets to a 10 degree shift in the temperature profile at ozone absorbing altitudes. Note that the selection of 321 nm as a short wavelength creates a triplet with strong temperature dependence that can be used to monitor temperature sensitivity and therefore temperature corrections. The specific choice of long wavelength has little or no effect on these results.

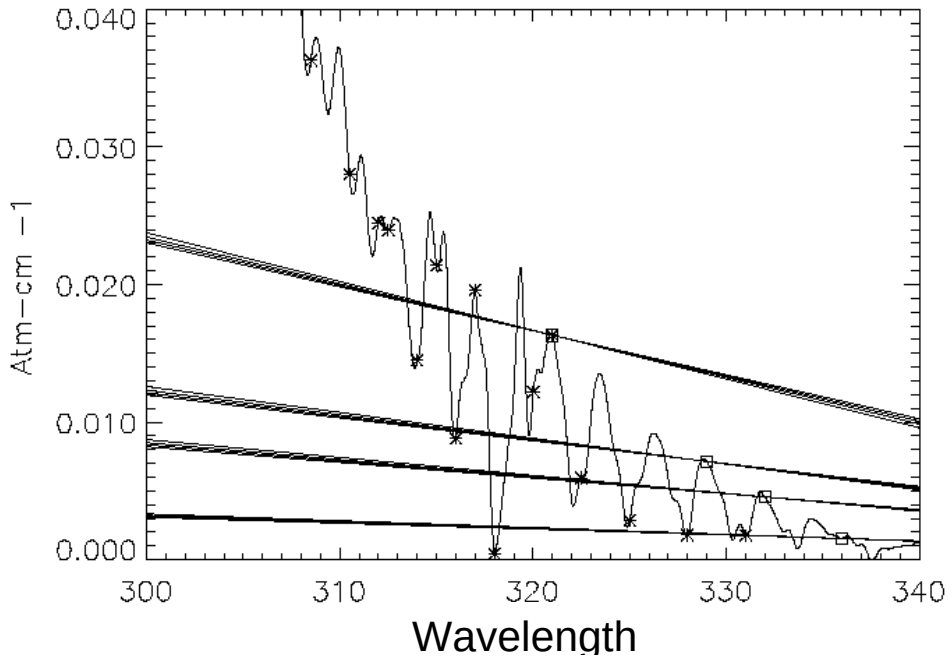

Figure 2.4-3. Impact of temperature changes on OMPS triplet channels

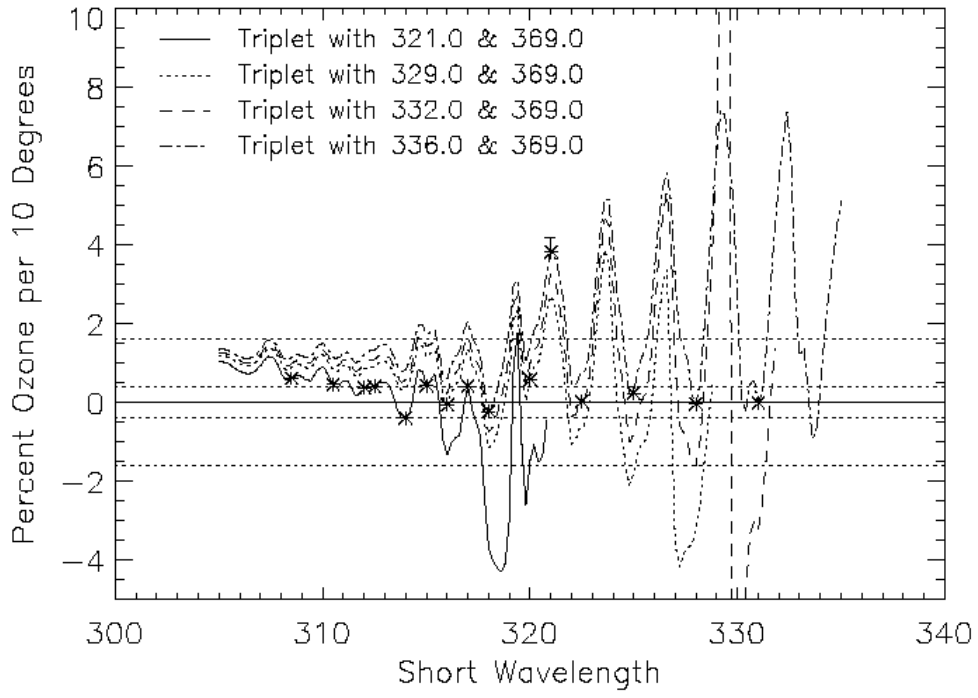

Figure 2.4-4. Impact of temperature changes on OMPS derived total ozone

Since the extreme in the temperature dependence are also extrema in the absorption (local absorption maximum corresponds with local minimum in temperature dependence), this selection procedure also minimizes sensitivity to shifts in the spectral scale. See **Figure 2.4-5**.

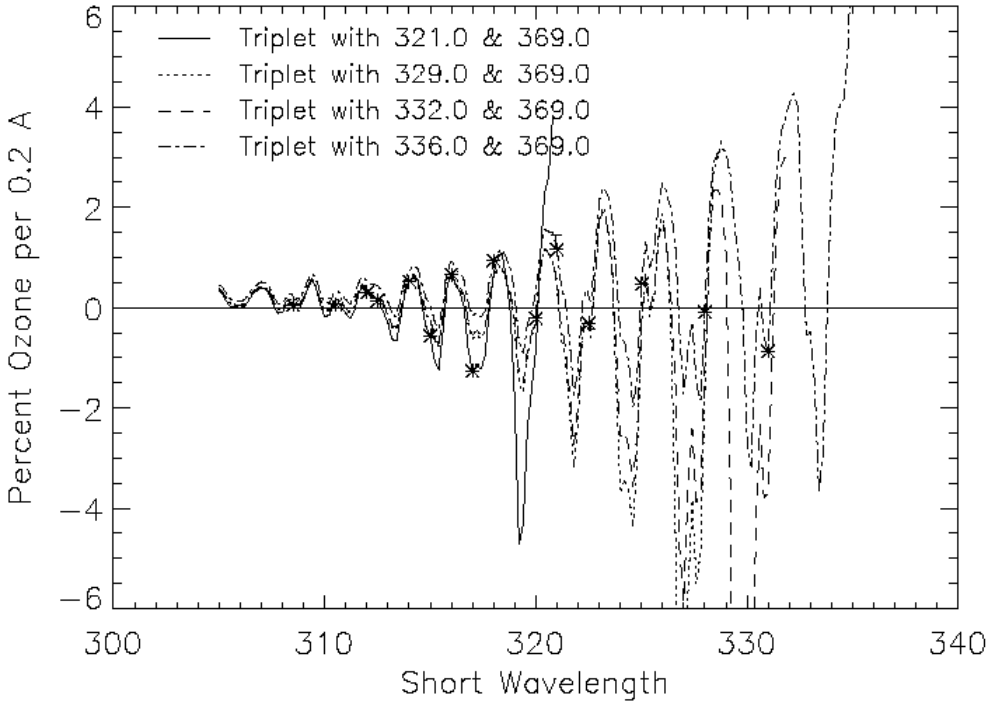

Figure 2.4-5. Impact of wavelength shift on OMPS derived total ozone

A third criterion for channel selection is minimization of the Ring effect. The OMPS channel selection is indicated in **Figure 2.4-6**, which also shows the nominal Ring effect for clear conditions. The Ring effect is the result of rotational Raman scattering, which modifies the wavelength of the scattered light and fills in spectral features (Fraunhofer lines) present in the incoming solar flux. Note that the Ring features are anti-correlated with the features of the relative solar flux included to illustrate this relationship. Because it is scattering induced, the Ring effect is pressure dependent. In general, the Ring effect is quite complicated to model. In the OMPS forward model, only a simple first order correction based on the pressure dependence is made in order to conserve processing time associated with a complete treatment of this complex problem. This is why channels are selected to minimize Ring dependence. As in the case of temperature dependence, two channels (316 and 317 nm) have also been selected to maximize the effect so that the Ring correction can be monitored.

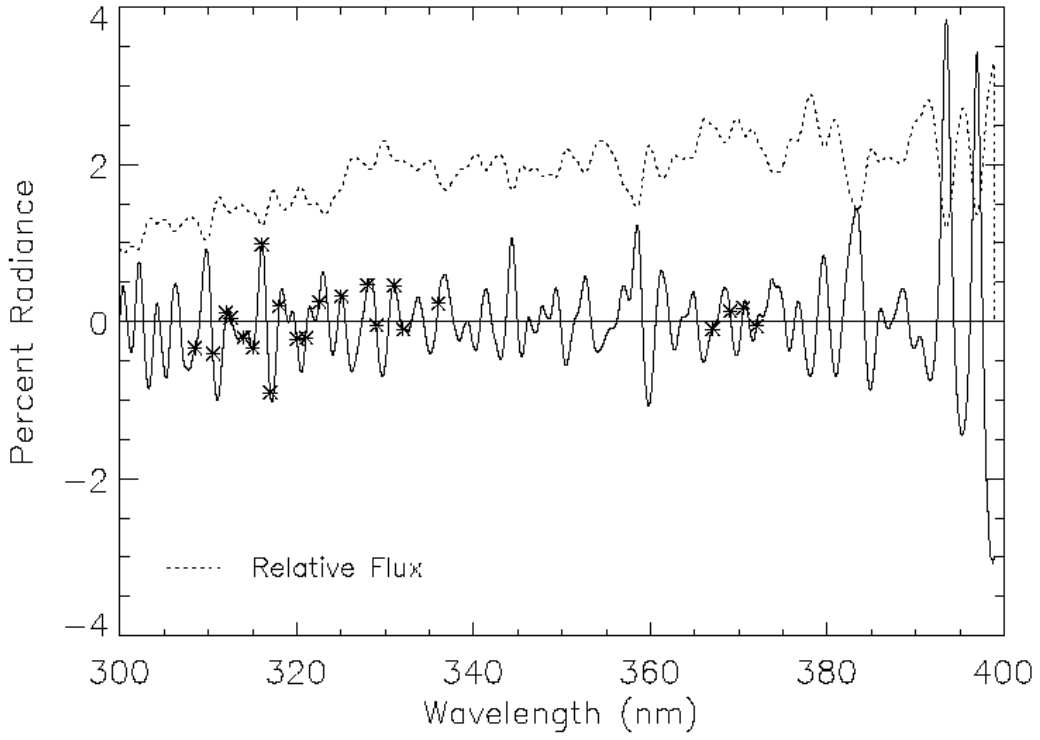

Figure 2.4-6. Impact of Ring effect on the OMPS channels

The selection of long wavelength channels is also effected by O_4 absorption. The abundance of O_4 (the O_2 - O_2 collisional complex) is proportional to the pressure squared, so it occurs close to surface. But the distribution of O_4 and its effect on ultraviolet backscatter has not yet been carefully studied. The effect is thought to be of the order of 1%. In order to avoid the problem of modeling this absorption, we plan to study the placement of the long wavelength channels of OMPS away from these O_4 absorption features. This study will take into account the effect of the different wavelengths on precision and accuracy (e.g., sensor noise, temperature sensitivity, aerosol corrections, and stray light corrections). **Figure 2.4-7** shows the O_4 absorption features and the long wavelength channels selected for the OMPS algorithm.

We note that the 360 nm and 380 nm channels are the heritage reflectivity channels for the EP/TOMS and the Nimbus7 TOMS respectively. Since O_4 absorption is affecting both of these channels, it is likely that GSFC/NASA will study these absorption features in the near future and suggest corrections to the retrieved ozone.

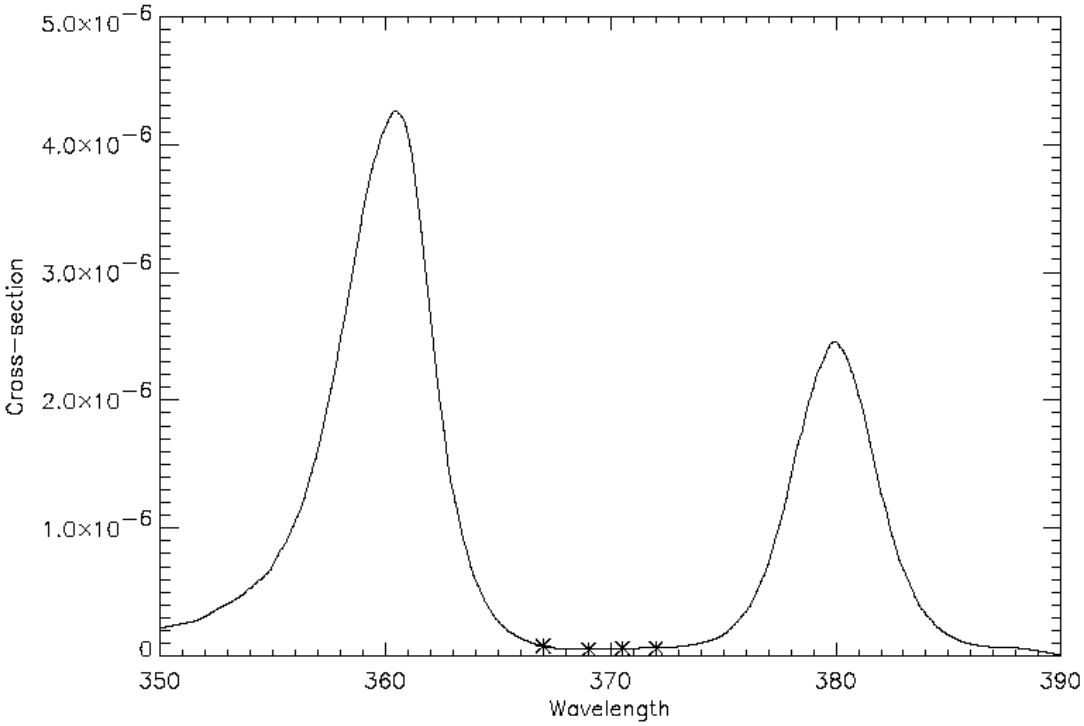

Figure 2.4-7. Possible long wavelength channels for future consideration to avoid O_4 absorption

Our channel selection scheme represents a significant improvement over the heritage channels as well as other potential schemes. Our selections for the OMPS channels have lower sensitivity to temperature effects and wavelength calibration shifts, as well as smaller Ring dependence. They maintain adequate separation between the long- and mid-wavelength channels to give sufficient sensitivity to the wavelength dependent scattering effects of tropospheric aerosols. The 312.0 nm channel provides increased sensitivity to SO_2, which is important for volcanic hazard detection.

2.4.11 Volcanic SO_2

Because of the similarity in absorption coefficients between O_3 and SO_2, the presence of SO_2 due to volcanic eruptions causes an error in determining ozone. The OMPS total column algorithm, while not designed to derive quantitative values for SO_2 amounts, does determine approximate SO_2 amounts. These values serve as flags to indicate the presence of SO_2 from volcanic eruptions and, therefore, an error in ozone determination.

After performing an ozone retrieval, the algorithm determines if there is any volcanic SO_2 present in the atmosphere by performing a Taylor series expansion about the retrieved ozone amount, Ω_{ret}:

$$r = N_m - N_{ret} = (\Omega - \Omega_{ret})\frac{dN}{d\Omega} + S\frac{dN}{dS} + a + b\lambda \tag{39}$$

where S is the amount of SO_2 in the atmosphere (because there is normally no SO_2 the initial estimate, S_0, is zero), N_m is the measured N value for a given wavelength, N_0 is the N value for that wavelength calculated from the tables, Ω is the true ozone in the atmosphere, and the $a + b\lambda$ term accounts for linear wavelength dependencies (either from calibration or atmospheric effects). We now have 4 unknowns, and we need 4 wavelengths to construct the 4 equations necessary to solve for S.

Along with one of the reflectivity wavelengths, the 310.5, 312.0, and 329.0 nm wavelengths are chosen to solve for SO_2. These wavelengths occur either at local maxima or minima with respect to the SO_2/O_3 cross-section ratio and were selected based on the conclusions in Gurevich and Krueger (1997) that such a choice optimizes the retrieval of SO_2.

The ozone sensitivities, $dN/d\Omega$, are determined internally in the course of deriving Ω_{ret}. The SO_2 sensitivities are approximated by

$$\frac{dN}{dS} = \frac{\alpha_{SO_2}}{\alpha_{\Omega}} \frac{dN}{d\Omega} \tag{40}$$

where α_{SO2} and α_{Ω} are the absorption coefficients for SO_2 and ozone for the given wavelength. Since the algorithm is designed to detect contamination from volcanic eruptions, α_{SO2} and α_{Ω} are chosen so that the algorithmic sensitivity to SO_2 for a volcanic plume is large. The SO_2 absorption coefficients are therefore chosen for a temperature of 210 K, which is the temperature of many volcanic plumes, and the ozone absorption coefficients are chosen for a temperature of 223 K, which is the nominal temperature of the ozone maximum.

There are four unknowns in the Taylor series expansion (Ω, S, a, and b). Using the OMPS reflectivity wavelengths with no ozone or SO_2 absorption (377 nm, for example), the four unknowns can be reduced to three by writing the a term as a function of the b term. The other 3 wavelengths are then used to solve the resulting three equations for S. Four estimates of S can be made using the 4 reflectivity wavelengths, thereby reducing the effects of sensor noise.

It should be noted that these equations can be used to simultaneously solve for the "uncontaminated" ozone amount Ω as well as S. However, since the SO_2 sensitivities are approximations designed to be most effective for volcanic eruptions, their use leads to errors in the calculation of Ω. Furthermore, the similarity in absorption between ozone and SO_2 also contribute to the errors when simultaneously retrieving both quantities. For these reasons, this algorithm is not used to determine ozone but, rather, to detect the presence of volcanic SO_2.

Because these errors exist in the calculation of S, it is reported not as the actual SO_2 amount but as an index indicating contamination. We call S the SO_2 index (SOI).

Determination of the SO_2 Contamination Flag Value. The calculation of SOI is not exactly zero in the absence of volcanic SO_2 but is, instead, distributed about zero in a peak whose standard deviation (σ) depends on the noise of the algorithm-sensor system and the approximations discussed above.

ADEOS TOMS is an example of a modern TOMS instrument that uses the above algorithm to flag data contaminated with SO_2. Since the calibration has been finalized and the data have been recently archived, we use it to serve as an example of how the data was flagged in the heritage Version 7 algorithm and how we plan to set this flag for OMPS. **Figure 2.4-8** shows a histogram indicating the frequency of SOI values calculated for March 20, 1997. This date, which represents a background day with no volcanic SO_2, was chosen because of the maximum latitudinal coverage of the data. The histogram is sharply peaked about zero with a σ of about 3 Dobson Units. For the TOMS the SO_2 contamination flag was set for any value of SOI greater than 4σ. In the case of ADEOS TOMS, this is 12 Dobson Units.

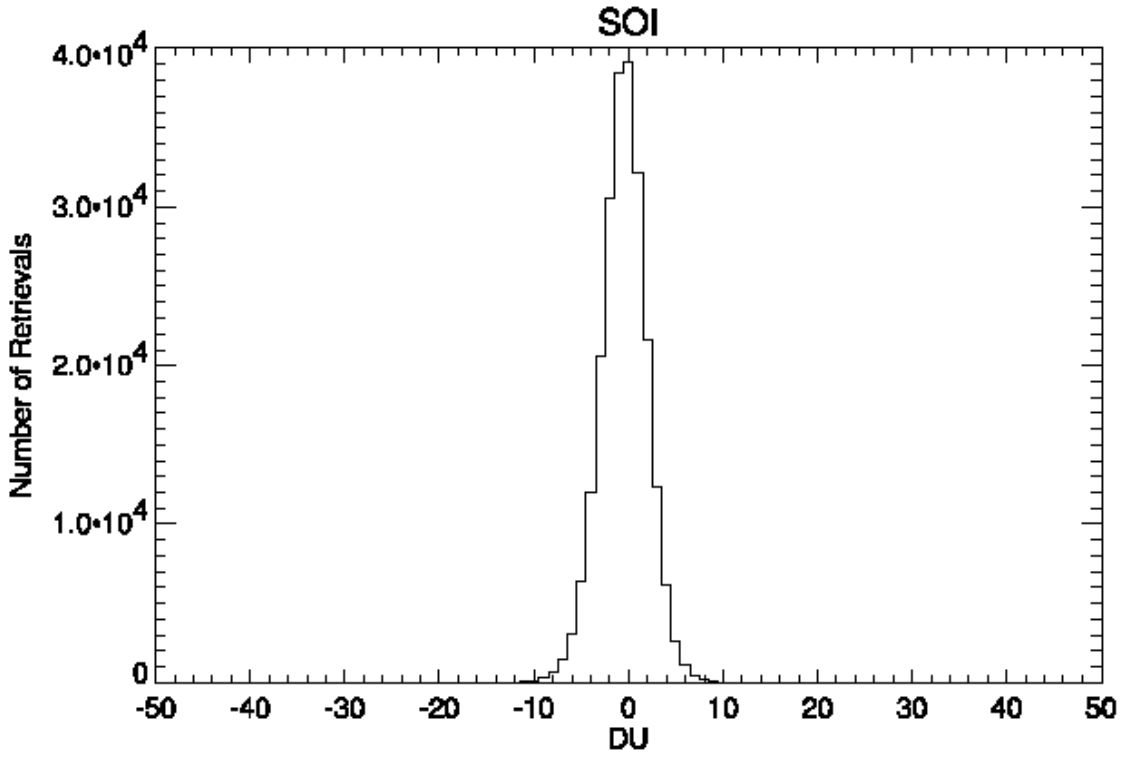

Figure 2.4-8. Distribution of SOI for ADEOS TOMS, Mar. 20, 1997

Figure 2.4-9 shows the number of retrievals flagged as contaminated by SO_2 for each day of the 10 month ADEOS TOMS data record. It indicates that the flagged samples represent less than 0.01% of the total number of samples for a given day.

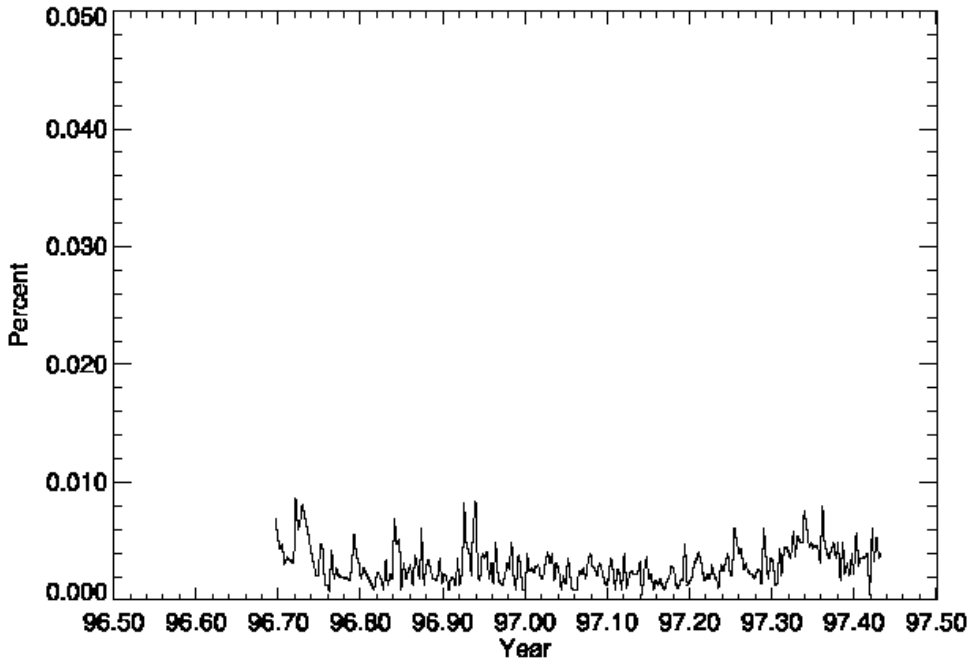

Figure 2.4-9. Percentage of ADEOS TOMS daily retrievals flagged as SO_2 contaminated

It should be noted that there was volcanic SO_2 contamination due to the eruption of Nyamuragira in December 1996. The number of retrievals contaminated by SO_2 due to this eruption, however, is small (approximately 10-20 measurements per day) and is barely discernable in Figure 2.4-9. A contaminated plume can be seen on a map showing the global distribution of SO_2 in latitude and longitude. In such a map, the cluster of contaminated values due to the volcanic eruption can be easily picked out from the rest of the flagged values that are scattered randomly.

Simulations of the SOI algorithm using the OMPS algorithm, wavelengths, signal-to-noise ratio, and slit functions indicate an SOI σ of approximately 1.5 DU. With 4 measurements of SOI this value can be further reduced by a factor of 2 to 0.75. An SOI flag set at 3 DU would lead to an equivalent percentage of the data eliminated as in TOMS. It should be emphasized that the SOI algorithm is not precise enough to provide a quantitative correction to the ozone amount. It can, however, be reliably used to flag volcanic SO_2 contaminated retrievals.

2.5 Error Sources

Table 2.5-1 summarizes the sources of error in the total column algorithm. Section 7 provides more detail about each error and how it affects the algorithm.

Table 2.5-1. Factors Contributing to the Accuracy and Precision Error Budgets

Sensor Accuracy	Algorithm Accuracy
Wavelength dependent albedo calibration Wavelength independent albedo calibration Pixel-to-pixel calibration (includes linearity) Wavelength calibration Wavelength shift Polarization Out-of-field stray light Out-of-band stray light	Rayleigh scattering coefficients Absolute ozone absorption coefficients Temperature dependent ozone absorption coefficients Tropospheric aerosols Cloud top pressure Table pressure interpolation Non-homogenous scene (including clouds vs. snow/ice) Ozone profile shape Multiple scattering Ring effect Interpolation
Sensor Precision	**Algorithm Precision**
Radiance noise Solar calibration noise	Tropospheric ozone Temperature dependent ozone absorption coefficients Cloud-top and surface pressure Cloud fraction (non-homogeneous scene) Ozone profile Tropospheric aerosol correction

3. Algorithm Description

3.1 SDR Production

This section describes the process by which Sensor Data Records (SDRs) are generated. The discussion follows ICSR# E8092402. SDR processing is either "Earth view" or "calibration," the end result of which is two separate SDRs." SDR processing is illustrated in Figure 3.1-1. Each SDR is primarily an archival product containing both calibrated and raw counts. We designed the earth and calibration SDRs to contain all the information necessary, under normal circumstances, for a retrospective processing of the raw data into EDRs. As such, the SDR contains all calibration factors and ancillary information needed to convert raw sensor counts to calibrated radiances. SDR processing uses inputs from the following sources:

- RDR headers and records
- Time-dependent calibration factors and signal correction data
- CCD pixel map and database of utilized pixels
- Climatological databases
- OMPS LP EDR products
- EDR products from other NPOESS sensors
- Reference solar irradiance

External data, either static climatology values or EDRs from other NPOESS sensors, are stored in the SDR. Climatological data include:

- Terrain height
- Cloud top height
- Atmospheric profiles of temperature, pressure, and neutral number density
- Snow/ice coverage

In the case of EDRs, the data are appropriately co-located with OMPS data cells. External EDRs include:

- Atmospheric profiles of temperature, pressure, and neutral number density – CMIS and CrIS
- Cloud cover – VIIRS
- Cloud top pressure – VIIRS, CMIS, and CrIS
- Snow/ice coverage – VIIRS and CMIS
- Profile ozone – OMPS-Limb Profiler

The threshold horizontal and vertical cell sizes specified by the VIIRS, CMIS, and CrIS SRDs for the external EDRs listed above are sufficient for OMPS. The co-location of the external EDRs with OMPS data cells is performed as part of SDR processing and is based on time tags.

Calibration data are collected and processed separately from Earth view data in the SDR data stream. Some, but not all, results from the calibration analyses are fed back automatically as calibration updates for use in subsequent SDR processing. All derived calibration parameters are part of an extensive monitoring database which is used to assess the quality of SDR (and

ultimately EDR) products. This database alerts the science team to problems with the products, and points the way to further data studies.

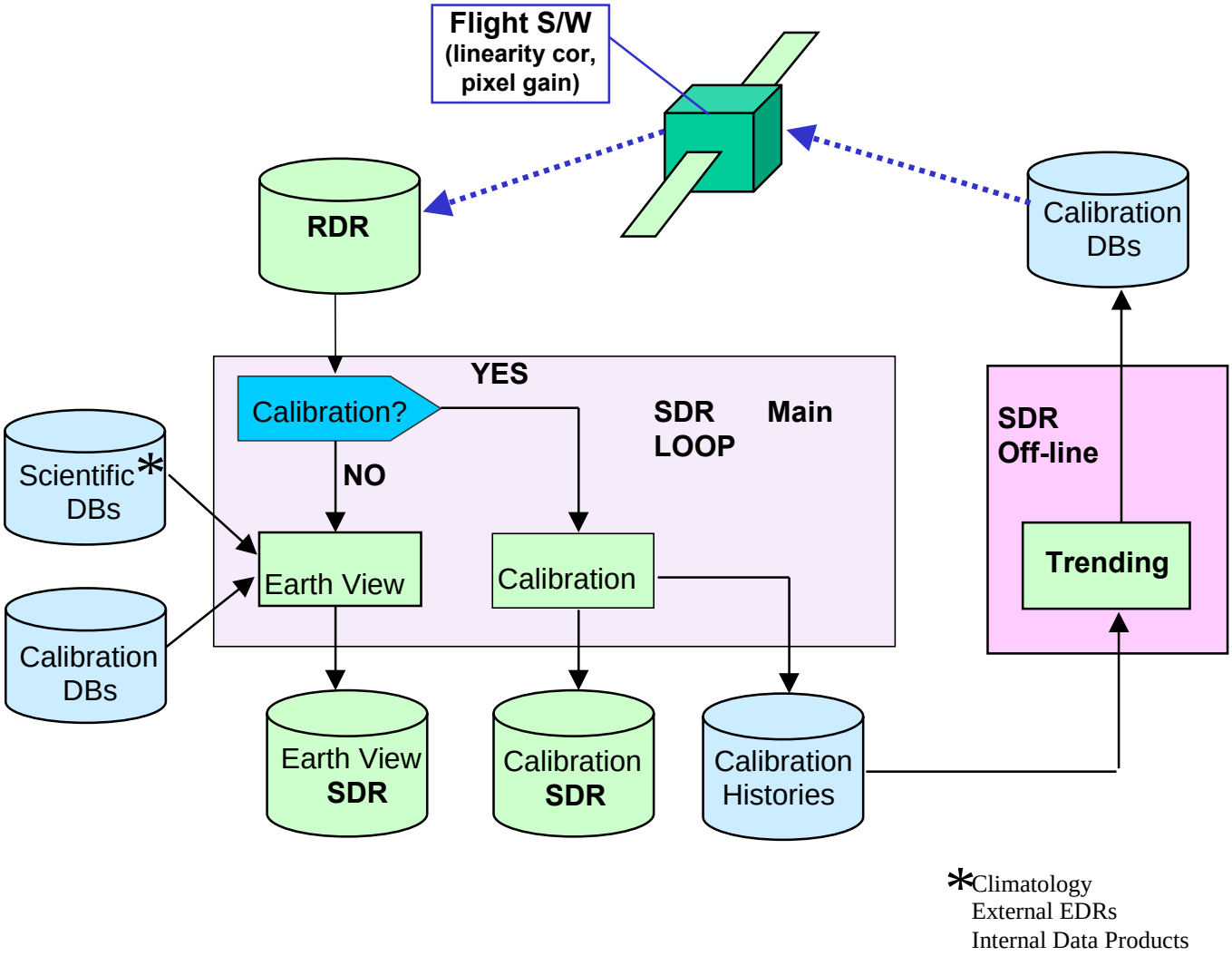

Figure 3.1-1. Schematic Showing SDR Generation

Sufficient information is contained in the SDR to permit complete retrospective processing and subsequent analysis of the data. Records such as uncalibrated raw counts are included, since it is likely that these data would be re-calibrated in any reprocessing. The processes of housekeeping data conversion and radiance data geolocation are unlikely to be repeated, so their precursors are not saved in the SDR.

The SDR files contain all Earth view data, observation information, and the state of the Nadir sensor needed to produce EDRs. An SDR file can cover any length of time, but because downlinked RDR data must be sorted and ordered sequentially prior to SDR processing, the nominal coverage of an operational SDR file is one full orbit. The SDR file contains a single major record and 800 (nominally) minor records.

The major record includes information and data that remain constant for the period covered by the file. The following information is written in the major record header of each OMPS-TC SDR file:

- Spacecraft identification tag
- Sensor identification tag
- SDR product identification tag
- Flight software version
- RDR software version
- SDR software version
- Generation date and time
- Ancillary data file names and version numbers

The following data are written in the major sensor/calibration record:

- Wavelength of channel band centers
- Reference solar flux
- Radiance calibration coefficients
- Smear correction data
- Dark current correction data

The minor record or individual sensor data record is associated with a group of data cells representing one report period. Each minor record contains a header and data record. The following information is written in the minor record header:

- Unique SDR identification tag
- Orbit number
- Logical sequence number
- Operation mode
- Date and time at start & end of period
- Attitude and ephemeris source flag
- Subsatellite latitude and longitude at start & end
- Spacecraft altitude at start & end
- Solar right ascension at start & end
- Solar declination at start & end
- Spacecraft-centered solar azimuth at start & end
- Spacecraft-centered solar elevation at start & end
- Spacecraft geocentric position (X,Y,Z) at start & end
- Spacecraft attitude (difference from nominal; in Roll, Pitch, Yaw) at start & end
- Data quality flags

The following data are written in the minor data record:

- Sensor status bits
- Sensor housekeeping data
- External data source flags
- FOV Latitude, Longitude

- FOV solar zenith angle, satellite zenith angle, and relative azimuth angle
- Cloud top pressure – VIIRS, CMIS, *or* climatology
- Cloud fraction (coverage) – VIIRS *or* climatology
- Terrain pressure – database
- Surface category and UV reflectance – database
- Snow/Ice coverage – VIIRS and CMIS *or* climatology
- Ozone profile amounts – OMPS Limb Profiler *or* climatology
- Temperature profile – CMIS and CrIS *or* climatology
- Pressure profile – CMIS and CrIS *or* climatology
- Neutral number density profile – CMIS and CrIS *or* climatology
- Raw sensor counts
- Normalized calibrated Earth radiances

A more precise description of the SDR content is given in the Algorithm Specification Document.

3.1.1 Earth View

The processing flow for each raw data record (RDR) is shown in Figure 3.1-2. SDR generation for Total Column begins by ingesting the RDR product for the time period of interest. Normally, the RDR file represents one orbit of data, although it may contain less. The next process consists of inputing all necessary databases. CCD spectral and spatial mapping is performed using some of these database inputs. Spacecraft clock time tags for all Earth view elements are refined with a simultaneous adjustment process using all time tags contained within the RDR. The above processing is performed only once per RDR.

The remainder of the processing is executed sequentially once for each minor record (i.e., set of radiance observations) within an RDR. Housekeeping data are converted to appropriate temperatures, voltages, etc. and stored. Initial signal corrections are performed to remove dark current and smear. The appropriate spacecraft attitude (as previously determined by the flight software) for each Earth view data element is corrected using auxiliary data sources. Earth data are geolocated and view and solar angles are computed. All external data (climatology, external EDRs, and LP EDRs) are interpolated to match the TC earth view observations. The final process involves computing normalized radiances using corrected earth-view signals, calibration constants, the reference solar spectrum, and time-dependent calibration factors.

After all records within the RDR are processed, the normalized radiances and all supporting data are written to the SDR. More detailed discussions of the individual processes within the Earth view SDR algorithm are now presented.

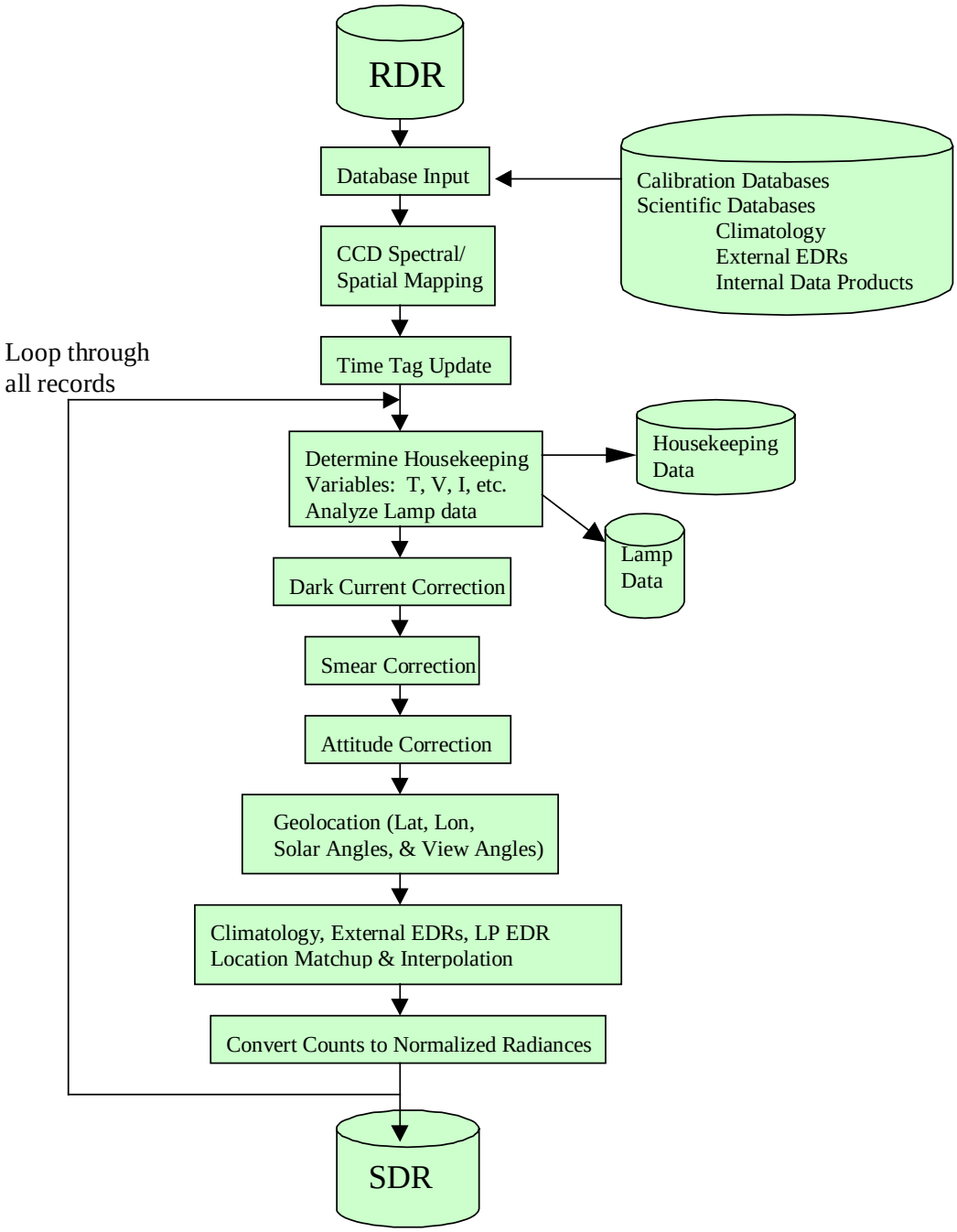

Figure 3.1-2. Schematic showing Earth View SDR generation process

Database Input.
The following databases are read for use during processing:

- Dark current
- Calibration factors
- Bad pixel
- Bandcenters
- CCD pixels utilized by flight software
- CCD pixel map
- Climatology
- OMPS-LP EDRs
- non-OMPS EDRs

CCD Spectral/Spatial Mapping.
Spectral/spatial mapping determines the transformation between pixel location and sensor view angle and wavelength for those pixels utilized by the flight software. This process also deletes bad pixels and integrates binned pixels accordingly. The output is an array of wavelengths and spatial locations mapping directly to each Earth view observation.

Time Tag Update.
Start and end times (of the data collection integration period) are assigned to data cells using stored spacecraft clock values. As stored, these values are somewhat imprecise. Clock values from many minor records can be combined with timing information from the Timing Pattern Generators to more precisely determine the time of each minor record. These enhanced time tags accompany the data elements and are written in each SDR.

Housekeeping Data.
Sensor housekeeping data generally include information from thermistors as well as any feedback from mechanical systems, command verification, etc. Most housekeeping data, particularly from thermistors, are telemetered in raw form and must be converted to a physical quantity. Only converted quantities are written to the SDRs. Conversion algorithms are provided by the OMPS sensor contractor. These data generally do not require time tagging because they vary slowly. In cases where multiple measurements are available for a single data cell, results are averaged. A historical summary of housekeeping data is maintained for use in offline analysis.

Initial Signal Correction.
The radiance data require initial corrections prior to applying the calibration. The dark signal on the OMPS CCD results when electrons are thermally emitted into the conduction band and collected within the parallel and serial shift registers. It is not possible to distinguish the dark signal from the integrated photogenerated signal effectively offsetting observations from each

pixel. Dark signal is characterized during calibration and is removed as a bias during SDR processing.

At the conclusion of the designated photon integration period, the image signal in the light sensitive region is quickly transferred into the light shielded region, which acts as an image storage area. During this transfer period, the impinging image is still present. Thus, each pixel collects signal from other pixels in the same column as it is clocked out. The accumulation of extraneous photons before and after the desired integration time is known as smear. The smear signal is measured with several rows of CCD pixels dedicated exclusively to this purpose. Smear data are scene dependent and are included in the input RDR. SDR processing performs the necessary smear correction. Since the dark signal bias is present in all CCD pixels (even the CCD smear rows), it must be removed prior to smear correction.

Attitude Correction.

A nominal spacecraft attitude is computed for any point in time using ephemeris information. The RDR contains attitude knowledge for adjustments from nominal. Attitude corrections are assigned to data cells via the time tag. Earth radiance data can then be geolocated.

Geolocation.

Solar illumination and sensor view angles are calculated for the center of each data cell. Spacecraft-centered solar illumination angles are calculated for solar radiance data. All angles accompany data elements and are in each SDR.

External Data Matchup.

Each SDR contains EDR information from OMPS Limb Profiler, VIIRS, CMIS, and CrIS, if available. The geophysical quantities from each are listed in 3.1. EDR information will overwrite existing climatological values if available. In the event that an EDR parameter has been flagged as having poor quality, those data will not be used. EDR information will require minimal additional processing. Temperature profile information from CMIS and or CrIS is used to compute the tropopause height for each Total Column data cell.

Following geolocation of radiance data, external database quantities will be read in for the correct latitude, longitude and time. The threshold horizontal and vertical cell sizes specified by the VIIRS, CMIS, and CrIS SRDs for the EDRs listed above are sufficient for OMPS. Multiple horizontal cells may need to be combined to match the coverage of a single Total Column data cell. The co-location of the external EDRs with OMPS data cells is performed as part of SDR processing and is based on time tags. Once the orbital altitude and mounting angles for the various sensors are known, the relative geometry of all relevant data cells can be computed for each instrument, and is then constant. The overlap of two data cells from different sensors is then solely a function of the time difference between the cells. Differing integration times may require the summation of multiple and/or fractional EDR reporting intervals. In the case of interval fractions, an appropriate interpolation scheme for the sensor in question will be used. During SDR processing, the appropriate external EDRs are selected for each OMPS data cell using a

matchup table and time tags from each sensor. The matchup table consists of an EDR data cell mask for each Total Column data cell which will be generated prior to or soon after launch.

Determine Normalized Radiances.

Following the signal corrections outlined in Section 3.1.1.5, normalized radiances are computed. Counts are converted to radiances using pre-launch calibration constants, then corrected for sensor drift using calibration factors read in from the CF database. Finally, these radiances are normalized by the reference solar irradiance.

3.1.2 Calibration

The calibration concept for the Total Column sensor follows closely that of TOMS and SBUV/2. The TOMS calibration procedures are described in Jaross, et al.,1995, Seftor et al., 1997, and McPeters, et al., 1998. The implementation for OMPS has been described in ICSR-8092402. The use of diffusers is described in ICSR-8110501.

Backscatter ultraviolet instruments measure the response to solar irradiance by deploying a ground aluminum diffuser plate to reflect sunlight into the instrument. The three-diffuser system aboard TOMS reduces the exposure and degradation of the diffuser used for the solar measurements and allows calibration through comparison of signals reflected off diffusers with different rates of exposure. An identical concept is employed on OMPS, but only two diffusers are used because mechanical design differences obviate the need for the third diffuser. The diffusers, designated Working and Reference, are arranged around an annulus so that a given diffuser can be rotated into view on demand. The Reference diffuser is exposed for one sequence every 6 months, and the Working diffuser is exposed every week. The Working diffuser is the primary sensor calibration diffuser. Periodic comparisons with Reference diffuser solar measurements are used to detect changes in the Working diffuser.

3.1.2.1 Theoretical Basis: Radiometric Calibration

Conceptually, the calibration of measured Earth radiance and solar irradiance may be considered separately. The measured Earth radiance in a single channel can be written as a function of the corrected instrument counts in the following way:

$$I_m(t) = \frac{C_r k_r}{\tau(t)} \tag{41}$$

Where

$I_m(t)$ = derived Earth radiance
C_r = radiance counts, corrected by Initial Signal Corrections algorithms

k_r = radiance calibration constant (from pre-launch calibration)
$\tau(t)$ = sensor throughput changes ($\tau(t=0) = 1$)

The measured solar irradiance, F_m, can be written as:

$$F_m(t) = \frac{C_i k_i}{g\rho(t)\tau(t)} \tag{42}$$

where

C_i = irradiance mode counts (corrected)
k_i = irradiance calibration constant (from pre-launch calibration)
$\tau(t)$ = sensor throughput changes ($\tau(t=0)$ = 1)
$\rho(t)$ = solar diffuser plate reflectiviity ($\rho(t=0)$ = 1)
$g(t)$ = relative angular correction for diffuser reflectivity

The constants k_r and k_i are not accurately determined separately. The primary quantity measured by bacscattered ultraviolet (BUV) sensors, and from which ozone is derived for the Total Column sensor, is the normalized radiance $I_m(t)/F_m(t)$. The advantage of this approach is that sensor throughput changes τ affecting both Earth and solar measurements cancel in the ratio. The expression for normalized radiances becomes:

$$\frac{I_m}{F_m} = K\frac{C_r}{C_i} g\rho(t) \tag{43}$$

where K is a combined calibration constant for normalized radiances, often referred to as the Albedo Calibration Constant. This and g are determined in pre-launch calibrations. Since the sensor changes affecting both the Earth and solar measurements cancel in the ratio, the quantity critical to time-dependent calibration of the normalized radiances is the diffuser plate reflectivity, $\rho(t)$.

Monitoring of this quantity is carried out periodically by deploying the Reference diffuser. The initial deployment frequency will be once every 6 months, and may decrease once adequate statistics of Working diffuser change $\rho(t)$ are obtained. A more detailed discussion of diffuser monitoring follows below. Diffuser deployment frequencies are described in ICSR-8110501. We expect several percent changes in the Working diffuser. Though we do not expect these changes to significantly affect ozone, our plan is to provide for automatic corrections for diffuser change once the change exceeds a threshold amount. The threshold value will be determined based upon the resulting ozone error, and is TBD.

The expression for normalized radiances $I_m(t)/F_m(t)$, given above, implies that time-dependent calibrations (apart from diffuser changes) are obtained by merely computing the ratio of sensor radiance signal to sensor irradiance signal. But this is not possible, since solar irradiance measurements are obtained only once per week. The solution is to characterize changes in the solar signal in order that the ratio can be computed as though irradiance measurements had been simultaneous with Earth radiance measurements. This is performed via trending and extrapolation algorithms.

Diffuser Degradation

In the multi-diffuser approach to calibration employed by OMPS the quantity derived from solar calibrations is the Working to Reference signal ratio

$$r = \frac{W}{R} \tag{44}$$

where W and R represent the mean signals from the Working and Reference diffusers, respectively, normalized to their baseline (initial post-launch) calibration values. A small fractional change in the value of this ratio, due to the degradation of either surface or a relative goniometric error, is then written as

$$\frac{dr}{r} = \frac{dW}{W} - \frac{dR}{R} \tag{45}$$

The multi-diffuser calibration approach relies on the assumption of exposure-dependent degradation of the flight diffusers. As discussed in ICSR E8110501, almost all evidence indicates that this assumption is valid. This implies

$$W = f(t_W) \qquad\qquad R = f(t_R) \tag{46}$$

where *f(t)* is an arbitrary function of the exposure time *t*. The differential changes are then

$$\frac{dW}{W} = \frac{f'(t_W)}{f(t_W)}dt_W \qquad\qquad \frac{dR}{R} = \frac{f'(t_R)}{f(t_R)}dt_R \tag{47}$$

Since a solar measurement sequence is the same for Working and Reference surfaces, exposure times can be rewritten in terms of the number of Working and Reference measurements, n_W and n_R.

$$\frac{t_R}{t_W} = \frac{dt_R}{dt_W} = \frac{n_R}{n_W} \tag{48}$$

Results from TOMS Cover diffusers indicate that degradation is truly an exponential process (see ICSR E8110501). In the specific case where *f(t)* is an exponential, the change in the working surface reflectance as a function of the change in the quantity *r* is

$$\frac{dW}{W} = \frac{n_W}{n_W - n_R}\frac{dr}{r} \tag{49}$$

For situations where the number of Working measurements far exceeds the number of Reference measurements, as with OMPS, the Working change is nearly equal the change in the ratio of diffuser surfaces. Any uncertainty ε_r in the value of *r* translates via this relationship to an uncertainty in *W*.

$$\frac{\varepsilon_W}{W} = \frac{n_W}{n_W - n_R}\frac{\varepsilon_r}{r} \tag{50}$$

It is the uncertainty in *W* that ultimately determines the long-term calibration uncertainty.

The value of ε_r is actually a time-dependent quantity because, assuming Gaussian statistics, it varies roughly as $\varepsilon_r = \sigma_r/\sqrt{n_R}$. The current operations schedule calls for Reference measurements every 6 months. Thus there will be 2 values of *r* derived per year. Each data point will have a variance σ^2_r associated with it. We will be employing linear regression to these data of the form

$$\ln(r) = b \cdot t_R \tag{51}$$

to determine the Working degradation at a time *t*. An uncertainty ε_W can be estimated (see Bevington, for instance) at a time *t* using σ_r and the proposed exposure schedule.

$$\frac{\varepsilon_W}{W} = \frac{n_W}{n_W - n_R}\sigma_b \cdot t \qquad \sigma_b^2 = \frac{1}{\Delta}\sum_i^{n_R}\frac{1}{\sigma_r^2} \qquad \Delta = \sum_i^{n_R}\frac{1}{\sigma_r^2}\sum_i^{n_R}\frac{t_R^2}{\sigma_r^2} - \left(\sum_i^{n_R}\frac{t_R}{\sigma_r^2}\right)^2 \tag{52}$$

We note that the uncertainty does not depend on the rate *b* of degradation. Each value σ_r depends upon several factors, but is predominantly related to the errors in the goniometric corrections applied to the solar data. Provided that the relationship

$$\frac{\varepsilon_W}{W} > \frac{dW}{W} \tag{53}$$

holds, we do not intend to apply a correction for Working surface degradation.

3.1.2.2 Operational Processing

The processing flow for calibration data shares many elements and proceeds in much the same way as for earth-view data (Section 3.1.1). A fundamental difference is that calibration data are not binned prior to downlink from the spacecraft. Also, several of the data corrections are derived from the calibration data (eg. dark currents), so these corrections would not always be applied as they are for earth-view data.

There are two basic parts to SDR processing of calibration data: in-line processing and routine off-line processing. The former refers to processing of data as it is encountered in the RDR. This data flow is illustrated in Figure 3.1-3. Additional automated analysis of calibration data, shown in Figure 3.1-4, will occur on a routine (at present, weekly) basis. We begin by describing in-line processing steps.

Time Tag Update

As described in Section 3.1.1, an improved time is computed for each data report period using data collected over a substantial fraction of an orbit. This calculation is performed before the record type is identified since it relies only on the spacecraft time stamp. Thus there is no algorithm that is specific to calibration data.

Database Input

Information stored in databases is required for calibration data reduction. These databases are read in prior to the record loop and stored in memory. While Figure 3.1-3 indicates three required databases, in fact dark currents and bad pixels will already exist in memory for earth-view data processing. Only the goniometry data need be ingested when calibration data is encountered.

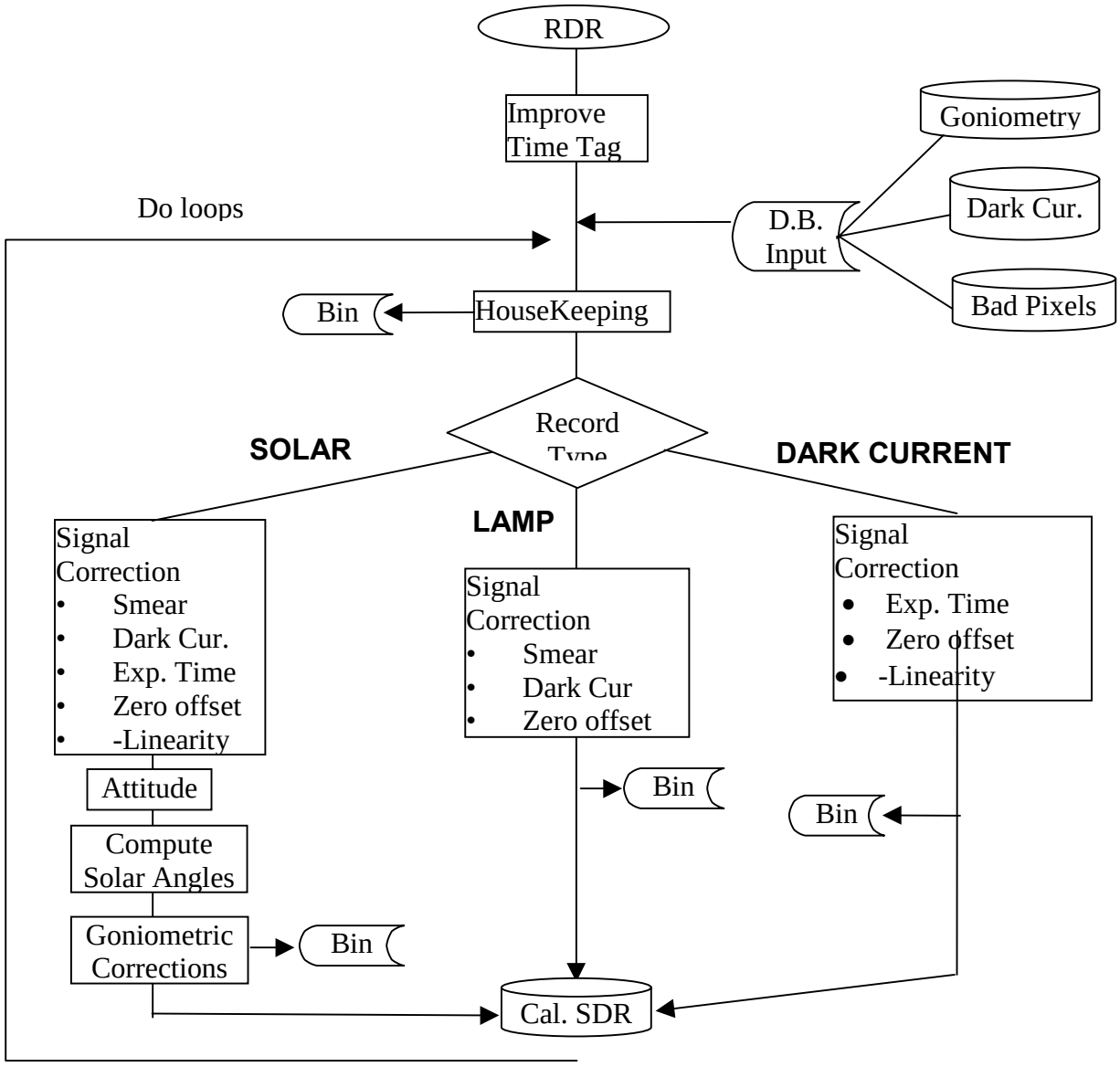

Figure 3.1-3: In-line SDR flow for calibration records

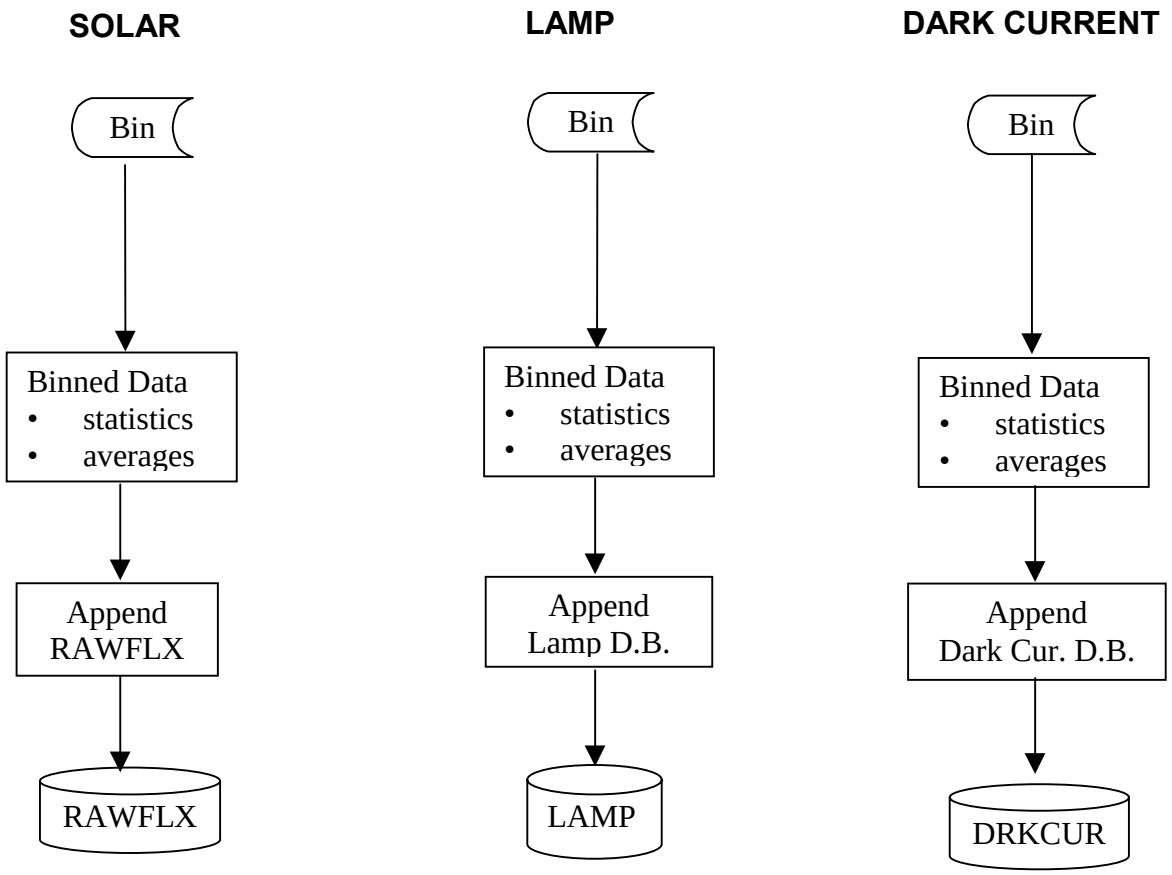

Figure 3.1-3: In-line SDR flow for calibration records (continued)

Housekeeping

The housekeeping analysis function is essentially the same as performed for earth-view data. It is likely that several additional housekeeping parameters will be tracked during calibration periods.

Signal Corrections

Data corrections will begin once the record type is determined. These corrections are, for the most part, the same as for earth-view data except that they are performed on unbinned pixels. The smear correction, based upon the average of the 16 over-clocked rows is applied to all but dark current data. The offset voltage, applied before the CCD output amplifier, is subtracted from all data. The zero offset is determined using calibration data. A dark current subtraction is applied to all but the dark current data itself.

Solar: Attitude

If spacecraft attitude information is used, the spacecraft axes are computed in geocentric coordinates. This process is identical for earth-view and solar-view data.

Solar: Compute solar angles

Using satellite ephemeris information, solar angles relative to the spacecraft axes are computed. This calculation will probably be performed as part of a general geolocation algorithm used for both earth-view and solar-view data.

Solar: Goniometric corrections

A correction *g(t)* is applied that accounts for variations in irradiance sensitivity as the spacecraft-centered solar angles change. This is a dimensionless quantity with a value of 1 at the angle at which radiometric calibrations were performed prior to launch. Each quantity $C_i(t)/g(t)$, within a range of elevation angles during a solar sequence, is independently binned for each pixel. From the expression for $F_m(t)$ in Section 3.1.2.1, this quantity is

$$\frac{C_i(t)}{g(t)} = \frac{\rho(t)F_m(t)\tau(t)}{k_i} \tag{54}$$

From the baseline irradiance measurement immediately following launch,

$$\frac{C_i(0)}{g(0)} = \frac{F_m(0)}{k_i} \tag{55}$$

The goniometry-corrected solar signals are normalized by the baseline value and the results *T(t)* written to the file RAWFLX. The expression for each value *T(t)* is:

$$T(t) = \frac{C_i(t)}{g(t)}\frac{g(0)}{C_i(0)} = \rho(t)\tau(t)\frac{F_m(t)}{F_m(0)} \tag{56}$$

For the Total Column sensor wavelengths the solar fluxes are practically constant, and the values $\rho(t)$ are nearly 1. Thus the quantities in RAWFLX are nearly equal to the sensor throughput changes since the baseline calibration.

Lamp data

Following signal corrections, per pixel lamp data $C_l(t)$ are binned independently for each different integration time.

Dark current data

Following signal corrections, per pixel dark data $C_d(t)$ are binned independently for each different integration time.

Data binning and statistics

Following the completion of a calibration sequence for a single orbit, all binned calibration data are averaged and standard deviations calculated. Results per pixel for the solar data are appended to the RAWFLX database. Lamp results are appended to the LAMP database, and dark results are appended to the DRKCUR database. All records are uniquely identified by pixel location and orbit number.

3.1.2.3 Off-line Processing

Calibration data will be analyzed in more detail on a periodic basis using results stored in the LAMP, RAWFLX, and DRKCUR databases. This off-line analysis occurs on a preset schedule,

generally soon after a solar calibration orbit. These analyses are distinct from in-line SDR processing because they are not time-critical, all calibration data must be downlinked before initiating, and they utilize information in databases, not from an RDR. The flow for off-line processing is shown in Figure 3.1-4.

Bad pixel update

The bad pixel database is updated based upon information from solar, lamp, and dark data. We would expect that all three data sources would expose a truly bad pixel. However, none of the three is a perfect source of bad pixel information. We expect to use a combination of the three to identify pixels that have gone bad since launch. Examples of changes include increases in dark current or charge trapping and decreases in quantum efficiency.

Pixel response non-uniformity

The primary source of information on changes in relative sensor response across the CCD are the solar data. The change in response along a CCD column or row is primarily due to changes in pixel quantum efficiency, sensor optics changes, and solar variability. Since these changes affect earth radiance and solar irradiance data the same, it is not necessary to separate the effect of the three. However, a significant radiometric error can occur if the individual pixels are binned prior to correction for pixel response non-uniformity (PRNU).

The flight software sums groups of 20 pixels in a column (spatial direction) prior to storage in an RDR. A PRNU correction is applied in the flight hardware prior to binning earth-view signals. The PRNU correction, derived initially from pre-launch calibration, can change for the reasons described above. The off-line processing computes a new set of PRNU corrections and stores the results in the FLTFLD database. This database can be periodically loaded into the flight hardware as deemed necessary. Since the correction is needed to prevent binning errors, only local (20 pixels along a column) PRNU changes are considered. By correcting variations relative to the average of the 20 pixels (a macro-pixel), PRNU changes between macro-pixels are left alone. These macro-pixel PRNU changes are then handled via the radiance normalization described in Section 3.1.2.1.

PRNU changes can pose a challenge for spectral monitoring since a change in relative pixel response can be mistaken for a shift of the Fraunhofer spectrum along a CCD row. The Fraunhofer structure is well known, so the PRNU change across the full CCD resulting from a spectral shift is well defined and unique. Our spectral monitoring relies on the exceedingly small probability that optical and quantum efficiency changes can mimic this unique pattern. The result of these changes, assuming they are random along rows and columns, is a reduction in the shift resolution of the solar Fraunhofer technique. Depending upon the final design of the TC lamp and focal plane assembly, it may be possible to use lamp data for monitoring pixel quantum efficiency changes. This, in turn, would improve spectral shift resolution.

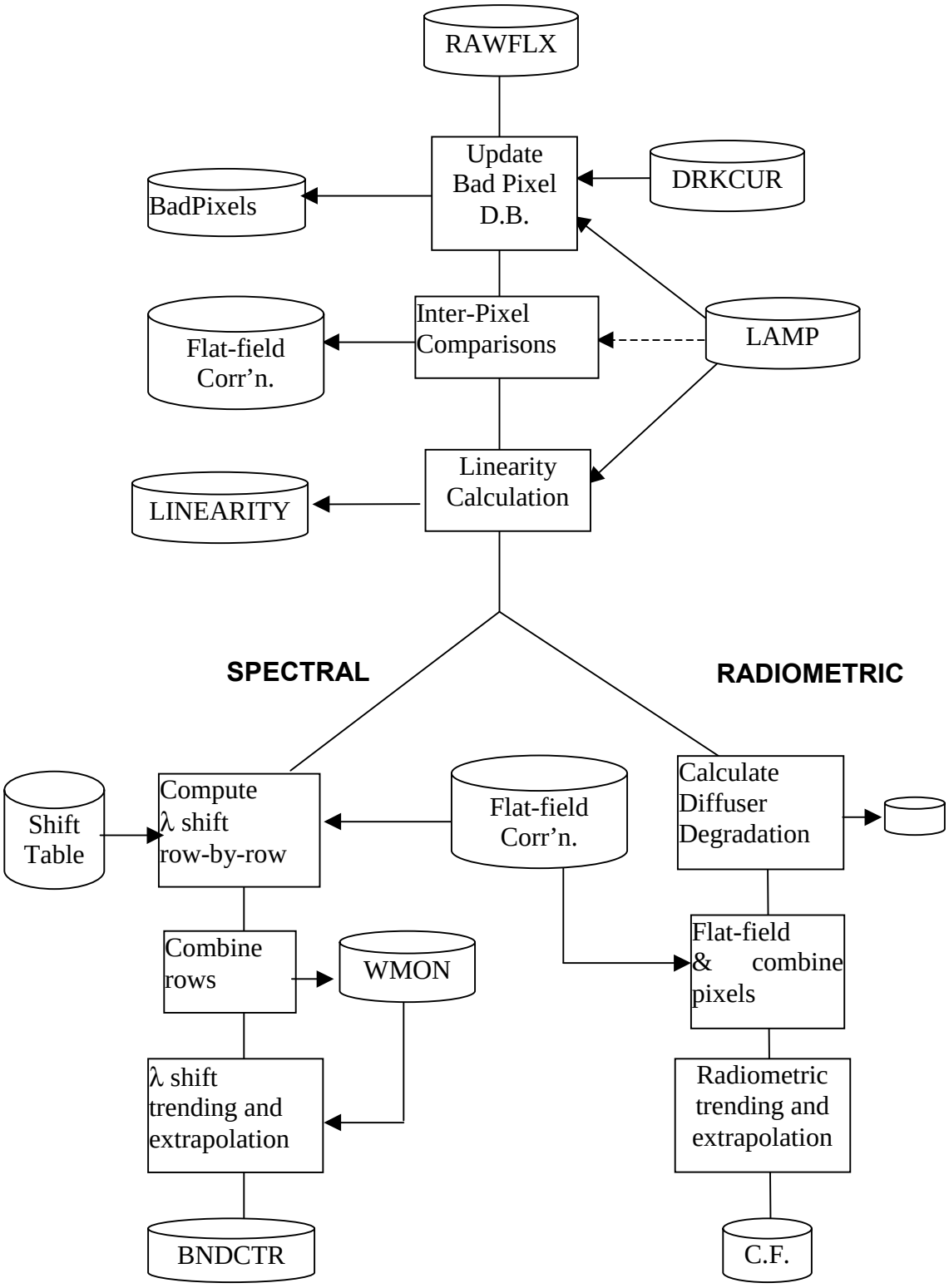

Figure 3.1-4: Off-line SDR flow for calibration data

Linearity

Linearity of sensor response is monitored using lamp results stored in the LAMP database. This database contains average lamp signals at a series of integration times. This analysis will determine the signal deviations at each integration time relative to expected values. Expected values are those determined prior to or at launch. There is evidence for change in the linearity of sensor response if these deviations vary with integration time. Deviations are stored in the LINEARITY database.

Diffuser Degradation

The basic approach for determining Working diffuser changes is described in Section 3.1.1. There the Working to Reference signal ratio

$$r = \frac{W}{R} \tag{57}$$

was introduced. W and R represent the individual pixel signals from the Working and Reference diffusers, respectively, that are stored in RAWFLX. Each pixel along a row (spectral dimension) measures a unique diffuser change. Since the solar diffusers are near a sensor aperture, each pixel's view of the diffuser surface overlaps that of adjacent pixels. Consequently, the value r from many pixels along a column can be combined without loss of information. Since optical degradation is thought to be a smooth, monotonic function of wavelength, pixels r values can also be combined in the spectral direction. The width of these spectral and spatial bins is TBD. Since we expect diffuser change to occur uniformly across the diffuser surface, we can envision applying a diffuser correction based upon the average of r along a full column. Monitoring will take place on a finer scale to check the uniformity assumption.

Pixel combination

Calibration corrections applied to earth-view data must ultimately be applied on a per-scene rather than a per-pixel basis. In earth-view mode, measurements from 20 pixels along a column are combined in the flight software to yield a single earth scene measurement. Prior to this combination, the PRNU correction is applied. Since the earth-view macro-pixels already include this radiometric correction, the same correction must be applied to calibration data. Note that this PRNU correction is the one to be utilized by the flight hardware, which is not necessarily the one derived from the current calibration data. The radiometric calibration for each earth scene is determined by combining calibration data from all 20 pixels. The PRNU correction Q_{ij} is applied to each pixel before adding, where i and j are row and column indices. The pixel signals.T_{ij}, are taken from RAWFLX. The new calibration quantity is then

$$T_{Ij} = \sum_{i=n}^{n+20} T_{ij} Q_{ij} \tag{58}$$

where I refers to a "macro-pixel" (20 rows). Macro-pixels are further combined into pairs and triplets. These are intended to duplicate the pair and triplet combinations formed in the retrieval

algorithm. The trending algorithm will operate on these combinations, rather than on individual channels, as a means of reducing the noise associated with the characterization.

Radiometric calibration

The radiometric calibration of the earth-view radiances amounts to multiplying corrected counts by an initial calibration constant and by a time-dependent correction factor

$$A_{Ij}(t) = \left[\tau_{Ij}(t) \left(\frac{F_m(t)}{F_m(0)} \right)_{Ij} \right]^{-1} \tag{59}$$

The quantity $\tau_{Ij}(t)$ are the total sensitivity changes per macro-pixel (20 pixels combined) since launch. When there is no solar flux change, *A(t)* is simply a reciprocal sensitivity change. Using the expressions derived in earlier in Section 3.1.2

$$A_{Ij}(t) = \frac{\rho_j(t)}{T_{Ij}(t)} \tag{60}$$

where

$$\rho_j(t) = 1 - \left(\frac{dW}{W} \right)_j \tag{61}$$

In fact the calibration factors *A(t)* are not a characterization but a prediction based on a characterization. In an operational environment with infrequent solar measurements, Earth radiance measurements always occur well in advance of solar measurements. The OMPS characterization algorithm adopts the TOMS procedure of using a first order regression of the preceding solar measurements to predict *A(t)* values. Predictions are made for at least one solar calibration period (1 week in this case) into the future, and are divided into discrete daily values. The new set of predictions begin the day following the calibration processing. A small discontinuity in an *A(t)* generally occurs between the two days. The daily values of *A(t)* for each channel are stored in the file CF. The expression for each macro-pixel normalized radiance becomes

$$\frac{I_m(t)}{F_m(t)} = C_r \bullet \left(\frac{Kg(0)}{C_i(0)} \right) \bullet A(t) \tag{62}$$

In the earth-view SDR processing flow each radiance signal C_r is multiplied by *A(t)*, read from CF, and then by the absolute calibration correction $Kg/C_i(0)$, obtained from pre-launch calibrations and the baseline post-launch calibration.

Wavelength Registration

The spectral wavelengths of the terrestrial observations are important because one must register the wavelengths to the laboratory ozone spectral cross sections in order to accurately measure ozone columns. The calibration algorithm determines wavelength shifts during the mission by periodically comparing a solar spectrum observed by OMPS with a reference solar spectrum. By

extrapolating in time from recent solar wavelength calibrations (see section 7.2), the algorithm predicts the wavelength scales for the terrestrial observations until the time of the next solar wavelength calibration. The wavelength scales are recorded in each terrestrial observation sensor data record (SDR). Thus, the accuracy of ozone mapping with terrestrial spectra depends on the accuracy of both the solar wavelength monitoring and initial wavelength registration.

Because OMPS data are spatially resolved, the wavelength scale is two dimensional, so the spectral analysis is conducted for each spatial sample. Every time a solar spectral-spatial CCD image is processed by the calibration SDR software, the wavelength monitoring subroutine analyzes and records wavelength shifts of the observed solar spectrum with respect to a solar reference spectrum. The reference solar spectrum is convolved to the OMPS nominal resolution (1 nm FWHM) and then sampled at the initial wavelength map of the CCD so that all wavelength shifts are with respect to the reference wavelengths. These reference wavelengths for each pixel are measured during or before the baseline solar observation.

Before analyzing the wavelengths, previously identified bad pixels are interpolated across or excluded by weighting them by an uncertainty equal to their value. We apply the irradiance calibration constants k_i to the counts to yield uncalibrated irradiances. These uncalibrated irradiances U_{ij} differ from true irradiances by the changes of the diffuser and sensor responses since the initial baseline solar measurement. If a time-dependent flat field from a lamp exists, it is applied to the CCD data.

Operational Algorithm for Detecting Wavelength Shifts

The operational algorithm computes wavelength shifts by varying the reference solar irradiances using several model parameters, and then minimizing the differences between these model irradiances and the observed uncalibrated irradiances over the entire usable spectrum. The algorithmn is based on Caspar and Chance (1997) [Caspar, C. and Chance, K., GOME Wavelength Calibration Using Solar and Atmospheric Spectra, Proc. 3rd ERS Symposium (ESA SP-414), p. 609, 1997.]

Additive wavelength shift and multiplicative shift are primary spectral parameters that are applied to the reference spectrum to obtain a model spectrum. The derived shifts are relative to the wavelength scale that contains the grating dispersion. The fitting parameters account for satellite motion Doppler shifts, as well as parallel translations between the grating and detector. Grating rotations are inherently non-linear, as given by the dispersion relation, but the change in the dispersion from the short to long wavelengths is about two percent, so a linear approximation is valid.

To account for large-scale diffuser and sensor response changes, we vary multiplicative parameters for a cubic scaling in wavelength of the model irradiances by a polynomial.

$$P(\lambda) = a + b\lambda + c\lambda^2 + d\lambda^3 \tag{63}$$

Small-scale irradiance variations due to diffuser and sensor response changes are reduced by spatially averaging the derived wavelength shift results for each spatial sample. To compute

optimal additive and multiplicative wavelength shifts that are actually present in the observed OMPS spectrum, the algorithm calculates a minimum chi-squared statistic over all wavelengths in common between the shifted (S) and model (I) spectra with noise sigma.

$$\chi^2(\delta,\beta) = \sum_{\lambda} \{[U(\lambda) - P(\lambda)\cdot I(\lambda[1+\beta]+\delta)] \ / \ [\sigma]\}^2 \tag{64}$$

$$\Delta_{\min} = \min\{\chi^2(\lambda[1+\beta]+\delta\} \tag{65}$$

$$\mathrm{B}_{\min} = \min\{\chi^2(\lambda[1+\beta]+\delta)\} \tag{66}$$

The wavelength algorithm determines spectral shifts, additive and multiplicative, separately for each spatial row of the unbinned solar RDR CCD data. However, the algorithm spatially bins the resultant shift information before storing it in a shift monitoring database (WMON). Stored uncertainties in the shifts are also calculated as the standard deviations across the spatially averaged region. The algorithm rebins the solar spectral output to match each terrestrial spatial region because the terrestrial ozone measurements in the terrestrial RDR have already been spatially binned by the onboard processor to a lower spatial resolution. Thus, every spatial region on the CCD, as defined by the terrestrial spectrum, has a separate wavelength scale determined by averaged shifts of the solar spectrum in the corresponding region, extrapolated in time to the day of the terrestrial observation. These individual trends can be combined if it is determined that there is little spatial variation in the shifts. The algorithm assumes that the wavelength scale does not change significantly within a day, even within an orbit, but additional software might have to be written to account for these potential short time variations if future studies so indicate a need.

Discrete Spectral Lines

As a non-parametric measure of the wavelength shifts, the algorithm also calculates shifts of narrow spectral absorption lines at discrete wavelengths across the solar spectrum. This has the advantage that no assumptions are needed regarding the sensor spectral dispersion. In contrast to the parametric shifts derived previously from the continuum, shifts are derived by comparing the irradiance differences between observed and reference solar spectra with a set of irradiance differences stored in a pre-computed reference shift table (M^j_{DS}). The pixel by pixel difference, D_{ij}, is determined from the uncalibrated radiances (U) of the observed spectrum and the reference spectrum (T) at t=0:

$$D_{ij} = T_{ij}(t=0) - U_{ij} \tag{67}$$

To remove large-scale changes in diffuser and sensor response, the differences on each side of a line with center at pixel j are subtracted from each other.

$$S_i^{\lambda} = (D_{i,j-1} - D_{i,j+1}) M_{DS}^{j} \tag{68}$$

Small-scale changes in diffuser and sensor response are removed by spatially averaging the shift results over i. The table contains these symmetric differences of the actual irradiance differences (M^{j}_{DS}) for several absorption lines with varying wavelength shifts (S). From the table, the algorithm linearly interpolates between subtracted difference irradiance signals to find a shift for each selected absorption line. In other words, the measured irradiance differences within the selected lines are matched by interpolation in the table to derive a shift (S) for each line. The shift linearity with wavelength is checked with a linear regression fit to the line shifts. Individual line shifts, group shift values, uncertainties, and linear fitting parameters are stored in the same wavelength monitoring database as stores the continuum shift parameters. The linear regression and individual line shifts thus provide a comparison for the assumed linear shift that was derived previously by continuum fitting.

Wavelength Trending in Time

For every day of the year, the wavelength trending algorithm predicts the spectral wavelengths for each spatial region on the CCD. Wavelengths are determined by adding a shift to the reference wavelength scale, so the analysis focuses on changes in the shifts. At the intervals (about weekly) that CCD shifts are monitored with the solar spectrum, the algorithm calculates a linear fit in time to the most recent measured shifts that were recorded during the previous eight to ten weeks. This bimonthly duration is used to track sensor changes and is much less than the period of the Earth's orbit around the sun, when orbital eccentricity induces changes in the Earth–Sun locations. A linear fit is used because changes in shifts during the short trending interval are expected to originate from small changes in a stable sensor. If OMPS has large oscillatory thermal changes during the orbit of the satellite around the Earth, then the trending algorithm will have to be altered for a shorter interval and sinusoidal functional variation.

The shift trend is determined separately for each CCD spatial region and uses only the additive and multiplicative shift values derived by the continuum method for that particular spatial region. The shifts derived from the discrete line method are not used in the trending, they are intended only for post-processing linearity checks. Also, measured shift values are never directly added to the reference wavelengths; instead, the fitted shifts are added to the reference wavelength scale to obtain the wavelengths for each day and for each detector spatial region. The wavelengths are written into a waveband database where they are available to be copied into terrestrial SDR data for a particular day. If the next wavelength monitoring occurs before the end of the last day for which wavelengths have been previously predicted, then new, updated wavelengths, based on more recent monitoring, are overwritten into the wavelength database, where they are propagated into the Earth scene SDRs.

3.2 EDR Production

The following sections describe the process of how the total column ozone EDR is produced from the OMPS total nadir column sensor measurements. **Figure 3.2-1** identifies the flow of the algorithm's modules as detailed below. **Table 3.2-1** identifies all the variables used in this algorithm flow-chart. The assumptions contained in the algorithm, data checks, and assessments that are performed in the algorithm are also discussed.

Figure 3.2-1 EDR Production
Shaded boxes denote further detail shown in following figures.
Variables above subroutines denote input values.
Variables below subroutines denote output values.

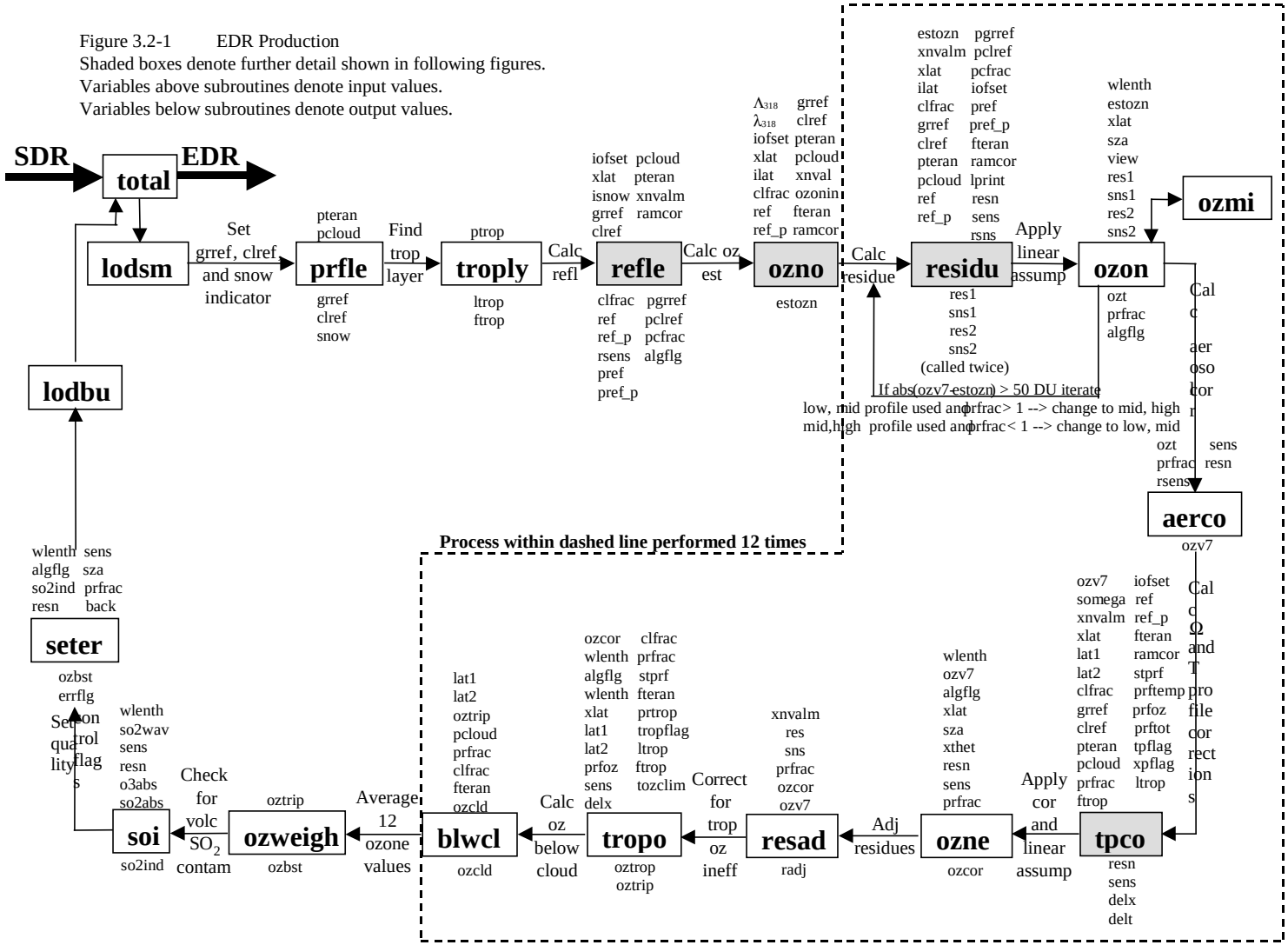

Figure 3.2-1. EDR Production

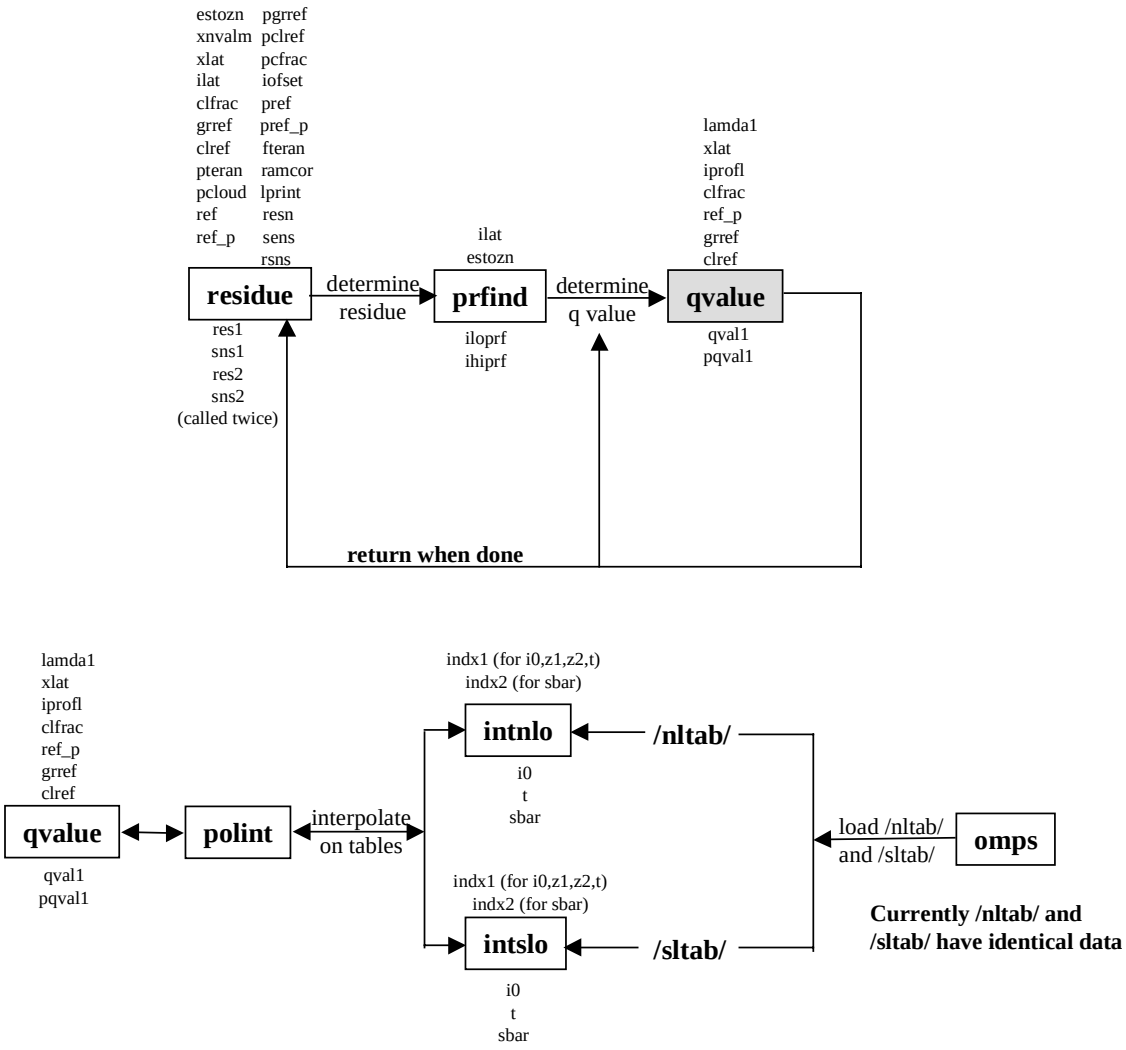
estozn
xnvalm
xlat
ilat
clfrac
grref
clref
pteran
pcloud
ref
ref_p
pgrref
pclref
pcfrac
iofset
pref
pref_p
fteran
ramcor
lprint
resn
sens
rsns
residue
determine residue
prfind
determine q value
qvalue
ilat
estozn
iloprf
ihiprf
lamda1
xlat
iprofl
clfrac
ref_p
grref
clref
qval1
pqval1
res1
sns1
res2
sns2
(called twice)
return when done
lamda1
xlat
iprofl
clfrac
ref_p
grref
clref
qvalue
qval1
pqval1
polint
interpolate on tables
indx1 (for i0,z1,z2,t)
indx2 (for sbar)
intnlo
i0
t
sbar
/nltab/
indx1 (for i0,z1,z2,t)
indx2 (for sbar)
intslo
i0
t
sbar
/sltab/
load /nltab/ and /sltab/
omps
Currently /nltab/ and /sltab/ have identical data

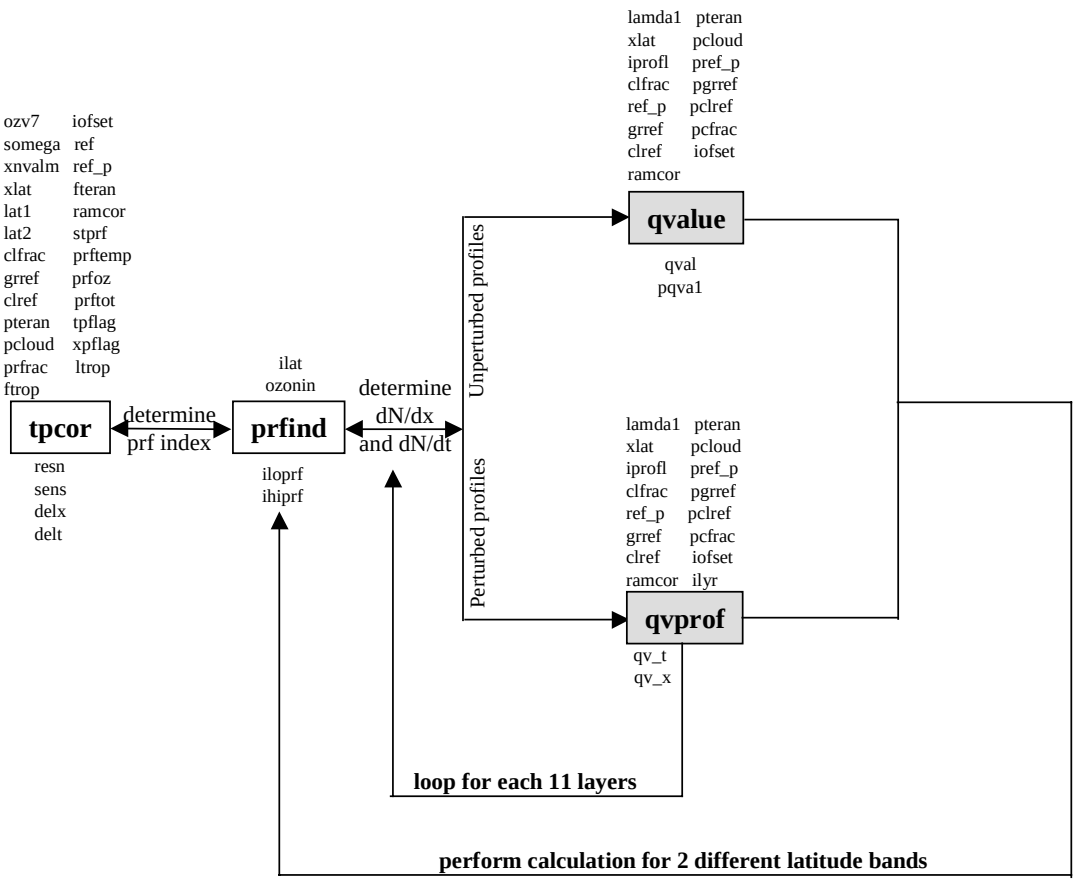
lamda1 pteran
xlat pcloud
iprofl pref_p
clfrac pgrref
ref_p pclref
grref pcfrac
clref iofset
ramcor
qvalue
qval
pqva1
ozv7 iofset
somega ref
xnvalm ref_p
xlat fteran
lat1 ramcor
lat2 stprf
clfrac prftemp
grref prfoz
clref prftot
pteran tpflag
pcloud xpflag
prfrac ltrop
ftrop
ilat
ozonin
determine
dN/dx
and dN/dt
Unperturbed profiles
tpcor
determine
prf index
prfind
resn
sens
delx
delt
iloprf
ihiprf
Perturbed profiles
lamda1 pteran
xlat pcloud
iprofl pref_p
clfrac pgrref
ref_p pclref
grref pcfrac
clref iofset
ramcor ilyr
qvprof
qv_t
qv_x
loop for each 11 layers
perform calculation for 2 different latitude bands

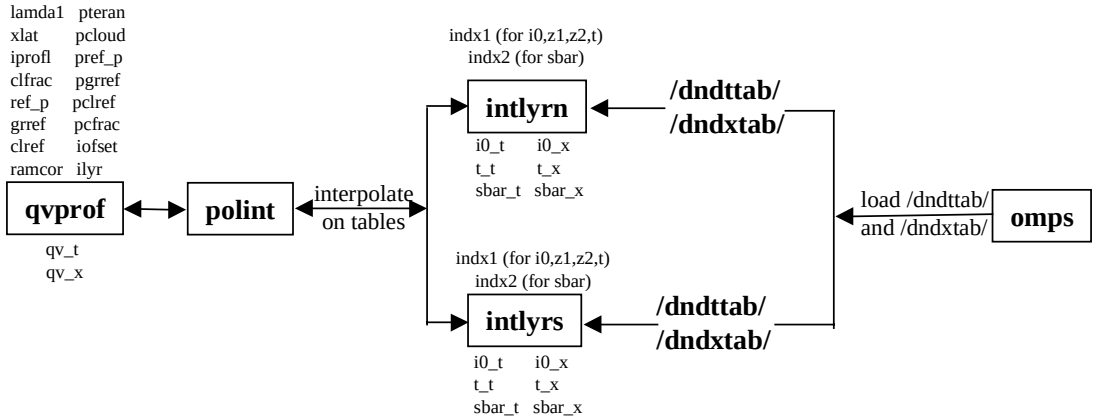
lamda1 pteran
xlat pcloud
iprofl pref_p
clfrac pgrref
ref_p pclref
grref pcfrac
clref iofset
ramcor ilyr
qvprof
qv_t
qv_x
polint
interpolate
on tables
indx1 (for i0,z1,z2,t)
indx2 (for sbar)
intlyrn
i0_t i0_x
t_t t_x
sbar_t sbar_x
/dndttab/
/dndxtab/
indx1 (for i0,z1,z2,t)
indx2 (for sbar)
intlyrs
i0_t i0_x
t_t t_x
sbar_t sbar_x
/dndttab/
/dndxtab/
load /dndttab/
and /dndxtab/
omps

Table 3.2-1. List of Variables Used in the Algorithm Flow Diagrams

Variable Name	Variable Type	Variable Dimension	Description
algflg	integer	1	Algorithm flag indicating which triplets are used
back	logical	1	Ascending/descending flag (if false, ascending)
clfrac	real	4	Cloud fraction
clref	real	1	Cloud reflectivity
day	integer	1	Julian day of year for measurement
estozn	real	1	Estimated ozone from 318/336 pair calculation
errflg	integer	1	Error flag
fteran	real	1	Terrain fraction (1 at 1 atm, 0 at 0.4 atm)
grref	real	1	Ground reflectivity
ilat	integer	1	Latitude index (1 for low, 2 for mid, 3 for high)
iofset	integer	1	Angular offset index for table pointer
isnow	integer	1	Snow/ice indicator (from ext EDR or database)
lat1	integer	1	Index corresponding to 1st latitude band used
lat2	integer	1	Index corresponding to 2nd latitude band used
o3abs	real	4	Ozone absorption coefficients (needed for soi)
ozbst	real	1	Final ozone
ozcld	real	1	Ozone below cloud
ozonin	real	1	Ozone estimate at beginning of algorithm (260 DU for low lat, 350 for mid, 360 for hi at beginning of day, previous measurement for rest of day)
pcloud	real	1	Cloud pressure
pclref	real	1	Perturbed cloud reflectivity
pcfrac	real	1	Perturbed cloud fraction
pgrref	real	1	Perturbed ground reflectivity
pref	real	4	Perturbed reflectivity for 4 wavelengths interpolated using pref_p
pref_p	real	4x4	Perturbed reflectivity for 4 wavelengths from 1.0, 0.7, 0.4, and 0.1 atm tables
prfrac	real	1	Profile mixing fraction
pteran	real	1	Terrain (ground) pressure
qval	real	1	Albedo
ramcor	real	22x4	Raman scattering correction for 22 wavelengths at 1.0, 0.7, 0.4, and 0.1 atm
ref	real	4	Reflectivity for 4 wavelengths interpolate using ref_p
ref_p	real	4x4	Reflectivity from 1.0, 0.7, 0.4, and 0.1 atm tables
rsens	real	22	Reflectivity sensitivity (dN/dR) for 22 wavelengths
res1	real	3	Residues for 1st latitude band used in calculation
res2	real	3	Residues for 2nd latitude band used in calculation
resn	real	22	Final residues
rngerr	real	1	Range error (true if ozone < 0, > 750 DU)
sens	real	18	Ozone sensitivities
sns1	real	3	Sensitivities for 1st latitude band used in calculation
sns2	real	3	Sensitivities for 2nd latitude band used
so2abs	real	4	SO_2 absorption coefficients (needed for soi)
so2wav	real	4	SO_2 wavelength indices
sza	real	1	Solar zenith angle
wav1	real	1	Strongly ozone sensitive wavelength used for estimate (318 nm)
wav2	real	1	Weakly ozone sensitive wavelength used for estimate (332 nm)
wlenth	real	22	OMPS wavelengths
xlat	real	1	Latitude
xnvalm	real	22	Measured normalized radiances for 22 wavelengths

3.2.1 Retrieval Algorithm Description

The following is a step-by-step description of the algorithm. It is limited to a description of the modules necessary to convert information in the SDR into the EDR ozone value and omits any references to the I/O and other routines. (Note: the equations in this section are not numbered.)

A) omps_tc

The main program **omps_tc** performs the following preliminary tasks:

1) It reads in entries contained in the main table as well as those for the dN/dx and dN/dt tables ($\log_{10}I_0$, Z_1/I_0, Z_2/I_0, T/I_0, and S_b).

2) Since the denominators of the Lagrange functions $L_i(X)$ and $L_j(Y)$ do not depend upon satellite measured quantities, these are computed for each sequential 4-point segment of tabular θ_0 and θ values.

3) It reads in the Raman scattering correction factors for each of the 22 wavelengths.

B) Total

The subroutine **total** is the main driver for the scientific algorithm. This subroutine obtains total ozone and determines SO_2 contamination for each OMPS measurement.

1) Using satellite latitude at the beginning of the first scan in the orbit, select an initial ozone estimate, Ω_{init}, based upon latitude as follows:

$\|lat\| < 45°$	$\Omega_{init} = 260$ DU
$45° < \|lat\| < 60°$	$\Omega_{init} = 340$ DU
$\|lat\| > 75°$	$\Omega_{init} = 360$ DU

2) lodsmp

Load satellite observed quantities.

Unpack θ, θ_0, ϕ, latitude, longitude, and day number.

If $\theta > 80°$ skip this measurement.

Set latitude flag for this sample:

$\|lat\| < 15°$	ILAT = 1
$45° < \|lat\| < 60°$	ILAT = 2
$\|lat\| > 75°$	ILAT = 3

Screen sample for possible contamination by an eclipse.

Read the cloud pressure p_c, the presence of snow or ice, and the surface category from the SDR. These are either values from external EDRs or, if not available, values from climatological databases. Read the terrain pressure and surface reflectivity from climatological databases.

Read in radiances for each of the 22 wavelengths.

Calculate angular quantities necessary to determine calculated N values:

$$Y = \ln(\sec\theta_0),\ s = \sec\theta + \sec\theta_0,\ \cos\phi,\ \cos 2\phi,\ Q_1, \text{ and } Q_2. \tag{69}$$

Find the 4 tabular values of $\theta_{0j}(j=l,l+3)$ that bracket the observed solar zenith angle and determine $L_j(X)$, $l = l+3$ (use n=4). Do the same for $L_j(Y)$ using the bracketing values of $\theta_I(I=k,k+3)$ (also with n=4).

3) prflec

Set R_t = surface reflectivity (from N7/TOMS UV surface ref database)
$R_c = 0.80$ (cloud reflectivity)

4) troplyr

Calculate the tropopause layer from external EDR temperature information.

5) reflec

For each of the 4 ozone-insensitive reflectivity wavelengths (364, 367, 372, and 377 nm):

1) Compute an effective cloud fraction, f^*, and an effective reflectivity, R^*.
2) Compute the terrain value of the normalized radiance, I_t, using R_t

$$I_c = I_0 + I_1 \cos\phi + I_2 \cos 2\phi + \frac{R_c T}{1 - R_c S_b} \tag{70}$$

$$I_t = I_0 + I_1 \cos\phi + I_2 \cos 2\phi + \frac{R_t T}{1 - R_t S_b} \tag{71}$$

and the cloud value of the normalized radiance, I_c, for the 1.0, 0.7, 0.4, and 0.1 atm tables:

Lagrange interpolation is used to obtain the calculated quantities I_0, Z_1, Z_2, T, and S_b; I_1 and I_2 are obtained using Z_1, Z_2, Q_1, and Q_2 values calculated in **omps.** A correction for Raman scattering (which is not accounted for in the radiative transfer tables) is applied to the normalized radiance (NR) at all 4 pressure levels and for both R_t and R_c. Lagrange interpolation is then used between the 1.0, 0.7, 0.4, and 0.1 atm parts of the table to obtain I_t and I_c for the correct terrain and cloud pressures.

If $I_{meas} \leq I_t$

1) Compute R^* for the 1.0, 0.7, 0.4, and 0.4 atm tables:

$$R^*(P) = \frac{I^{\lambda}_{meas} - I^{P}_{a}}{T + S_b(I^{\lambda}_{meas} - I^{P}_{a})} \tag{72}$$

where

$$I^{P}_{a} = I^{P}_{0} + I^{P}_{1}\cos\phi + I^{P}_{2}\cos 2\phi \tag{73}$$

2) Use Lagrange interpolation to determine R^* for the given terrain pressure.

3) Set the cloud fraction , f^*, equal to 0.

If $I_t < I_{meas} < I_c$:

1) Calculate cloud fraction according to:

$$f^* = \frac{I^{\lambda}_{meas} - I_t}{I_c - I_t} \tag{74}$$

2) If there is snow or ice on the ground

a) assume there are no clouds

b) calculate a reflectivity for the 1.0, 0.7, 0.4, and 0.1 pressure tables using

$$R^* = \frac{I^*_{meas} - I_a}{T + S_b(I^*_{meas} - I_a)} \tag{75}$$

c) Use Lagrange interpolation and the terrain pressure to get the terrain reflectivity

If $I_{meas} > I_c$:

1) Compute R* for the 1.0, 0.7, 0.4, and 0.1 atm tables:

$$R^* = \frac{I^{\lambda}_{meas} - I_a}{T + S_b(I^{\lambda}_{meas} - I_a)} \tag{76}$$

where

$$I^{P}_{a} = I^{P}_{0} + I^{P}_{1}\cos\phi + I^{P}_{2}\cos 2\phi \tag{77}$$

2) Use Lagrange interpolation to obtain R*

3) Set f* = 1.

4) If snow or ice is present

a) assume there are no clouds

b) calculate a reflectivity for the 1.0, 0.7, 0.4, and 0.1 pressure tables using

$$R^* = \frac{I^{\lambda}_{meas} - I_a}{T + S_b(I^{\lambda}_{meas} - I_a)} \tag{78}$$

c) Use Lagrange interpolation and the terrain pressure to get the terrain reflectivity

Subroutines called by **reflect:**

intnlr: perform table look-ups for the Northern Hemisphere
intslr: perform table look-ups for the Southern Hemisphere
polint: perform Lagrange interpolations

(Note: the tables for the Northern and Southern Hemisphere are currently the same).

The following steps (6 – 14) are performed for each of the 4 reflectivity wavelengths.

6) oznot

Compute Ω_0 using the 318.0/336.0 pair of wavelengths and the partial cloud algorithm. A single set of ozone profiles (low for |lat| ≤ 15°, mid for 15°≤ |lat| ≤ 60°, high for |lat| ≥ 60°) are used.

Start with the initial guess of ozone appropriate for latitude zone ILAT or, for measurements other than the first one, the result from the previous measurement.

Using the 1.0 atm tables and R_t find I_0, Z_1 (and, from it, I_1), Z_2 (and, from it, I_2), T, and S_b and calculate I_t(1.0 atm). Apply a correction for Raman scattering (which is not accounted for in the radiative transfer code) to the NR. Do the same thing with the 0.7, 0.4, and 0.1 atm tables. Use Lagrange interpolation on the calculated NRs at the 4 pressure levels to determine I_t at the terrain pressure. In a similar manner, determine I_c using the cloud pressure instead of the terrain pressure.

Use the cloud fraction, f*, calculated in Step 4 to interpolate between I_t and I_c to produce I_{calc}. Calculate $N_{calc} = N_{318} – N_{336}$ from $I_{calc} = I_{318}/I_{336}$.

If N_{calc} is lower than the measured N value, N_{meas}, perform the above calculation for the next higher ozone value in the table, If N_{calc} is higher than N_{meas}, go to the next lower ozone value. Continue searching through the profiles in the latitude zone designated by ILAT to find the two values of ozone, Ω_L and Ω_U, whose corresponding pair N values, N_L and N_U, bracket N_{meas} at the observed solar zenith angle, satellite zenith angle, and azimuth angle and for the reflectivity calculated previously.

The ozone amount between 1.0 and 0.4 is contained in a table for each of the 26 profiles. The terrain pressure is used to calculate the fraction of this ozone amount that is below the ground and this amount is subtracted from both Ω_L and Ω_U.

Linearly interpolate to obtain an estimate of ozone for the latitude zone:

$$\Omega_0 = \Omega_L + \frac{N_{meas} - N_L}{dN/d\Omega} \tag{79}$$

Where $dN/d\Omega$ is the ozone sensitivity given by

$$\frac{N_U - N_L}{\Omega_U - \Omega_L} \tag{80}$$

Using the procedure above, calculate ozone for two temperature sensitive triplets (including the 316./321. and 318./329. nm pairs).

Subroutines called by **oznot:**

nvbrac: determines whether N_{calc} is above or below N_{meas} in order to determine bracketing values;
prfind: determines profile index (the pointer that indexes the correct profile in the table);
qvalue: determines table values (**qvalue** calls **intnlr** and **intslr**)

7) residue

Compute two sets of residues and sensitivities for wavelengths comprising 3 different triplets from two sets of profiles (low and mid for |lat| < 45°, mid and high otherwise).

For each of the two latitude bands and wavelengths, use Ω_0 to determine I_0, I_1 (from Z_1), I_2 (from Z_2), T, and S_b for the 1.0, 0.7, 0.4, and 0.1 atm tables. Using f*, R_t*, R_c* and reversing the calculations in Step 5, determine N_{calc}.

Calculate residues:

$$r = N_{meas} - N_{calc} \tag{81}$$

Calculate sensitivities.

Subroutines called by residue:

prfind: determines profile index (the pointer that indexes the correct profile in the table);
qvalue: determines table values (**qvalue** calls **intnlr** and **intslr**)

8) ozone

Compute new ozone estimate for each of the 3 wavelength triplets.

Determine which three triplets to use by calculating the optical path length:

$$somega = \frac{\Omega_{est} \cdot (\sec\theta_0 + \sec\theta)}{1000} \tag{81}$$

For each of the 3 triplets:

Compute two separate values of Ω at two latitudes using the two sets of residues and sensitivities obtained in Step 6 and the following formula:

$$\Omega_{profile} = \Omega_0 + \frac{r_1\Delta\lambda_2 - r_2\Delta\lambda_1}{\eta_1\Delta\lambda_2 - \eta_2\Delta\lambda_1};\ \Delta\lambda_i = \lambda_i - \lambda_R \tag{82}$$

where subscripts refer to two selected wavelengths, η is the sensitivity, and r is the residue.

To account for the change in calculated ozone value, adjust residues using the following formula:

$$r_{adj} = \left[r_{prf1} \cdot (1 - f_m) + r_{prf} \cdot f_m\right] - (\Omega_{profile} - \Omega_0) \cdot \eta \tag{83}$$

Call **ozmix** to determine select mixing fraction between low- and mid- or mid- and high-latitude profiles.

Subroutines called by **ozone:**

9) ozmix

For somega ≤ 1.5, mix Ωs to get Ω using the latitude mixing fraction, f_m:

$$\Omega_{mix} = (1 - f_m) \cdot \Omega_{prf1} + f_m \cdot \Omega_{prf2} \tag{84}$$

where prf1 and prf2 are low- and mid- or mid- and high-latitude profiles, respectively, and

$f_m = 0$	for $\|lat\| \le 15°$,
$f_m = (\|lat\|-15)/30$	for $15° < \|lat\| < 45°$,
$fm = (\|lat\|-45)/30$	for $45° < \|lat\| < 75°$, and
$fm = 1$	for $\|lat\| \ge 75°$.

For somega > 1.5, use the following procedure.

3) For each triplet chosen in Step 7, use a 4th wavelength that is sensitive to ozone profile shape to select mixing fraction between low- and mid- or mid- and high-latitude profiles. For example, if the optical path length of the measurement is 1.7, the 3 triplets chosen in Step 7 are formed by using one of the 4 reflectivity wavelengths with the 312.5/321.0, 314.0/321.0, and 318.0/336.0 nm pairs. For these 3 triplets, the 308.5 nm wavelength is used to select ozone profile shape.

3) Calculate a residue for the 4th wavelength, r_4.

3) For each of the two profile sets, calculate the "triplet residue":

$$r_{trip} = r_4 - r_2 \frac{\lambda_4 - \lambda_R}{\lambda_2' - \lambda_R} \tag{85}$$

where r_2 is the middle wavelength of the wavelength triplet.

4) Calculate the mixing fraction:

$$f_m = \frac{r_{trip}(lower)}{r_{trip}(lower) - r_{trip}(higher)} \tag{86}$$

Calculate ozone using this mixing fraction:

$$\Omega_{mix} = (1 - f_m) \cdot \Omega_{prf1} + f_m \cdot \Omega_{prf2} \tag{87}$$

and readjust residues

$$r = \left\lfloor r_{prf1} \cdot (1 - f_m) + r_{prf} \cdot f_m \right\rfloor - (\Omega_{mix} - \Omega_0) \cdot \eta$$

5) Recalculate r_{trip}. If it is greater than 0.1, iterate once using Ω_{mix} determined in 4 above.

Ω_{mix} corresponds to the heritage V7 ozone amount, Ω_{V7}.

10) tpcor

Correct for differences between actual ozone and temperature profiles and standard ozone and temperature profiles

1) Calculate dN/dx and dN/dt using the two sensitivity tables.

   Unperturbed profile

   For each of the two latitude bands and wavelengths, use Ω_{V7} to determine I_0, I_1 (from Z_1), I_2 (from Z_2), T, and S_b for the 1.0, 0.7, 0.4, and 0.1 atm dN/dx and dN/dt tables. Using f_m, f*, R_t*, R_c* and reversing the calculations in Step 5, determine N_{calc}.

   Perturbed Profiles

   For each of the two latitude bands and wavelengths, use Ω_{V7} to determine I_0, I_1 (from Z_1), I_2 (from Z_2), T, and S_b for each of the 11 perturbed profiles for the 1.0, 0.7, 0.4, and 0.1 atm dN/dx and dN/dt tables. Again, use f_m, f*, R_t*, R_c* and reverse the calculations in Step 5 to determine N_{calc} for each of the perturbed profiles.

2) Using N values calculated for the unperturbed profile and the N values calculated for the perturbed profiles, calculate 11 dN/dx and dN/dt values (one for each of the 11 layer perturbations).

3) Using Ω_{V7} and f_m, determine the standard ozone and temperature profile used in the table lookup.

4) Use the EDR external temperature profile to determine the difference between the actual and standard temperature, Δt, for all 11 layers.

5) Use the limb retrieved ozone profile to determine the difference between the actual and standard ozone profile, Δx, for all layers for which there is a limb retrieval.

6) Form the two sums:

$$\sum_{layer}(t_{layer}-t^0_{layer})\frac{dN}{dt_{layer}} \qquad \sum_{layer}(x_{layer}-x^0_{layer})\frac{dN}{dx_{layer}} \tag{88}$$

11) oznew

Form the equation

$$r = N_m - N_{V7} = (\Omega - \Omega_{mix})\eta + \sum_{layer}(t_{layer} - t^0_{layer})\frac{dN}{dt_{layer}} + \sum_{layer}(x_{layer} - x^0_{layer})\frac{dN}{dx_{layer}} + a + b\lambda \quad (89)$$

and solve for Ω:

$$\Omega = \Omega_{mix} + \frac{r_1\Delta\lambda_2 - r_2\Delta\lambda_1}{\eta_1\Delta\lambda_2 - \eta_2\Delta\lambda_1}. \quad (90)$$

12) resadj

To account for the change in calculated ozone value, adjust residues using the following formula:

$$r_{adj} = \lfloor r_{prf1} \cdot (1 - f_m) + r_{prf} \cdot f_m \rfloor - (\Omega - \Omega_{V7}) \cdot \eta \quad (91)$$

13) tropoz

From the calculation of the tropopause pressure in Step 2, calculate the climatological amount of tropospheric ozone in standard profile used to determine Ω.

Calculate layer efficiencies:

$$\xi_{layer} = \frac{dN_{triplet} / dx}{dN_{triplet} / d\Omega} \quad (92)$$

where the numerators are obtained from Step 9 and the denominators are obtained from Step 7.

14) blwcld

Calculate ozone beneath the cloud for both appropriate latitude bands.

If the cloud pressure is greater than 0.5 atm, the cloud is in layer 1. Determine the fraction of ozone in layer 1 that is below the cloud for the bracketing ozone values (since pressure scales with height exponentially use logarithmic interpolation):

$$f_{cloud} = \frac{\log(1.013 / p_{cloud})}{\log(1.013 / 0.5)} \quad (93)$$

$$\Omega^{prflo}_{cld} = f_{cloud} \cdot \Omega^{prflo}_{layer1} \quad (94)$$

$$\Omega^{prfhi}_{cld} = f_{cloud} \cdot \Omega^{prfhi}_{layer1} \quad (95)$$

If the cloud pressure is less than 0.5, the cloud is in layer 2 (which ends at 0.253 atm). Determine the fraction of ozone in layer 2 that is below the cloud and add to the ozone in layer 1 (which is totally below the cloud):

$$f_{cloud} = \frac{\log(0.5/p_{cloud})}{\log(0.5/0.253)} \tag{96}$$

$$\Omega_{cld}^{prflo} = f_{cloud} \cdot \Omega_{layer\,2}^{prflo} + \Omega_{layer1}^{prflo} \tag{97}$$

$$\Omega_{cld}^{prfhi} = f_{cloud} \cdot \Omega_{layer\,2}^{prfhi} + \Omega_{layer1}^{prfhi} \tag{98}$$

Mix ozone below cloud from bracketing profiles for the two latitude bands:

$$f_{\Omega} = \frac{\Omega - \Omega_{prflo}}{\Omega_{prfhi} - \Omega_{prflo}} = \frac{\Omega - \Omega_{prflo}}{50}, \tag{99}$$

$$\Omega_{cld}^{lat} = \Omega_{cld}^{prflo} \cdot (1 - f_{\Omega}) + \Omega_{cld}^{lat\,2} \cdot f_{\Omega}. \tag{100}$$

Mix Ω_{cld} using the profile mixing fraction:

$$\Omega_{cld} = (1 - f_m) \cdot \Omega_{cld}^{lat1} + f_m \cdot \Omega_{cld}^{lat\,2}. \tag{101}$$

Finally, multiply by the cloud fraction:

$$\Omega_{cld} = f_{cld} \cdot \Omega_{cld}. \tag{102}$$

The previous steps (6 – 14) are performed for each of the 4 reflectivity wavelengths.

15) ozweight

Combine the 12 ozone values determined in Steps 6-14 to produce a final ozone value for the measurement

16) soi

Determine if SO_2 is present.

For each reflectivity wavelength

Calculate the ratio, Rat, of ozone to SO_2 absorption coefficients for the 310.5, 312.0, and 321.0 nm wavelengths.

Calculate SO_2 sensitivities:

$$\frac{dN}{d(SO_2)} = Rat \cdot \frac{dN}{d\Omega}. \tag{103}$$

Calculate the SO_2 index using

$$SO_2 = \frac{r_{23} \cdot s_{13} - r_{13} \cdot s_{23}}{so_{23} \cdot s_{13} - so_{13} \cdot s_{23}}, \tag{104}$$

where

$$s_{13} = \left(\frac{dN}{d\Omega}\right)_{310.5} \cdot (321.0 - \lambda_R) - \left(\frac{dN}{d\Omega}\right)_{321.0} \cdot (310.5 - \lambda_R), \tag{105}$$

$$s_{23} = \left(\frac{dN}{d\Omega}\right)_{312.0} \cdot (321.0 - \lambda_R) - \left(\frac{dN}{d\Omega}\right)_{321.0} \cdot (312.0 - \lambda_R), \tag{106}$$

$$so_{13} = \left(\frac{dN}{dSO_2}\right)_{310.5} \cdot (321.0 - \lambda_R) - \left(\frac{dN}{dSO_2}\right)_{321.0} \cdot (310.5 - \lambda_R), \tag{107}$$

$$so_{23} = \left(\frac{dN}{dSO_2}\right)_{312.0} \cdot (321.0 - \lambda_R) - \left(\frac{dN}{dSO_2}\right)_{321.0} \cdot (312.0 - \lambda_R), \tag{108}$$

$$r_{13} = r_{310.5} \cdot (321.0 - \lambda_R) - r_{321.0} \cdot (310.5 - \lambda_R), \text{ and} \tag{109}$$

$$r_{23} = r_{312.0} \cdot (321.0 - \lambda_R) - r_{321.0} \cdot (312.0 - \lambda_R). \tag{110}$$

Average the 4 reflectivity wavelengths to obtain the final SO_2 value. Rename SOI and use to flag data if larger than 4σ.

17) seterr

Assess the quality of the data. This assessment will include:

1) checks on the residues for deviation from linearity;
2) checks for volcanic SO_2 contamination; and
3) comparison of ozone determined from the 2 temperature sensitive triplets (see Table 2.4-1) with the 318/336 nm ozone estimate to determine large-scale temperature deviations from the standard profile

4 Assumptions

Table 4-1 summarizes the assumptions described in Sections 2.3, 2.4, and 3.2.1.

Table 4-1. List of Assumptions Made in Forward Model and in Retrieval

Forward Model
The atmosphere can be represented by a simplified Beer's Law, which includes Rayleigh scattering and ozone absorption.
The atmosphere's lower bound consists of two Lambertian reflecting surfaces, one for the ground and one for clouds.
Raman scattering can be treated as being independent of solar and satellite zenith angle.
Retrieval
The NR for an entire scene can be treated as coming from a point source with viewing conditions given by those at the center of the FOV.
The cloud fraction can be determined by linearly interpolating the measured normalized radiance of an ozone-insensitive wavelength between a normalized radiance calculated for the surface and one for the cloud.
The cloud's reflectivity is 0.8.
The surface's reflectivity is obtained by a table look-up.
A correction factor linear with wavelength corrects for most non-Rayleigh scattering atmospheric effects.
Tropospheric aerosols and sun glint can be corrected by requiring a reflectivity dependence that is linear with wavelength.
A correction factor independent of viewing angles can be used to correct calculated normalized radiances for Raman scattering.

5 Input Data Requirements

Primary Sensor Requirements

Table 5.1-1 outlines what the baseline algorithm needs and sensor allocations.

Table 5.1-1. Sensor Parameters and Performance Requirements to Meet EDR Requirements Using the Nadir Total Column Ozone Algorithm

Parameter	Baseline Algorithm Needs	Baseline Sensor Allocation	Comments
Wavelength range	308-377 nm	300-380 nm	Ozone and path length range
Bandwidth	1 nm	1 nm	Pair/triplet approach
Samples/FWHM	1 min.	2.4	λ shift, Ring effect
Number of channels	22*	192	Triplets, over-sampling, aerosols
Horizontal cell size	50 km @ nadir	50 km @ nadir	
Horizontal coverage	> 2800 km	> 2800 km	
SNR	> 1000 for SZA < 80 at specified radiances	> 1000 for SZA < 80 at specified radiances	Precision
λ registration	< 0.01 nm	< 0.01 nm	Ozone cross-section error
Albedo calibration	2%	2%	Accuracy and stability
Pixel to pixel calibration (includes linearity)	0.5% max.	0.5% max.	Accuracy
Albedo deviation error	< 1%	< 1%	Accuracy and stability

* The 22 wavelengths are: 308.5, 310.5, 312.0, 312.5, 314.0, 315.0, 316.0, 317.0, 318.0, 320.0, 321.0, 322.5, 325.0, 328.0, 329.0, 331.0, 332.0, 336.0, 364.0, 367.0, 372.0, and 377.0 nm

5.2 Other OMPS Sensor Data Requirements

Table 5.2-1 specifies other OMPS data required by the total column ozone algorithm.

Table 5.2-1. Other OMPS Data Required by the Total Column Ozone Algorithm

Sensor	Data	Form	Use
UV/Vis limb	Ozone profile	Co-located in 11 Umkehr layers Dobson Units	Ozone profile shape Tropospheric ozone correction
UV/Vis limb	Aerosol profile	Co-located	P^3I

5.3 Other NPOESS Sensor Data Requirements

Table 5.3-1 specifies data from other NPOESS sensors required by the total column ozone algorithm.

Table 5.3-1. Data Products from Other NPOESS Sensor Systems That Are Used by the Total Column Ozone Algorithm

Sensor	Data	Form	Use
CrIS	Temperature - pressure profile	Co-located in 11 Umkehr layers Kelvin	Temperature profile shape
VIIRS	Cloud top pressure	Co-located Atm	Partial cloud algorithm Calc of normalized radiances
VIIRS	Snow and ice cover	Co-located Percent	Snow/ice indication Calc of normalized radiances

5.4 Climatology Data Requirements

Table 5.4-1 specifies climatological data required by the total column ozone algorithm (note: some of the databases are only used if external EDRs are not available).

Table 5.4-1. Climatology Databases Used by the Total Column Ozone Algorithm

Data	Form	Source	Use
Surface pressure*	1° x 1.25°grid In mbars	TUG87 geophysical model (see Weiser, 1987)	Calculation of normalized radiances
Cloud pressure*	1° x 1.25° x 12 month In mbars	ISCCP	Partial cloud algorithm Calculation of normalized radiances
Snow/ice*	1° x 1.25° x 12 month In percent probability	Air Force	Snow/ice indication Calculation of normalized radiances
Surface reflectivity	1° x 1.25°	Herman and Celarier, JGR, 1997	Calculate radiances
Eclipse	Areal coverage	Astronomical almanac	Flag data

* Used if external EDR not available

6 Output Data Description

6.1 EDRs

Ozone total column is defined as the amount of ozone in a vertical column of the atmosphere measured in Dobson Units (milli-atm-cm). The specifications and specified performance for the EDR are given in **Table 6.1-1**.

Table 6.1-1. Total Column Ozone EDR Specifications

SRD Paragraph No.	Description	Allocated (Assured) Performance
SRDO3.2.1.1.1.1-1	Horizontal Cell Size	50 km @nadir
SRDO3.2.1.1.1.1-3	Horizontal Reporting Interval	50 km @ nadir
SRDO3.2.1.1.1.1-4	Vertical Cell Size	60 km
SRDO3.2.1.1.1.1-10	Horizontal Coverage	SZA < 80 degrees
SRDO3.2.1.1.1.1-11	Vertical Coverage	0 – 60 km
SRDO3.2.1.1.1.1-12	Measurement Range	50 – 650 m-atm-cm
SRDO3.2.1.1.1.1-15	Measurement Accuracy	15 m-atm-cm, 480 < Ω < 650 m-atm-cm 12 m-atm-cm, 250< Ω<450 m-atm-cm 9 m-atm-cm, Ω < 250 m-atm-cm
SRDO3.2.1.1.1.1-19	Measurement Precision	3 m-atm-cm + 0.5%, 450 m-atm-cm ≤ Ω m-atm-cm + 0.5%, 250< Ω<450 m-atm-cm 2.5 m-atm-cm + 0.5%, Ω < 250 m-atm-cm
SRDO3.2.1.1.1.1-24	Long term Stability	1%
SRDO3.2.1.1.1.1-26	Mapping Uncertainty	5 km
SRDO3.2.1.1.1.1-28	Mapping Local Average Revisit Time	24 hours

6.2 Additional Data Products

Table 6.2-1 specifies additional algorithm outputs that are not part of our baseline as verified data products but are available as P^3I.

Table 6.2-1. Additional, Non-Baseline Data Products Available from the Total Ozone Algorithm

Data	Form	Reference
Cloud fraction	$0.0 < f_{cld} < 1.0$	Section 2
Reflectivity	Percent	Section 2
Volcanic SO_2	Dobson Units	Section 2, ICSR 8091101
Aerosol index	Index	Section 2, ICSR 8100101

6.3 EDR Content

The output records of the Total Column Ozone EDRs will include the information listed in Table 6.1-1 and Table 6.2-1. (The additional, non-baseline P^3I data products are flagged as bold-italicized parameters) This data is organized into a header record followed by a number of Earth view data records. The recommended content of these records follows:

Header record with:

- EDR identification
- Spacecraft identification
- Sensor identification
- Date and time of EDR generation
- Date and start time of data in file
- Date and end time of data in file
- Earth view data records (approximately 14,000 IFOV per orbit) with:
  - Orbit number
  - Date and time of data
  - Data acquisition orbit number
  - Data transmission orbit number
  - Ascending node Julian date and time tag
  - Spacecraft altitude
  - Identification of SDR calibration parameters
  - EDR Algorithm identification number
  - EDR Algorithm version number
  - Channel identification
  - Latitude of scene
  - Longitude of scene
  - Solar zenith angle
  - Satellite zenith angle
  - Azimuth angle (the angle between the sun and the satellite IFOV)
  - Calibrated albedo (ratio of radiance to irradiance) per channel
  - Total ozone (from the OMPS Total Column Ozone Algorithm)
  - Total ozone (from the heritage TOMS Version 7 Algorithm)

- Residue, defined as the difference between measured and modeled N-values per channel
- Ozone sensitivity per channel (defined as dN/dΩ)
- Reflectivity sensitivity per channel (defined as dN/dR, where R is the scene reflectivity)
- ***Cloud fraction***
- ***Scene reflectivity***
- ***Surface category***
- ***Cloud pressure***
- ***Aerosol index***
- ***SOI (SO2 index)***
- Updated tropospheric ozone value for scene (if cloud free)
- Data quality flags

7. System Accuracy and Precision

Accuracy and precision in total column retrievals are allocated to the sensor and the algorithms. In this section, error sources are identified along with estimates of the error we expect to achieve based on our design.

7.1 System Accuracy

Total column ozone retrieval accuracy is allocated to sensor and algorithm systematic errors. The threshold and objective accuracies are 15 DU and 5 DU. We assure allocated performance at 9 DU from 50 to 250 DU; at 12 DU from 250 to 450 DU; and at 15 DU from 450 to 650 DU. The combined allocation of sensor and algorithm accuracy (not including margin which is carried at the system level) is shown in **Figure 7.1-1** as a function of total ozone, along with the threshold, objective, and assured performance. The allocated plot is curved due to the combination of driving errors such as the linear dependence from cross section errors and a constant contribution from wavelength-dependent calibration errors.

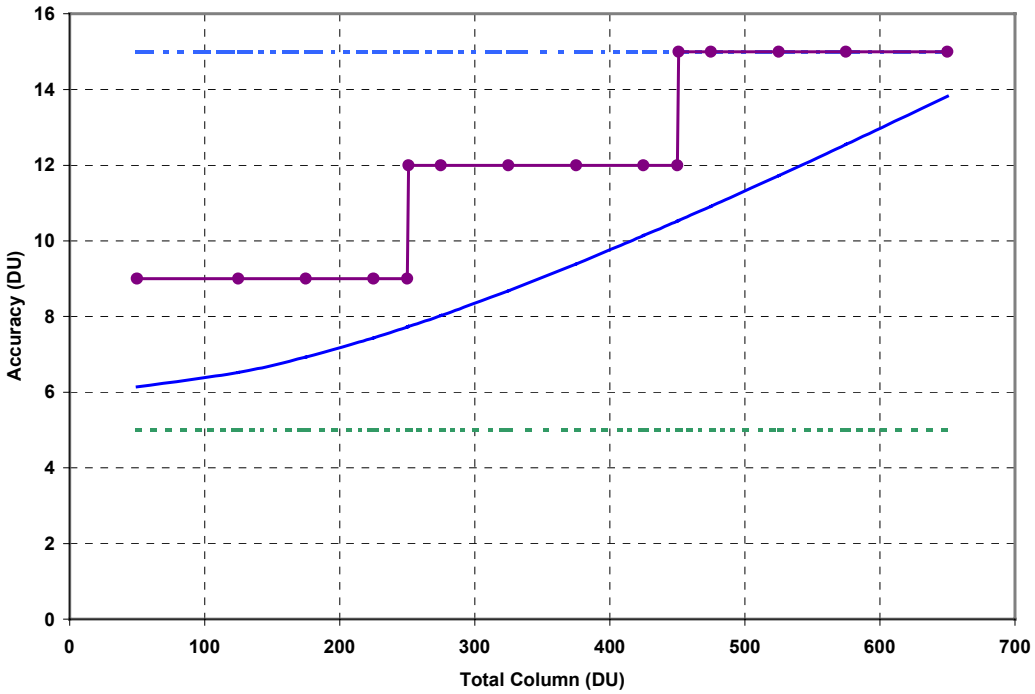

Figure 7.1-1. Plot of total allocated (assured) total column accuracy, including margin (solid line with filled circles); allocated sensor and algorithm accuracy, not including margin (solid line); and thresholds (dash-dot) and objectives (dotted) for total column EDR accuracy.

The tree showing the allocation between sensor and algorithm is shown in **Figure 7.1-2**. The allocation is done to the maximum ozone value of 650 DU because (as shown in Figure 7.1-1) the smallest margin with respect to threshold is encountered there.

Maximum Ozone	
650	DU

Total		
Available	15.0	Dobson units
Allocated	13.8	Dobson units
Margin	1.2	Dobson units

Sensor		
Available	10.0	DU
Allocated	8.7	DU
Margin	1.3	DU

Algorithm		
Available	11.0	DU
Allocated	10.8	DU
Margin	0.2	DU

Figure 7.1-2. Allocation of total column accuracy to sensor and algorithm for 450-650 DU

7.1.1 Sensor Accuracy

The sensor accuracy allocations for retrieved total column ozone values are given in the tree shown in **Figure 7.1-3**. Derivations of the allocations are given in the text and plots that follow the allocation tree.

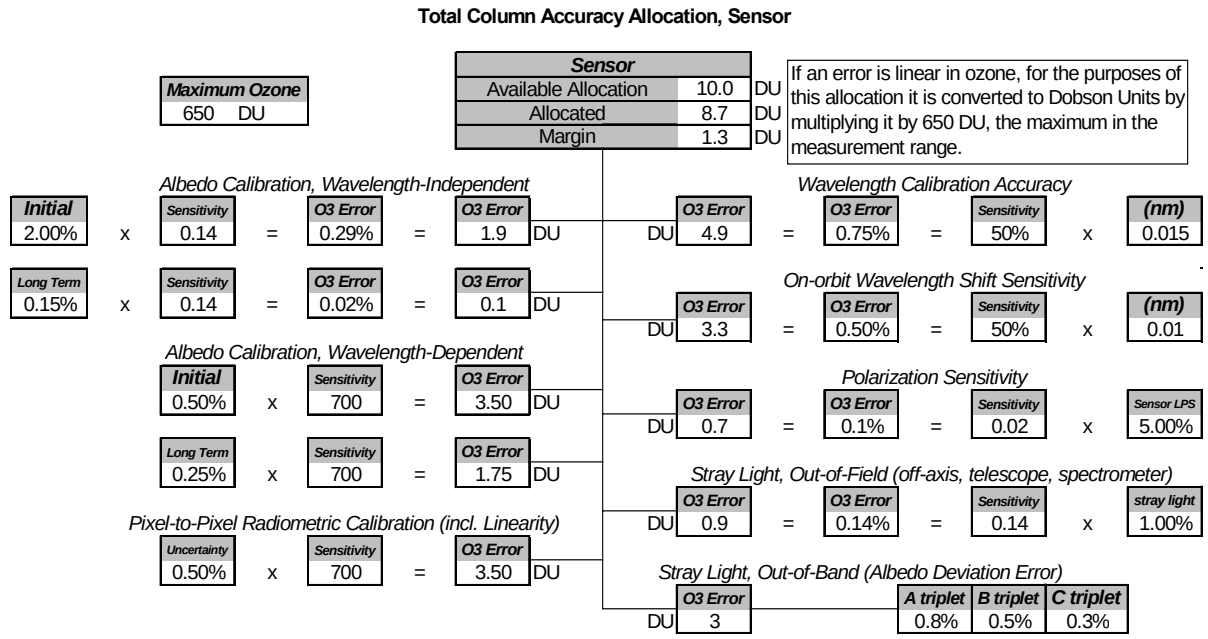

Figure 7.1-3. Allocation for sensor contributions to retrieved ozone accuracy

Albedo Calibration, Wavelength-Independent. Albedo calibration is the ratio of sensor sensitivity to spectral radiance (nadir scene) and spectral irradiance (solar calibration). In that ratio, absolute scales and sensor efficiency cancel out leaving only the spectral efficiency and geometry of the solar diffuser.

Our allocation of 2% accuracy of initial (pre-flight), wavelength-independent albedo calibration is based on experience with similar calibrations of SBUV/2. The in-flight accuracy pertains to the trend of diffuser degradation over time of exposure to the sun, as measured by comparison of working and reference diffusers (Section 7.1.3). Ordinary in-flight solar calibration does not detect or correct errors in the pre-flight baseline calibration, however, vicarious calibrations and data justification will allow evaluation of, and possible correction to, the pre-flight wavelength-independent baseline.

The triplet formulation has a small sensitivity to wavelength-independent albedo calibration, as shown by Wellemeyer et al. (1996). This sensitivity is approximately 1% ozone for 7% calibration error (Jaross et al., 1998a).

Albedo Calibration, Wavelength-Dependent. An absolute calibration error has a small effect on ozone derived using the triplet formulation. It is the difference in absolute calibration error between different wavelengths in the triplet that is important. Such errors are treated in analysis as uncorrelated between wavelengths. Jaross et al. (1998a) show such uncertainties estimated for retrievals using the TOMS wavelengths.

For TOMS, sensitivity of ozone to albedo variations depends strongly on total column and path length. For a well designed instrument such as OMPS with many wavelengths, we select triplets to essentially keep the sensitivity constant (Table 2.4-1). Thus the value of $s\Delta\alpha\Omega$ varies by no more than a factor of 2 over the full range of measurements. By Monte Carlo analysis we find that a 1% wavelength-dependent (but uncorrelated) albedo calibration error will result in about 7 DU ozone error. This value is essentially independent of total column amount, by design.

Pixel-to-Pixel Radiometric Calibration: This contribution includes the uncertainty of flat-fielding and system linearity calibrations. The sensitivity to this uncertainty is the same as to wavelength-dependent albedo calibration.

Wavelength Calibration Accuracy and On-Orbit Wavelength Shift Sensitivity: We allocate an initial wavelength calibration accuracy and a sensitivity to shifts on orbit. The allocations are based on analysis, the results of which are shown in Figures 3.1-4 and Figure 7.1.1-4. For the shift sensitivity analysis, the assumed sensor characteristics were 0.1% irradiance measurement noise and 1 nm FWHM sensor resolution. In order to derive the results, GOME 0.2 nm solar data were degraded to 1 nm FWHM resolution and the sensitivity using single absorption lines was determined. The result is that we expect better than 0.005 nm shift sensitivity.

The sensitivity of the Nadir Total Column sensor retrieved ozone to wavelength registration errors occurs predominantly via the absorption coefficients. A sensitivity study was performed as part of channel selection (see Section 2). The sensitivities of triplet-derived ozone to 0.02 nm wavelength registration errors is shown in Figure 2.4-5 for all triplet combinations. The results indicate less than 1% retrieval errors for most of the triplets (5% per 0.1 nm). Those triplets with greater sensitivity are not intended for standard ozone retrievals. For instance, triplets were chosen with maximum temperature sensitivity as a monitoring tool. These same triplets will also have large sensitivities to wavelength registration. We use the 5% per 0.1 nm as the sensitivity for the wavelength calibration allocations.

We have also performed an end-to-end simulation of wavelength registration errors in the Nadir Total Column ozone retrieval. For this study we selected three triplets which will cover the full range of atmospheric slant paths encountered during ozone retrieval.

- A triplet: 312.0 nm, 321.0 nm, 364.0 nm
- B triplet: 316.0 nm, 329.0 nm, 364.0 nm
- C triplet: 322.5 nm, 336.0 nm, 364.0 nm

For each triplet, the forward model was run assuming the nominal wavelengths. Ozone was then retrieved from the generated radiances using a modified ozone table. This modified table was created by shifting the band centers of all channels 0.1 nm from nominal. The retrieved ozone was then compared to the original input amounts. The differences are shown in **Figure 7.1-5** as a function of total ozone amount. For each triplet a solar zenith angle (SZA) and satellite zenith angle (SatZA) were chosen to maximize the error. The resulting sensitivities are approximately 1.5%, 4%, and 3% per 0.1 nm for the A, B, and C triplets, respectively. These sensitivities are all less than the maximum 5% per 0.1 nm shown in Figure 2.4-5 for triplets used in ozone retrievals.

Based on the above analysis, we make a conservative allocation of 0.01 nm shift sensitivity. The accuracy allocation accounts for the calibration transfer uncertainty from wavelength standards to the reference solar spectrum.

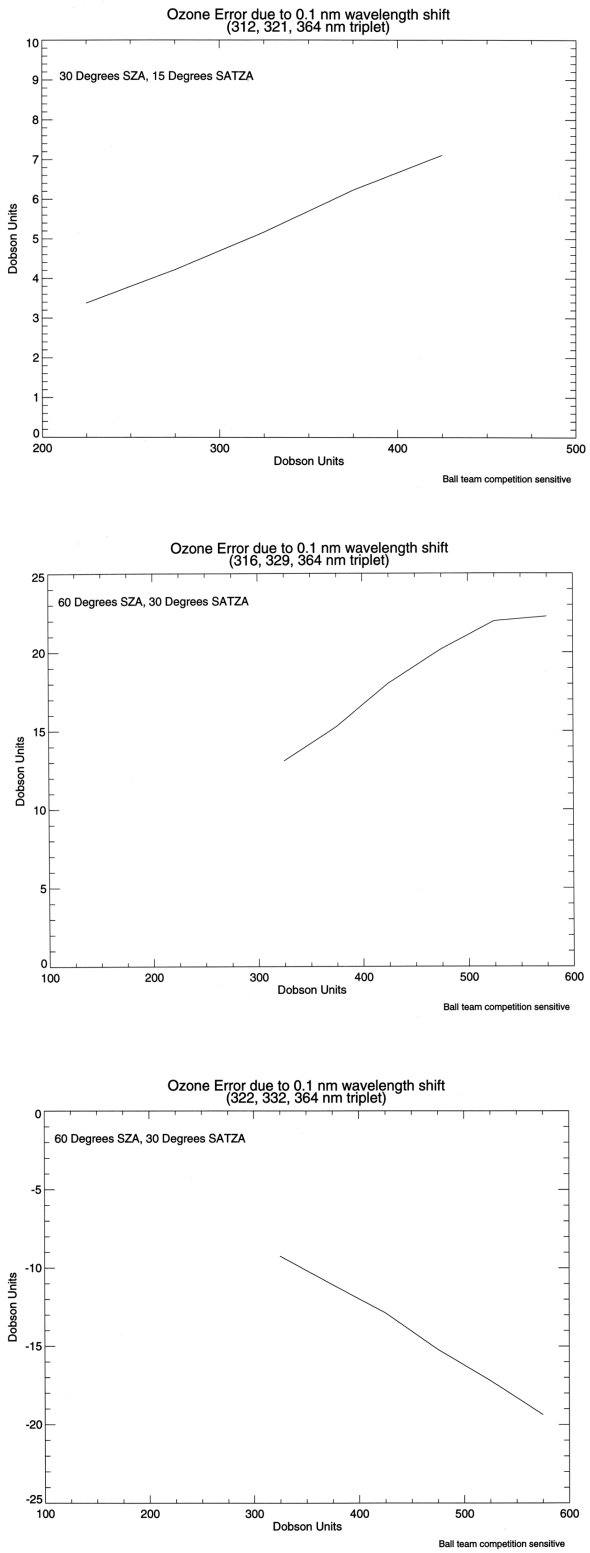

Figure 7.1.1-5. Simulated retrievals of ozone are shown using an ozone table with 0.1 nm sensor wavelength errors. The percent error for each triplet varies little with viewing conditions or with total ozone amount.

Polarization Sensitivity. We have estimated the sensitivity of the Nadir Total Column retrieval algorithm to polarized radiances. Polarization of backscattered radiation poses a particular problem in the UV where Rayleigh scattering cross sections are high. Reflective surfaces in the sensor can enhance incident radiation of one polarization state more than the other. This in itself is not a problem, except that the relative amplitudes, S and P, of polarized light will vary with viewing conditions. The result would be cross-track and latitude dependences in the retrieved ozone amounts. BUV sensors typically use depolarizers in the fore-optics to reduce the polarization sensitivity of the sensor to acceptable levels. Both Nadir and Limb sensors are designed with depolarizers at their entrance apertures.

We took advantage of existing radiative transfer simulations to first estimate the percent polarization in each of the two polarization states for backscattered UV radiation. This information is available from the Dave forward model, which has been used to generate radiances for TOMS and OMPS viewing conditions and at TOMS wavelengths. To compute the sensitivity to polarized light, we make the assumption that radiances will be in error by the percentage of polarization present in the incoming radiances. For our studies, we also assumed that the Nadir depolarizer reduces the linear polarization sensitivity to 5%. Thus, if 20% of the incoming radiation is plane polarized, we say in our conservative model that radiances have a 1% error. The optical designs have no scanning optics and fairly small apertures, making polarization scrambling through use of depolarizers very effective at reducing polarization sensitivity; expected polarization sensitivity of the sensor will actually be 1% or less.

We computed radiance errors at three TOMS wavelengths under a variety of viewing conditions. The wavelengths, 313 nm, 331 nm, and 360 nm, correspond to the TOMS A triplet and are not far from A triplet wavelengths on the Nadir sensor. The triplet formulation, discussed in Section 2, forms a linear combination of the N values from the three measured radiances. We express an error in the N values, ΔN_λ, in terms of an error in the radiances, ΔI_λ:

$$\Delta N_\lambda = \ln\left(\frac{I_\lambda + \Delta I_\lambda}{I_\lambda}\right) \tag{111}$$

The effective radiance error in the A triplet is the difference between the true error at 313 nm and the error predicted by the linear extrapolation of the two longer wavelengths,

$$\Delta N_A = \Delta N_{313} - \left[f\left(\Delta N_{331} - \Delta N_{360}\right) + \Delta N_{360} \right] \tag{112}$$

where f is a ratio of wavelength separations from 360 nm of the two short channels. The ozone error $\Delta\Omega$ is then simply computed using the sensitivity, $dN_A/d\Omega$=0.135 DU^{-1}.

$$\Delta\Omega = \frac{\Delta N_A}{dN_A/d\Omega} \tag{113}$$

These formulas state that no ozone errors will exist due to polarization if the fractional radiance error caused by sensor polarization sensitivity varies at most linearly in wavelength. This fact

can be used to explain, in large part, the simulation results shown in **Figure 7.1-6**. These results indicate that, under the worst viewing conditions, ozone errors do not exceed 0.02 DU. The 0.1% error allocation is therefore conservative.

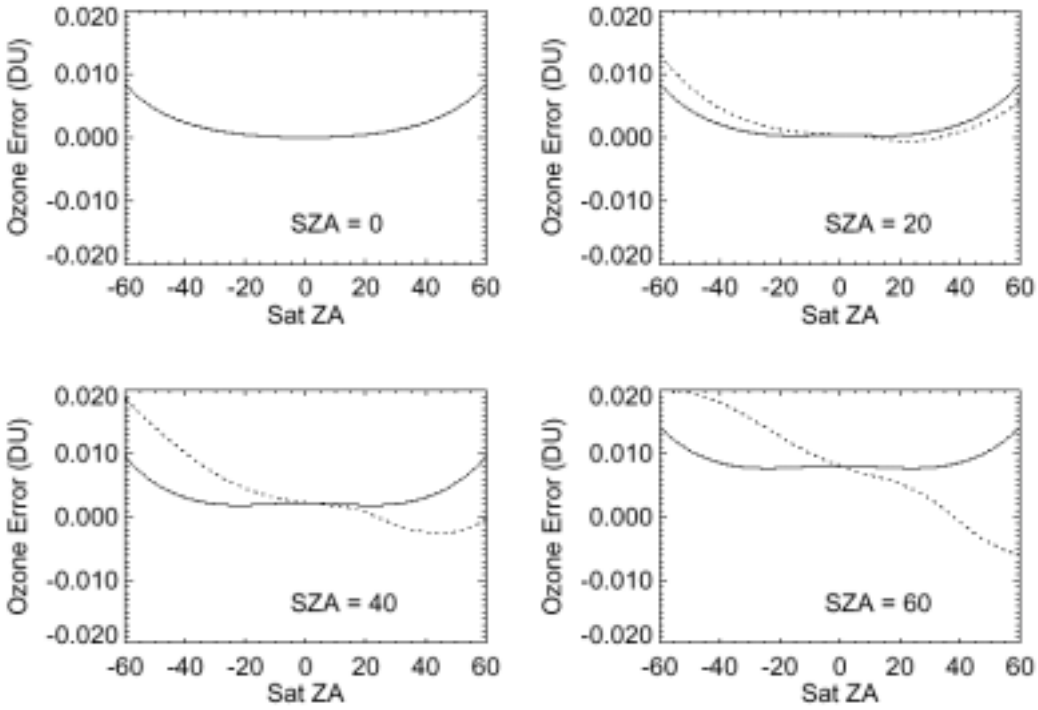

Figure 7.1-6. Plots of ozone error due to polarization sensitivity are shown as a function of satellite zenith angle for four solar zenith angles. Errors are for A-triplet ozone. A 5%-residual depolarizer is assumed for the sensor. The solid line represents the situation in a near-noon orbit (relative azimuth = ±90°), and the dotted line is for a 4PM or 8AM orbit (relative azimuth = 30°, 150°)

In this analysis we have used TOMS wavelengths and ozone sensitivities. Because the ozone errors are so small, we hypothesize that the slight changes in these quantities for OMPS wavelengths will make little difference. Also, we have neglected triplet combinations other than the A triplet. These other triplets, which tend to be used at higher latitudes, all use wavelengths longer than 313 nm to decrease ozone sensitivity. Thus the linear extrapolation of radiance errors in wavelength should work even better. On OMPS, the values of $dN/d\Omega$ are the same within a factor of 2 for all triplets.

Stray Light, Out of Field. Out-of-field stray light has three sources: off-axis scatter into the telescope's field-of-regard, scatter within the telescope (before the slit) and scatter within the spectrometer (after the slit). We expect that this error is predominantly wavelength-independent before and after the slit. The ozone sensitivity to out-of-field scatter is therefore similar to that of a wavelength-independent albedo calibration error. Current analysis of the sensor optical scatter indicates worst-case off-axis and telescope stray light of 1% albedo error. We have made this our allocation for total out of field stray light.

Stray Light, Out of Band. The effect of out-of-band stray light on the total column algorithm is detailed in ICSR E8093001 (titled "Explanation of the ozone total column algorithm's linear wavelength assumption and its use in stray light analyses", 30 Sep 98). Studies show that the sensitivity of the ozone retrieval to albedo "deviations" (departures from the linear wavelength dependence expected in the N-values) is different for different wavelength triplets. To stay within the allocated 3 DU, the A triplet deviation can be no bigger than 0.8%, the B triplet 0.5%, and the C triplet 0.3%. This allocation is flowed down to the requirement that irradiance or radiance stray light be no more than 1.2% at wavelengths used in the retrievals.

7.1.2 Algorithm Accuracy Errors

The algorithm accuracy allocations for retrieved total column ozone values are given in the tree shown in **Figure 7.1-7**. Derivations of the allocations are given in the text and plots that follow the allocation tree.

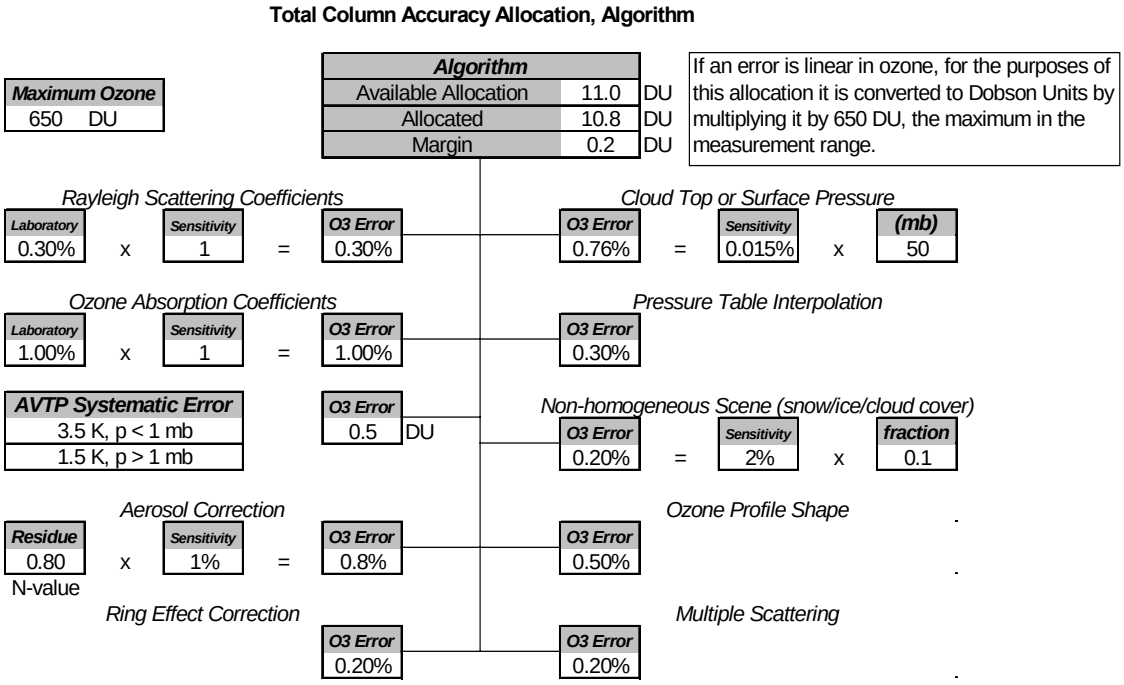

Figure 7.1-7. Allocation for algorithm contributions to retrieved ozone accuracy

Rayleigh Scattering Coefficients. We allocate the 0.3% accuracy for total column given by Fleig et al. (1990, Table 7.2).

Ozone Absorption Coefficients, Absolute. We allocate 1.0% based on analysis by C. Wellemeyer comparing Bass-Paur and French measurements of ozone absorption coefficients.

Ozone Absorption Coefficients, Temperature Dependence. The allocation is based on the selection of temperature-insensitive wavelengths (Section 2.4.10) and the use of the external

atmospheric vertical temperature profile (AVTP) EDR. We allocate constant 0.5 DU error for both precision and accuracy. The derivation is given in the section on the precision allocation.

Tropospheric Aerosol Correction. Both the Torres and the R_λ correction for aerosols remove most of the systematic error due to aerosols. We expect stray light to affect the tropospheric aerosol correction, with an ozone error of no more than 0.3% (ICSR E8093001, 30 Sep 98). We also expect some systematic error due to the variation in aerosols optical properties. **Figure 7.1-8** shows that the worst-case difference between the ozone error for smoke (moderately absorbing carbonaceous aerosol, C2) and desert dust (D) is about 0.4%. Worst case, these combine additively to result in 0.7% systematic ozone error. We allocate 0.8% ozone error.

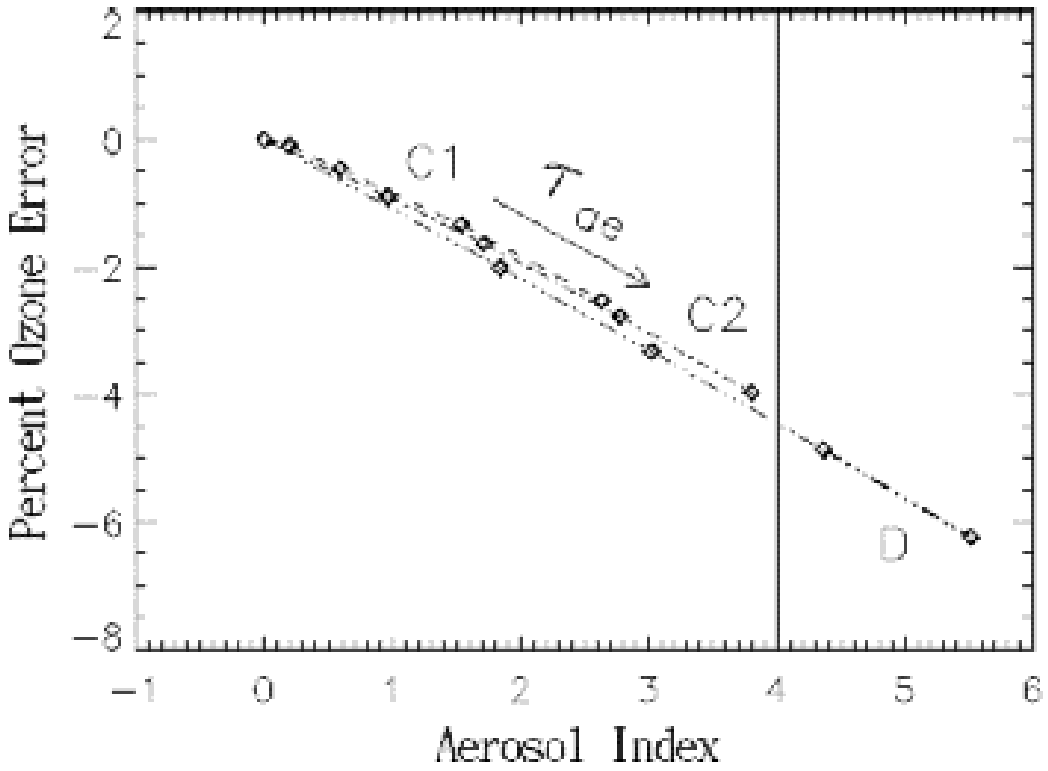

Figure 7.1-8. The systematic error in ozone retrieval due to the presence of tropospheric aerosols (before applying the Torres or R_λ correction) is shown for three models of tropospheric aerosols. C1 is weakly absorbing carbonaceous. C2 is moderately absorbing carbonaceous. D is desert dust. τ_{ae} is the optical thickness

Cloud Top Pressure. The accuracy allocation for cloud top pressure (CTP) is based on the global amount derived for the VIIRS CTP EDR precision listed in section 7.3.2. The global weighted average is 0.38% based on the 25 mb threshold precision at 400 mb; consequently, for the 50 mb threshold CTP accuracy, the allocation is 0.76%.

Pressure Table Interpolation. This allocation accounts for the greatly reduced error due to interpolation in pressure when using the new OMPS radiative transfer tables. This improvement over TOMS is due to the availability of the external cloud top pressure data from VIIRS. The

fidelity of the table is enhanced by increasing the number of pressure node points from 2 to 4 and changing from linear to Lagrangian interpolation. The improvement is demonstrated in **Figure 7.1-9**.

The radiative transfer interpolation errors in solar and satellite zenith angles are the same as heritage and are negligible (<0.1%, Klenk et al., 1982).

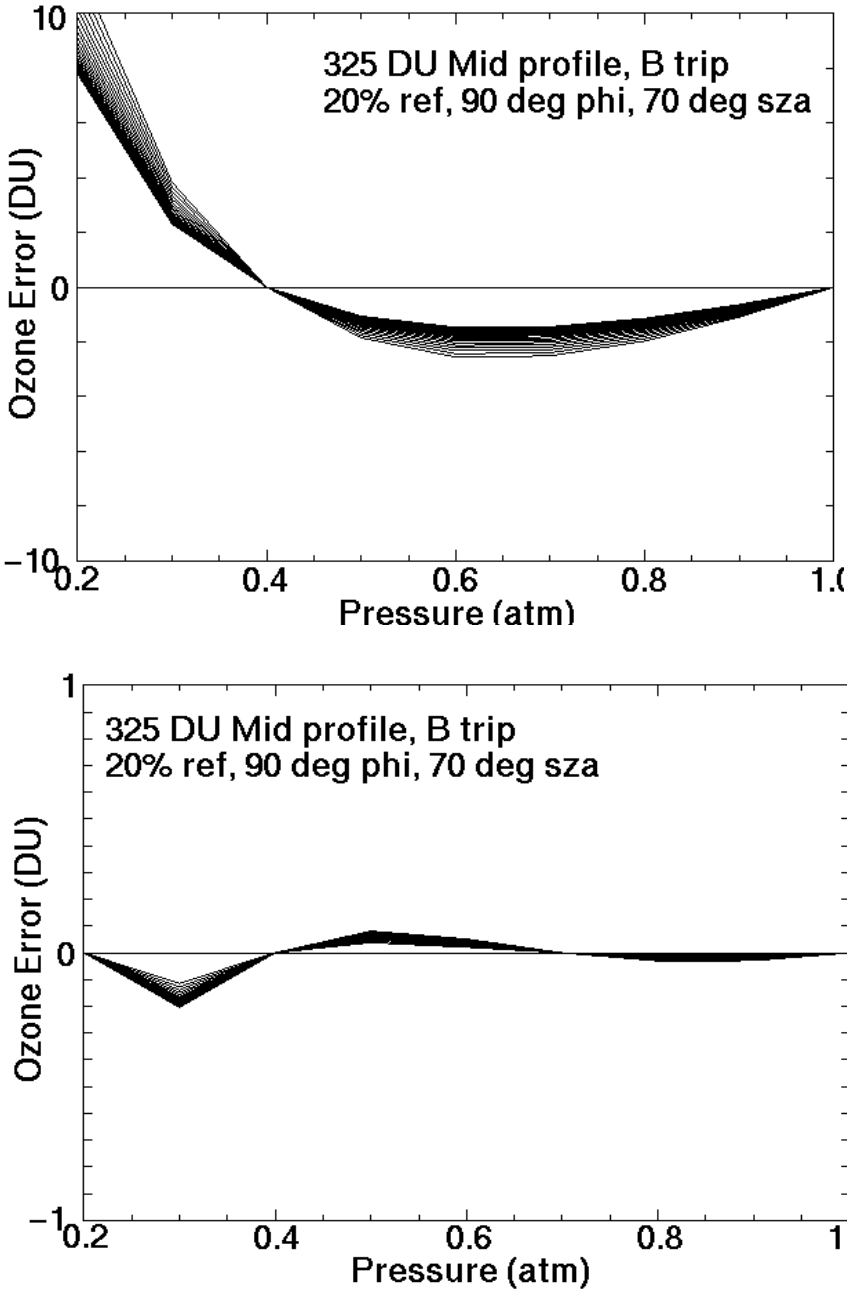

Figure 7.1-9. Ozone error in DU using the TOMS pressure node points (TOP) and the new OMPS pressure node points (BOTTOM). Note the difference in the vertical scales.

Non-Homogeneous Scene (Snow/Ice/Cloud Cover). The UV reflectivity of a clear scene with snow is similar to that of a partly cloudy scene with no snow (Klenk et al., 1982). The heritage algorithm uses a monthly snow/ice climatology (1x1 degree latitude-longitude grid) based on probabilities from the Air Force Global Weather Center to determine whether there is snow or ice in a high reflectivity scene. If the probability is > 50%, the assumption is that snow or ice is present. Then it assumes that cloud and ground contribute equally (if the measured radiance is greater than the radiance calculated for cloudy conditions) (McPeters et al., 1996). This assumption represents a fractional area accuracy of 1 (i.e., the scene may have from 100% to 0% cloud cover). Calculations show that, for a fractional area accuracy of 1, the heritage total column uncertainty is 6 DU (2% for a nominal 300 DU total column). Heuristically, for the 0.1 fractional area accuracy threshold of the cloud cover EDR, the ozone column accuracy allocation is 0.2%.

Ozone Profile Shape Errors. The uncertainty due to assumed ozone profile shape reaches 1% at 80 SZA (Wellemeyer et al., 1997). We allocate improved performance (0.5%) through the use of measured profiles from limb and nadir in place of the climatology used in previous retrievals from other instruments.

Multiple Scattering. Klenk et al. (1982) report <0.2% error in multiple scattering using six iterations of Dave's auxiliary equation solution to the radiative transfer equation.

Ring Effect Correction. We allocate a 0.2% systematic error based on the following considerations.

TOMS V7 makes a Ring effect (rotational Raman scattering) correction based on the work of Joiner et al. (1995). The following angular assumptions are made: SZA = 45 deg, scan angle = 0. Dependences on solar and scan angles are neglected but are small under most conditions (a major exception is SZA > 80 deg). Corrections are calculated for two boundaries: surface (1 atm, R = 0.08) and cloud (0.4 atm, R = 0.8). The magnitude of the correction is <1%. The two N7 TOMS wavelengths most sensitive (~–0.9% radiance correction at 1 atm, R = 0.08) are 317.35 nm and 359.88 nm. We have not selected 360 nm as an ozone insensitive wavelength for OMPS, but we have included 317 nm in our set of ozone sensitive wavelengths for the purpose of measuring our sensitivity to the Ring effect, as described below. The correction is 0.27% for 312.34 nm, which is close to our 312.5 nm baselined wavelength for ozone retrievals.

We have included this correction in our baseline total column retrieval algorithm. Accuracy concerns are twofold: wavelength errors and the incomplete angular modeling described above. C. Wellemeyer selected triplet wavelengths for the operational retrievals that are insensitive to temperature and minimize sensitivity to Raman scattering. He also selected some triplets that are particularly sensitive to Raman scattering. Retrievals using the sensitive and insensitive wavelengths were compared not only to estimate the magnitude of the error but also to provide an additional correction. A talk by J. Joiner at NASA Code 916 in 1994 showed that wavelengths that are insensitive to Raman scattering are also insensitive to the angular dependence of radiance error.

7.2 Long Term Stability

Without retrospective processing, the long term stability of the total column ozone depends on the schedule of on-orbit solar calibrations and the expected optical degradation of the solar diffusers. This section contains a discussion of the planned calibration operations and the anticipated change in diffuser reflectances and its effect on retrieval algorithms.

Operational Calibration Approach. Our recommended SDR algorithms rely on the current TOMS calibration approach for operational processing (see ICSR E8092402). In this approach, calibration data are analyzed automatically on a regular basis, but the implied changes are not immediately applied to the radiance data. This follows from our discussion above concerning the uncertainty of individual solar measurements.

In order to obtain sensor calibrations for operational processing, the TOMS solar measurements (and the OMPS measurements) are fit to a low order polynomial and extrapolated for a short period. This regression is updated as new solar data is obtained. An estimate of the true calibration for the TOMS is shown in **Figure 7.2-1**. The resulting TOMS Earth Probe operational calibration is shown in **Figure 7.2-2**. For an operating OMPS, a plot or plots analogous to Figure 7.2-2 will exist for each spatial channel. The TOMS predicted values in Figure 7.2-2 have a standard deviation about an estimate of the true calibration of about 0.2 DU. The implication is that the predicted calibration introduced less ozone error than a calibration based on the most recent solar measurement (0.3 DU). The prediction error is a function of the amount of solar data included in the regression. We simulated the operational calibration of TOMS using 4 regression periods for the data in Figure 7.2-1. The results, shown in **Figure 7.2-3**, indicate that an optimum regression interval exists for a given set of data. This is the result of a trade between following changes in sensor throughput and not following individual solar measurements. TOMS does not currently use the optimum interval.

Anticipated Diffuser Changes. Our estimates of diffuser reflectance changes are based on observations of TOMS and SBUV (including SBUV/2) diffuser reflectances. A discussion of these observations can be found in Jaross et al. (1998b). The primary mechanism for reflectance decreases appears to be photo-deposition of outgassed contaminants. There is no evidence for significant degradation of either a stowed or exposed diffuser surface in the absence of UV radiation. The diffuser degradation rate is therefore a function of the solar measurement frequency. There is some evidence that initial rates depend on the diffuser material (Hilsenrath, 1994), but in the long term contaminants and UV exposure appear to be the dominant parameters (Hall, 1994).

Degradation rates observed on TOMS, SBUV and SBUV/2 instruments have differed by as much as a factor of 30. The underlying causes of these differences are not completely understood, and may be related to conditions on the individual spacecrafts. We base our assumptions concerning OMPS diffuser degradation on the results from TOMS/ADEOS, the sensor with the greatest diffuser degradation rate. The multi-diffuser monitoring system on that instrument indicated rates with equivalent exponential time constants of 500 hr at 360 nm and 300 hr.at 309 nm. Assuming weekly solar measurements each with an equivalent solar exposure of 0.05 hr, the reflectance of the OMPS Working surfaces will have decreased by about 3.5% at 360 nm after 7 years. Semi-annual use of the Reference diffuser will result in less than 0.2% reflectance change.

Thus far we have ignored the sensitivity of ozone retrieval to the calibration changes caused by diffuser degradation. In Section 1 the A triplet combination of wavelengths was used to show the connection between wavelength dependent calibration changes and ozone errors for the Nadir sensor. The same wavelength combination can be used to look at diffuser degradation. In fact, the TOMS triplet approach was developed primarily to deal with diffuser degradation. Triplets are insensitive to changes (sensor or diffuser) which occur as a linear function of wavelength. As **Figure 7.2-4** demonstrates, the wavelength dependence of BUV diffuser reflectance time constants has been nearly linear for wavelengths longer than 300 nm. This spectral relationship holds for moderate degradation (<10%). **Figure 7.2-5** contains a plot of the A triplet degradation of the TOMS Earth Probe Working diffuser. There is no statistically significant change in the Working/Reference ratio after over 5 hours of Working exposure. This is nearly 1/3 the total anticipated exposure for the OMPS Nadir Working diffuser. Consequently, we expect diffuser degradation that is moderate and, at worst, linear in wavelength and time.

In the preceding discussions we have assumed that any Reference diffuser degradation represents a calibration error. This is not necessarily the case. Any degradation of this surface will be linear in exposure time. Using the relationship between degradation and exposure established through use of the Working diffuser, a correction can be derived for the Reference diffuser as well. In the unlikely event that we have underestimated diffuser degradation rates, we can apply such a correction. Such a correction is not expected to be necessary given the long-term stability requirements, retrieval algorithms, and estimated diffuser changes.

Summary. We present results from TOMS Earth Probe to show the anticipated uncertainty in individual solar measurements. We do not expect short-term sensor variations to exceed this uncertainty, so calibrations more frequently than once per week are unnecessary. More frequent measurements also increase uncertainties caused by diffuser degradation. Less frequent calibrations remain a possibility if observed rates of sensor change are smaller than observed on TOMS, SBUV and SBUV/2.

Our operational calibration approach involves a regression of the latest solar measurements. The sensor calibration used in the ozone retrievals is based on extrapolating the regression results for a short period. We demonstrated that the calibration error in such an extrapolation is less than using true solar measurements, provided the regression is optimized.

Sensor calibration is based on solar measurements using the Working diffuser. Our baseline schedule for Working measurements means this diffuser will degrade. The Reference diffuser is employed to monitor changes in the Working diffuser through periodic comparison of the two sets of measurements. The Reference measurement frequency is ultimately determined by the lifetime of the sensor and the uncertainty in the comparison between Working and Reference measurements. We will apply regressions to the Working/Reference measurement ratios in order to determine the correction required for working diffuser degradation. Since the uncertainty in this correction will decrease with time, the Reference deployment frequency can also decrease as the mission progresses. Semi-annual Reference deployments will be adequate to meet long-term stability requirements on the nadir sensor.

We base estimates of OMPS diffuser degradation on worst-case observations of TOMS, SBUV and SBUV/2 diffuser degradation. We predict that an OMPS Working diffuser could degrade by as much as 3.5% at 360 nm for a 7 year mission. Rates will be greater at shorter wavelengths, and smaller in the visible. Reference diffuser degradation will be 20-30 times less. At these moderate degradation levels, reflectance changes are nearly linear in wavelength. The retrieval algorithms for both Nadir and Limb sensors are relatively insensitive to such changes, so corrections for diffuser degradation, if any, will be infrequent and minimal.

Based on this analysis, the allocations for long term stability are 0.15% for wavelength-independent errors and 0.25% for wavelength-dependent errors (Figure 7.1-2), sufficient to meet the 1% long term stability requirement. These allocations assume weekly working diffuser and semi-annual reference diffuser deployments for seven years. A reduced uncertainty can be achieved by increasing the frequency of the reference diffuser deployment.

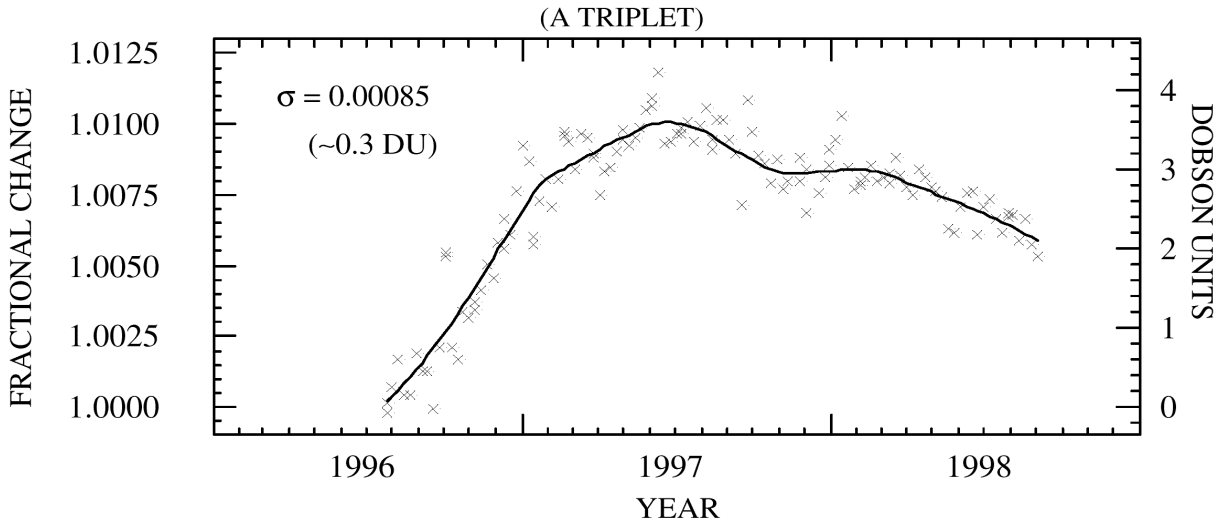

Figure 7.2-1. A plot of TOMS Earth Probe Working diffuser solar signal (corrected for goniometry and sun/earth distance) is shown for the A triplet combination of wavelengths (313nm, 331nm, 360 nm). A smooth fit indicates an estimate of the true instrument calibration. The standard deviation about the fit is translated into an ozone uncertainty of ~0.3 DU via the A triplet sensitivity of 0.3%/DU.

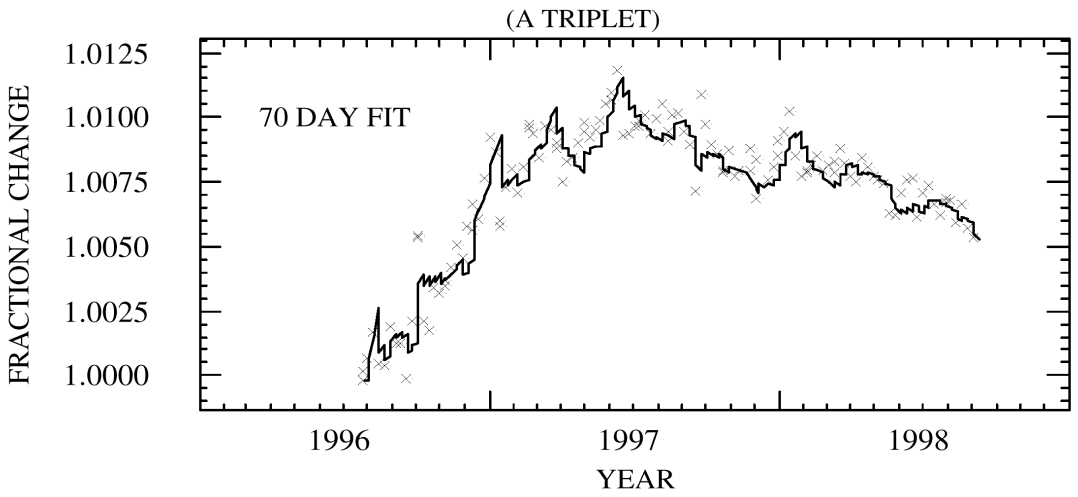

Figure 7.2-2. The TOMS Earth Probe operational calibration for the A triplet is shown superimposed over the solar data. Predicted calibrations for 1 week into the future are determined from a 1st order regression of the previous 10 Working diffuser measurements

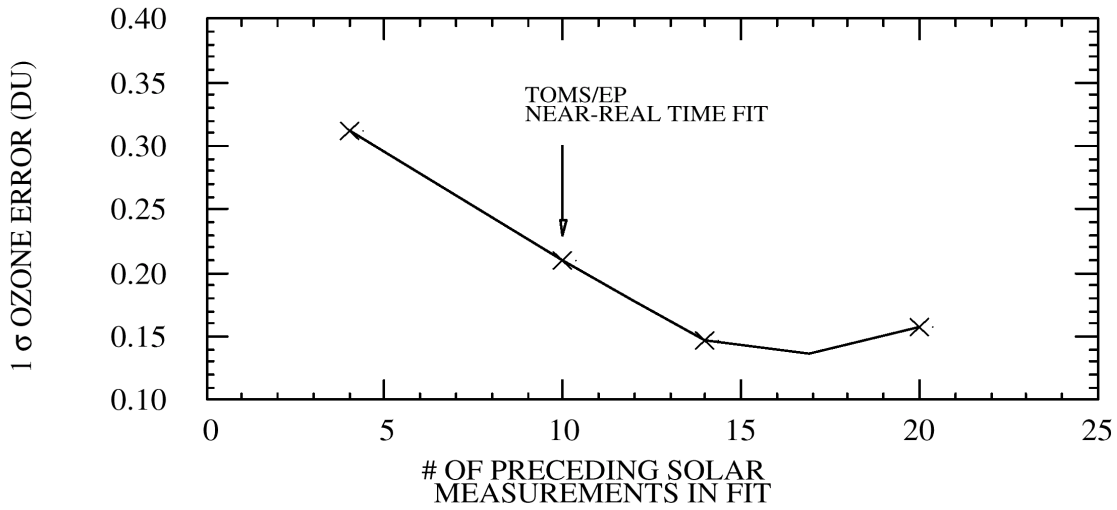

Figure 7.2-3. The standard deviation of predicted calibrations (translated into column ozone) about the "true" sensor calibration of Figure 7.2-2 is shown. The variance depends on the amount of solar data included in the regression. The plot indicates that an optimum data selection exists for a given sensor. This optimum period will depend on the specific sensor response and the solar measurement uncertainty.

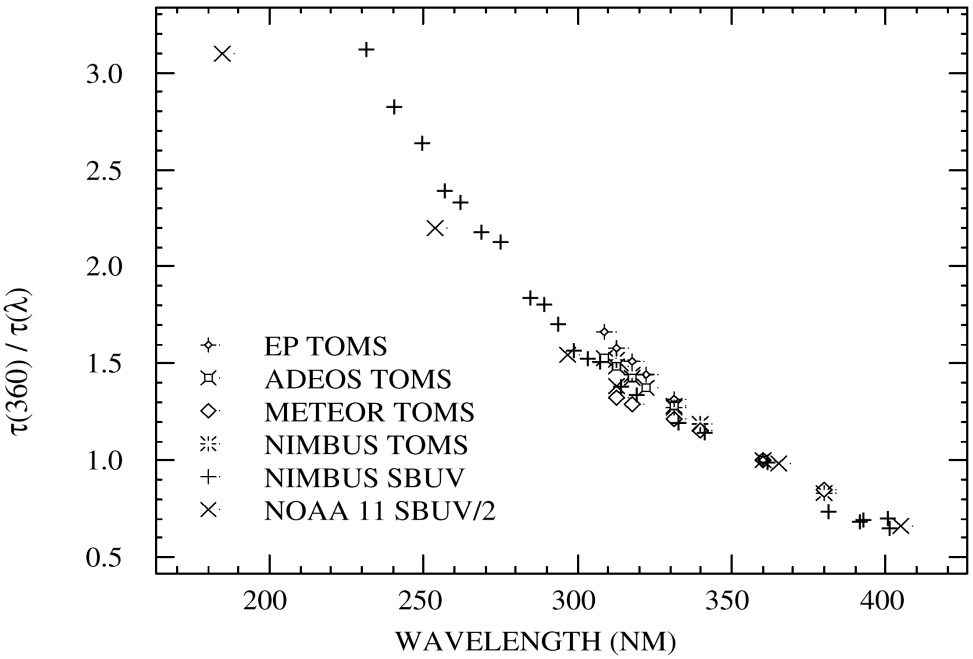

Figure 7.2-4. This figure contains the diffuser degradation rates (1/time constant) for several TOMS and SBUV instruments plotted as a function of wavelength. The data, which have been normalized to the time constant at 360 nm, demonstrate the similarity in spectral dependence of diffuser degradation in the UV. The data also show that this dependence is nearly linear for wavelengths longer than 300 nm.

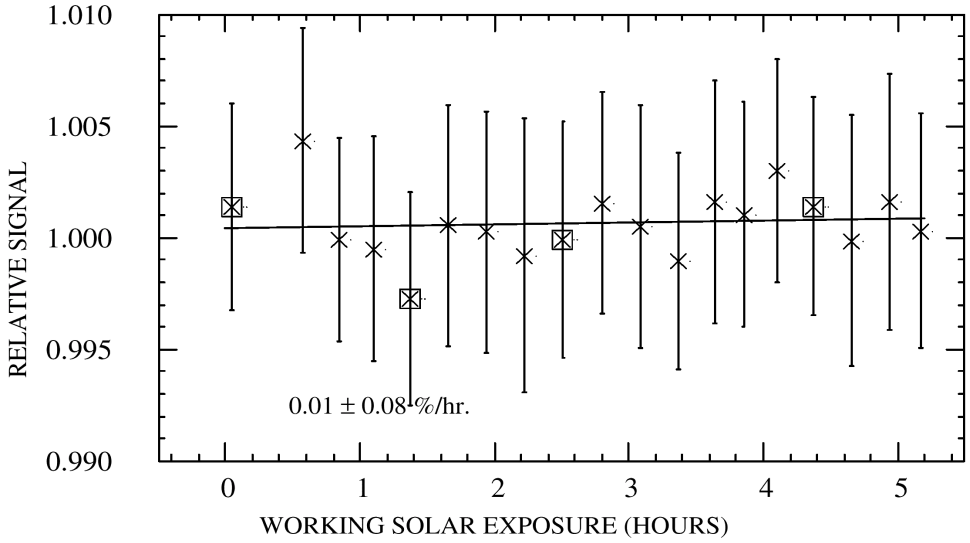

Figure 7.2-5. The TOMS Earth Probe Working/Reference solar measurement ratio is plotted for the A triplet combination (313 nm, 331 nm, 360 nm) of wavelengths as a function of Working diffuser exposure. Error bars are ±1σ. A 1st order regression applied to the data indicate that no statistically significant change has occurred in the Working diffuser (relative to the Reference) for the A triplet combination. Boxed points indicate data that would result from a semi-annual Reference deployment frequency (TOMS/EP Reference measurements occurred every 5 weeks).

7.3 System Precision

The allocated precision performance is shown in **Figure 7.3-1**. The assured performance is to the allocation including margin. We assure precision performance at or better than threshold, depending on the measured total column amount. As with accuracy, total column precision applies to a global ensemble of measurements having the same total column amount (IPO ICSR 3999, 29 Jan 99). Therefore, this allocation applies to a global ensemble.

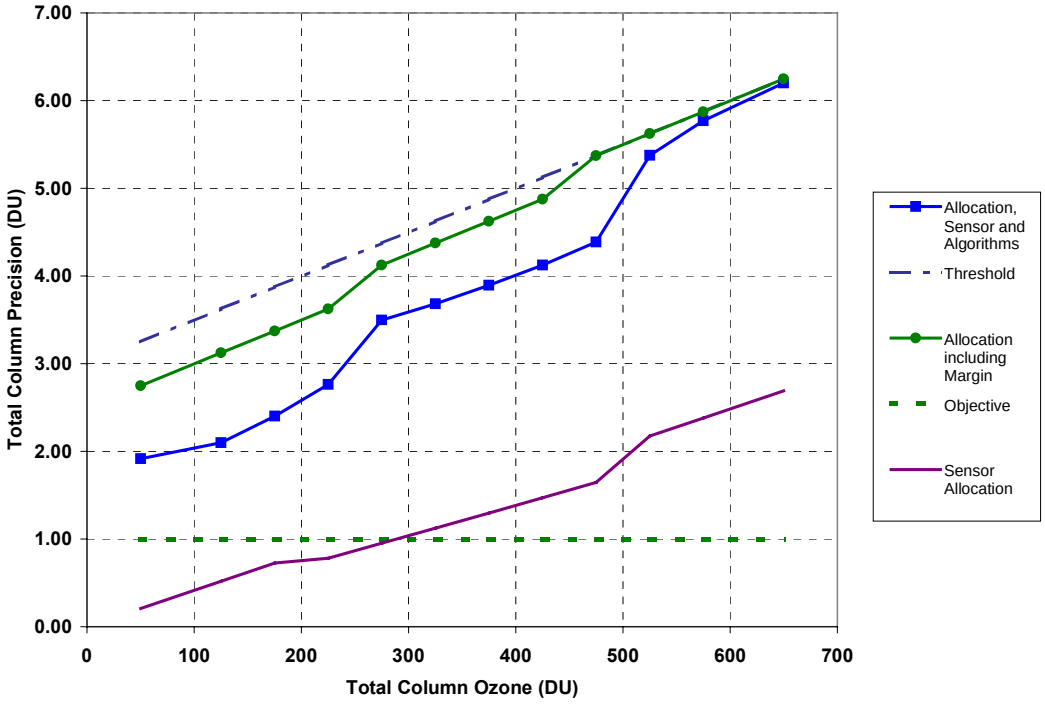

Figure 7.3-1. Allocated precision of total ozone retrievals over the required measurement range of total column values. The allocated performance (including margin) is: 2.5 DU + 0.5%, Ω ≤ 250 DU; 2.75 DU + 0.5%, 250 < Ω ≤ 450 DU; 3 DU + 0.5%, 450 DU < Ω.

Section 7.3.1 describes the allocations to sensor noise. Section 7.3.2 describes the allocations to algorithm precision errors. Section 7.3.3 describes how the global ensemble is estimated.

7.3.1 Sensor Precision Errors

The sensor uncertainties contributing to precision errors are just due to the signal to noise ratios of the wavelength channels used in the retrieval. Improving the signal-to-noise ratio (SNR) of the sensor can reduce the effect of sensor noise. The precision error due to random noise in the earth radiances and solar irradiances observed by the spectrometer is derived from equation (21) of McPeters et al. (1996):

$$\frac{\sigma_\Omega}{\Omega} = \sqrt{\frac{(\lambda_2-\lambda_3)^2 e_1^{\,2} + (\lambda_1-\lambda_3)^2 e_2^{\,2}}{\left[(\lambda_2-\lambda_3)s_1 - (\lambda_1-\lambda_3)s_2\right]^2}} \tag{114}$$

where e_n is the normalized standard deviation of the albedo random noise:

$$e_n^2 = \left(\frac{\sigma_A}{A}\right)^2 = \left(\frac{\sigma_I}{I}\right)^2 + \left(\frac{\sigma_F}{F}\right)^2 \quad (115)$$

and s_n is the sensitivity at wavelength n to ozone (percent albedo per percent ozone).

We have allocated SNR = 1000 for radiance and for irradiance noise due to the sensor. **Figure 7.3-2** shows the sensitivity to SNR = 1000 for a wide range of cases. The solid curves represent bright cases (low ozone, cloudy scene) while the dashed curves represent dark cases (high ozone, clear scene). Based on these results, the allocations are 0.20% for 0 < SZA < 60 deg, 0.25% for 60 < SZA < 70 deg, and 0.33% for 70 < SZA < 80 deg.

Irradiance noise is dominated by goniometric errors associated with the solar diffuser. The noise is reduced (yielding SNRs of 1000) by 1 week extrapolations based on the previous 10 weekly calibrations, as shown in Figures 3.1-3 and 7.2-2.

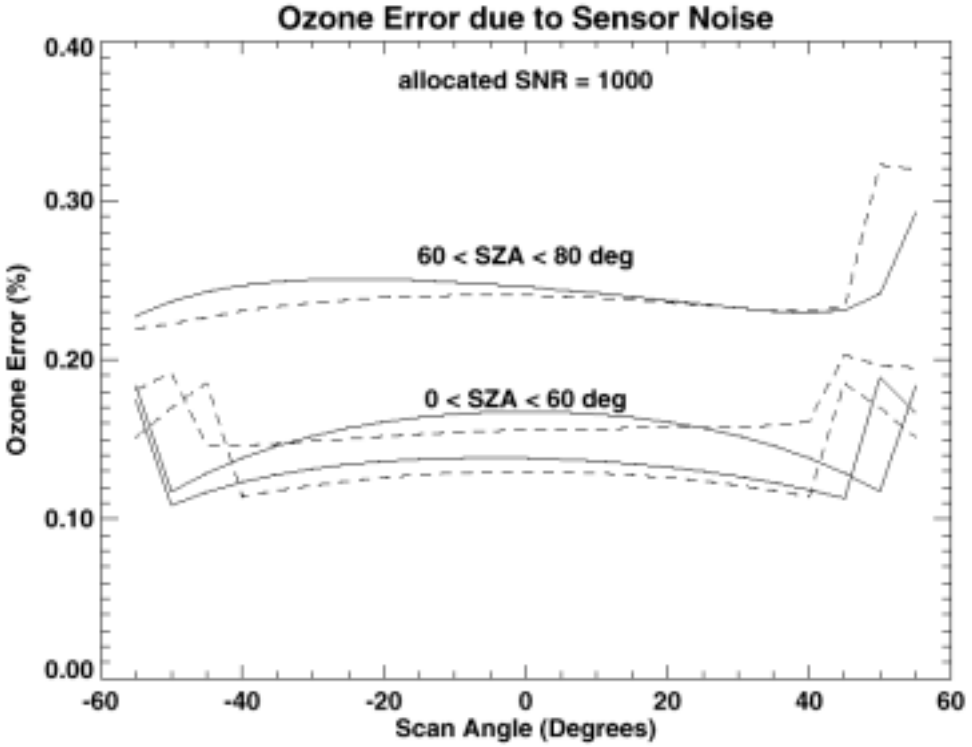

Figure 7.3-2. Ozone error due to sensor SNR = 1000 for a wide range of scenes. The solid curves represent bright cases (low ozone, cloudy scene) while the dashed curves represent dark cases (high ozone, clear scene). The curves for 0 < SZA < 60 deg include two cases for low SZA and two cases for moderate SZA. The cases for low SZA are Ω = 300 DU, R = 0 and Ω = 200 DU, R = 1. The cases for moderate SZA are Ω = 450 DU, R = 0.2 and Ω = 200 DU, R = 1. The two curves for 60 < SZA < 80 deg represent Ω = 75 DU, R = 1 and Ω = 650 DU, R = 0. Clearly, the cases for SZA < 60 deg are similar. The cases for higher SZAs show larger errors, with the error largest for edge of scan (SZA = 80 deg).

7.3.2 Algorithm Precision Allocations

Ozone Absorption Coefficients, Temperature Dependence. In the SBUV and TOMS heritage algorithms, the variation of the actual temperature profile about the climatological profiles used in the forward model causes a precision error. Fleig et al. (1990) and McPeters et al. (1996) give it as 1%. For the OMPS baseline design, the allocation for this error is based on the selection of temperature-insensitive wavelengths (Section 2.4.10) and the use of the external atmospheric vertical temperature profile (AVTP) EDR from CrIS. We allocate constant 0.5 DU error for both precision and accuracy based on assumed 10K temperature variation simulations shown in **Figure 7.3-3**. The largest error in DU is for 425 DU at low SZAs (0.4 DU), so this constant allocation should account for the required measurement range (50-650 DU) and horizontal coverage (SZA < 80 deg).

Cloud Top/Surface Pressure. In general, a terrain pressure database is sufficient for our uses. However, surface pressure can vary by more than 100 mb from ambient. Since such a deviation corresponds to a 0.3% total column ozone error (significant in the context of a 3 DU + 0.5% threshold), we baseline the use of the pressure profile EDR (ICSR E7121806, 19 Dec 97). The precision threshold for this EDR is 4 mb, corresponding to ~0.01% error, so we allocate 0.05% ozone precision due to surface pressure for totally clear scenes.

For totally cloudy scenes, our allocations are based on simulation results shown in **Figure 7.3-4**. The uncertainty in the cloud top pressure (CTP) causes two errors that cancel to some degree but not entirely: the error in the ozone estimated to be beneath the cloud, and the error in the ozone measured above the cloud by the BUV technique. For example, if the algorithm places a cloud at a lower pressure than it actually is, the amount of ozone estimated beneath the cloud for the assumed CTP will be larger than it should be (independent of other errors in the estimate). At the same time, with the higher altitude, the algorithm expects less backscatter and hence less ozone absorption above the cloud to match the measured radiances than it should. The magnitude of the former error is larger than the latter.

The results in Figure 7.3-4 are for low, mid, and high latitude scenes, assuming clouds at 0.4 atm (>7 km) and a cloud top pressure precision of 30 mb. The effect on the reflectivity is included self-consistently. The most serious error was 0.7% for low-mid latitude ozone and 0.9% for high latitude ozone (both corresponding to high ozone amounts). The allocations are based on the use of the external CTP EDR. For the 25 mb threshold precision, the allocations are 0.6% and 0.75% for low-mid and high latitude ozone, respectively.

Cloud Fraction (Non-Homogeneous Scene). This allocation is driven by the case when there is snow or ice cover on the ground. Based on the same reasoning as the accuracy allocation, for the 0.15 fractional area precision threshold of the cloud cover EDR, the ozone column precision allocation is 0.3%.

Ozone Profile Shape Errors. As the SZA increases, the incident solar irradiance penetrates less into the atmosphere. Consequently, the sensitivity to the shape of the ozone profile increases. A correction technique based on profile climatology and total column radiances can achieve about

1% precision at 80 deg SZA, using the Nimbus 7 and Meteor TOMS wavelengths (Wellemeyer et al., 1997, Figure 5). We expect to improve this performance from 1% to 0.5% by using the ozone profile measured by our limb sensor. We allocate 0.5% for 70 < SZA < 80 deg, and 0.1% for lower SZAs.

Tropospheric Aerosol Correction. There are two sources of precision error in the aerosol correction. The first is due to sensor and algorithm noise. A unit of N value is equal to a 2.3% change in albedo (Torres et al., 1998). Consequently, for SNR = 1000, we expect the equivalent N value noise to be 0.14/2.3 = 0.06 N-value. The combined algorithm and sensor noise is about 0.1 N-value in the aerosol index. The algorithm error is probably associated with errors in the forward model. Based on **Figure 7.3-5**, this error is equivalent to about 0.1% ozone error.

The dominant source of error is due to the scatter of actual ozone error about the Torres or R_λ correction. Figure 7.3-5 (from Torres et al., 1998) shows the scatter due to different aerosol types, layer heights, and optical depths, and different relative azimuth angles and satellite zenith angles. The actual R_λ correction implemented in the OMPS algorithm, described in section 2.4.6, is more general. The quality of this correction, as shown in **Figure 7.3-6**, is consistent with the Torres aerosol correction. To account for the scatter as well as the noise effects, we allocate 0.5% precision for an aerosol-laden scene after the aerosol correction.

Tropospheric Ozone. The random error associated with tropospheric ozone has basically two causes: the variable sensitivity of the buv technique to tropospheric ozone and the natural variability of tropospheric ozone about the mean or climatology. In addition, the buv technique is totally insensitive to ozone under clouds, so the error is increased in the presence of clouds.

The precision allocation to tropospheric ozone is expressed as:

$$\Delta_{\sigma t} = (1-\varepsilon)\sigma_t \tag{116}$$

where ε is the fractional sensitivity of buv remote sensing to tropospheric ozone and σ_t is the natural variability of tropospheric ozone. For clear conditions, we use values of ε that are representative of the values calculated by Klenk et al. (1982) for different SZAs. Under cloudy conditions, $\varepsilon = 0$ for ozone below the cloud top.

We have estimated σ_t by finding the standard deviation of tropospheric ozone measured by balloon-borne ozonesondes at various stations around the world and organizing the measurements by tropopause pressure. The results of these regression analyses are shown in **Figure 7.3-7**. We use the tropospheric ozone amounts (in the lowest two Umkehr layers) from the TOMS standard profiles as the basis for these fractional amounts. (The tropospheric ozone correction method is described in section 2.4.8.)

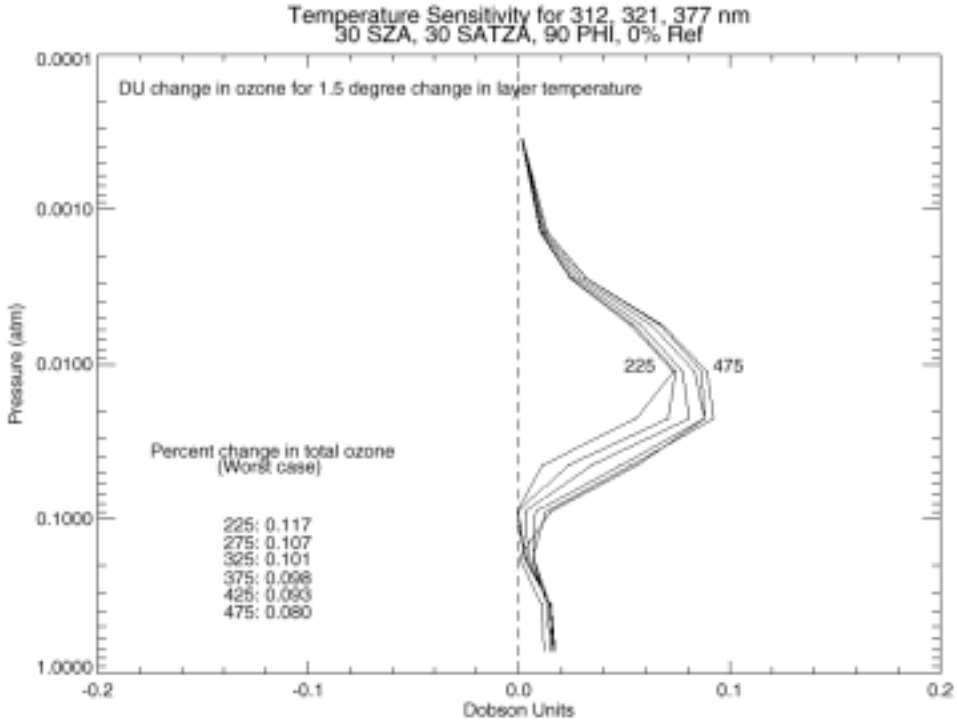

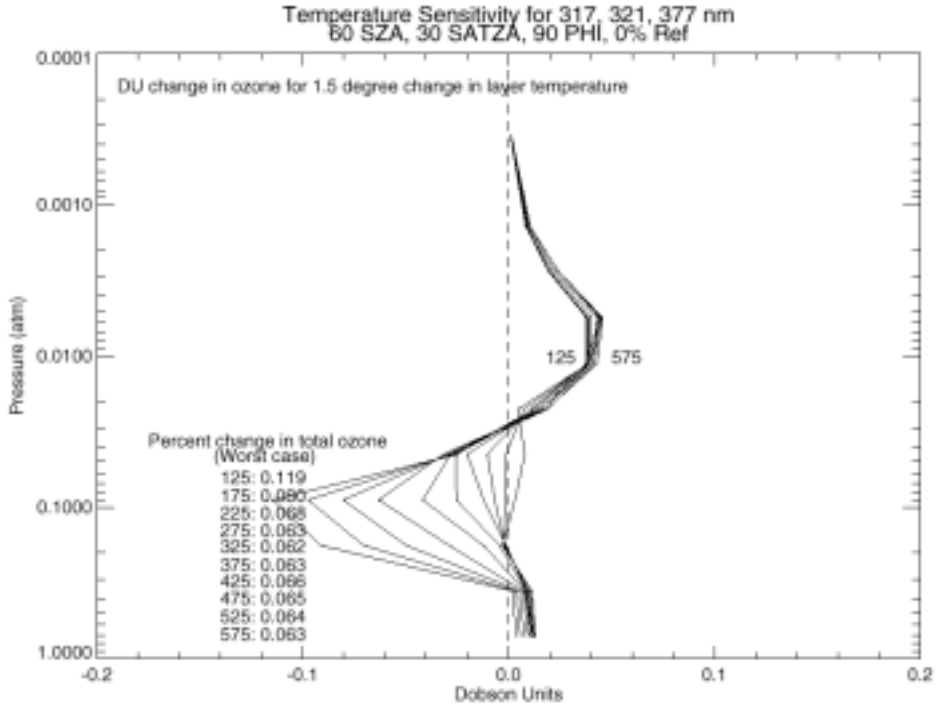

Figure 7.3-3 (a) and (b)

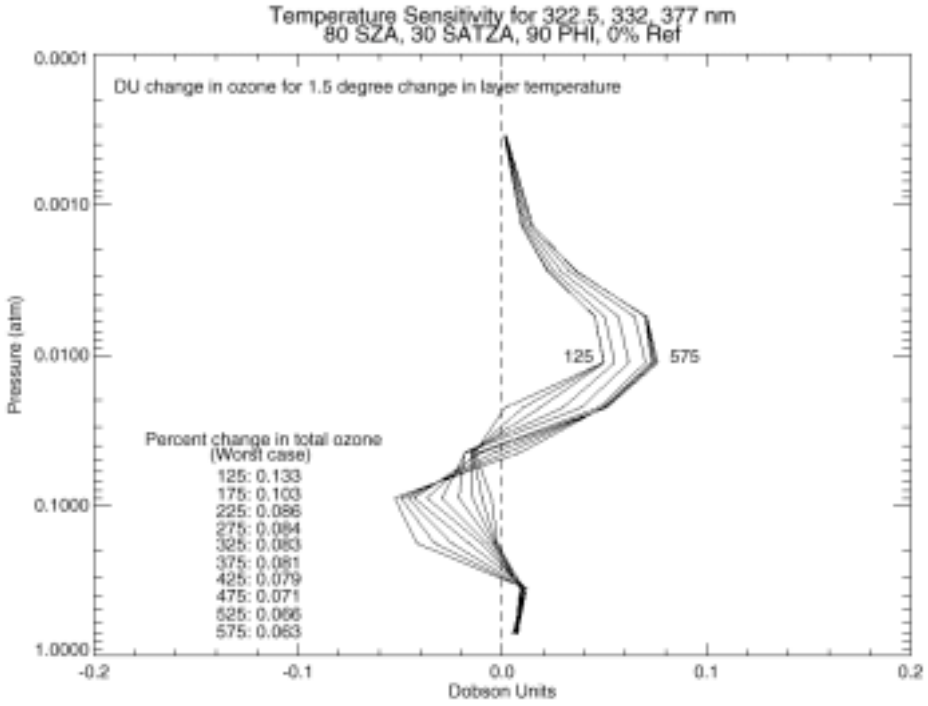

Figure 7.3-3. Ozone temperature sensitivity for (a) low, (b) mid, and (c) high solar zenith angles as a function of altitude for the TOMS standard ozone profiles. The total column error for a 1.5 K temperature precision is given in each figure in the lower left hand corner. The largest error in DU is for 425 DU at 30 deg SZA (0.4 DU). The allocations account for the 3.5 K temperature threshold above the 1 mb level.

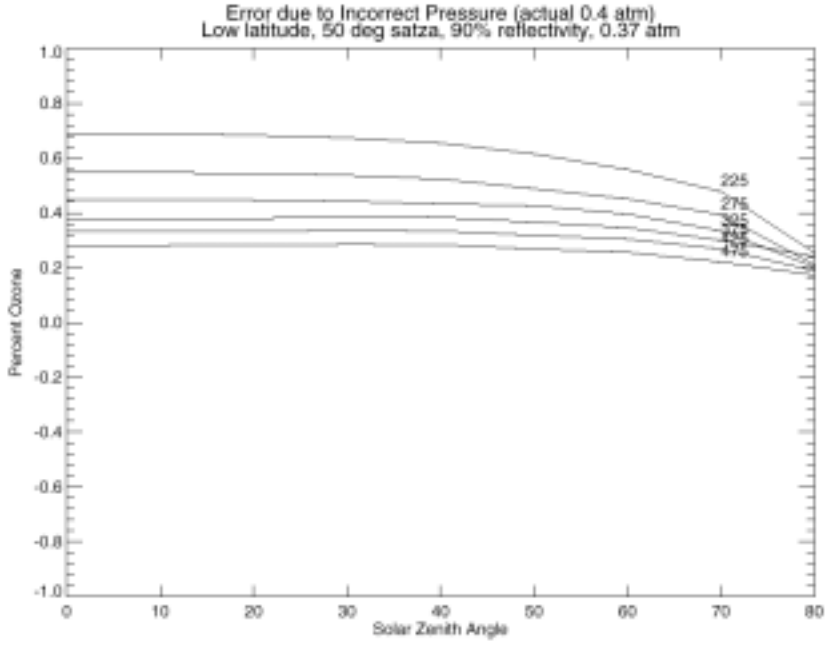

Figure 7.3-4 (a)

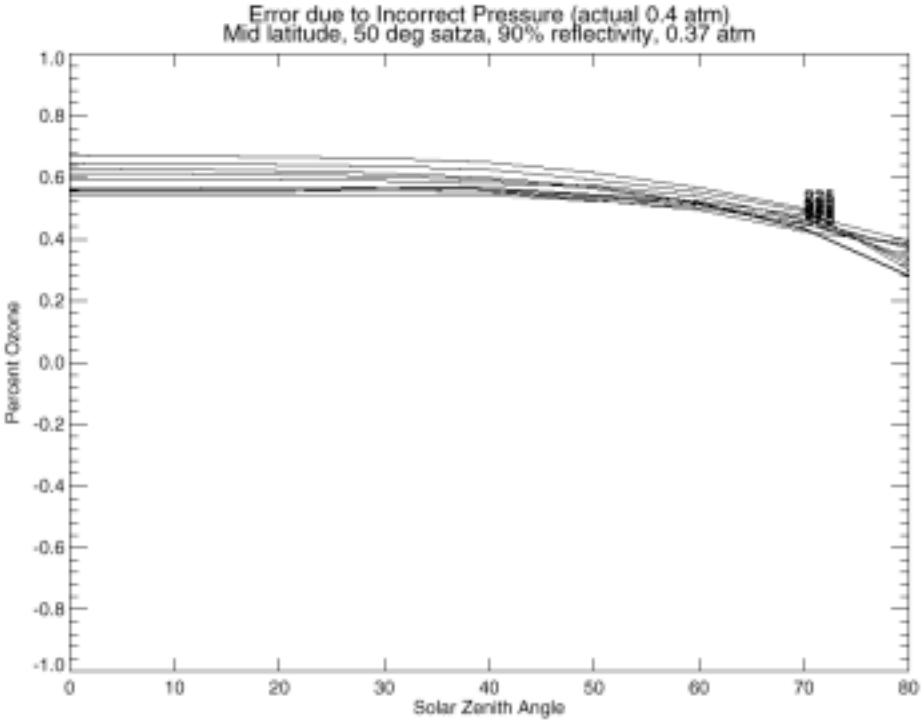

Figure 7.3-4 (b)

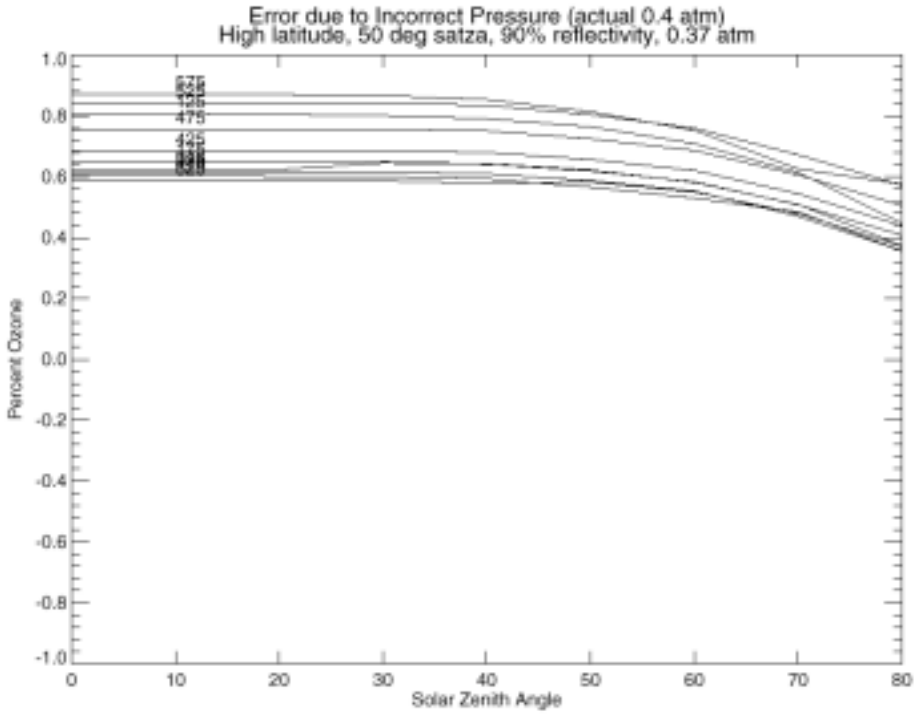

Figure 7.3-4. Error due to cloud top pressure error for (a) low, (b) mid, and (c) high latitude ozone. The curves are parametric in total column ozone in Dobson Units.

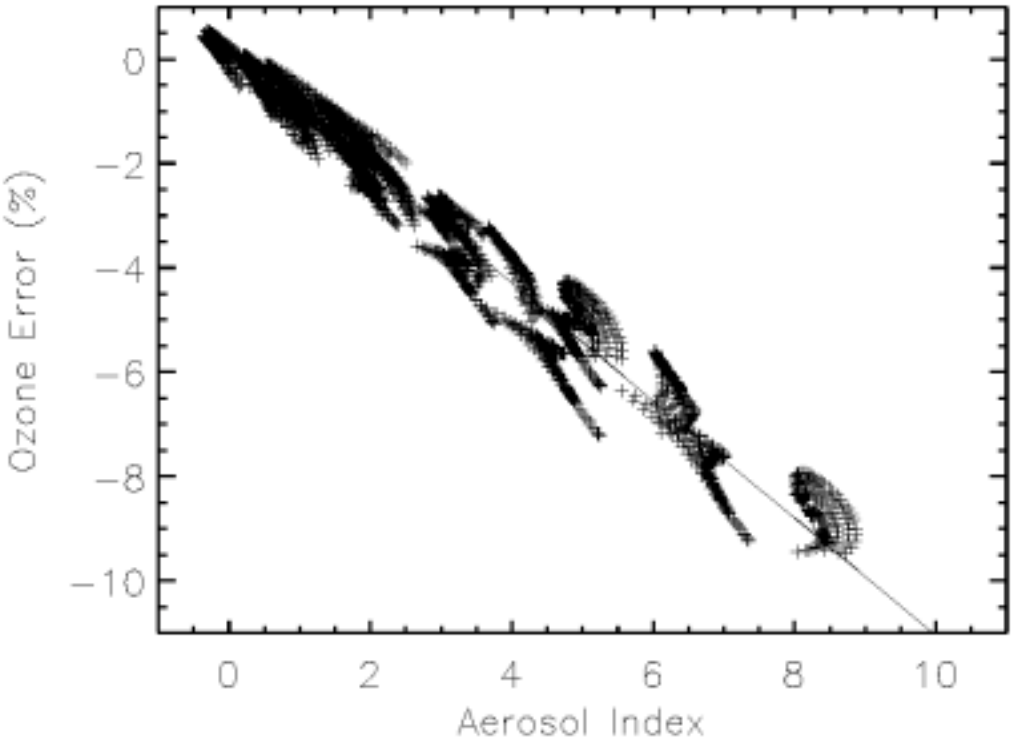

Figure 7.3-5. Systematic ozone error as a function of aerosol index and the linear ozone correction developed by Torres et al. (1998). [after Torres et al., 1998]

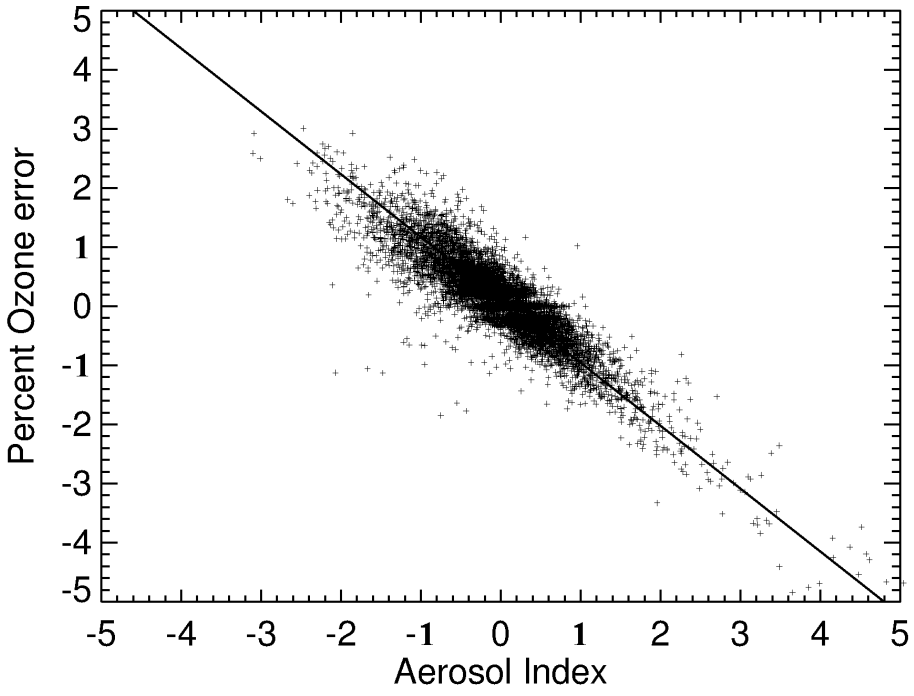

Figure 7.3-6. The OMPS R_λ correction applied to TOMS data from 10 Sep 81, showing results similar to the Torres correction

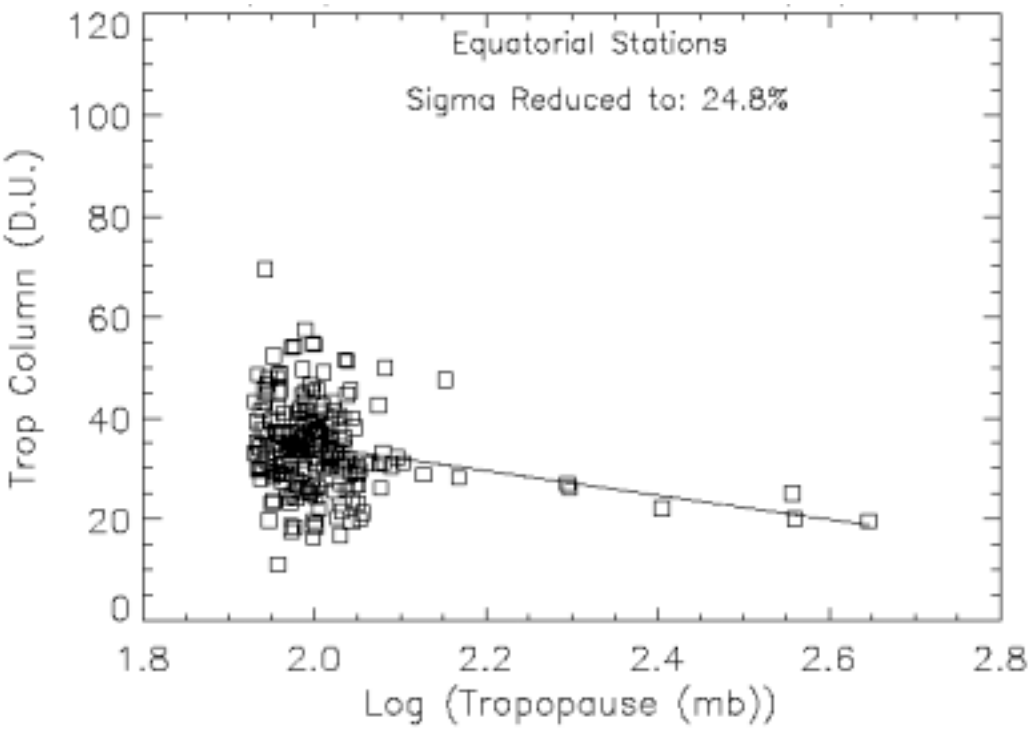

Figure 7.3-7 (a)

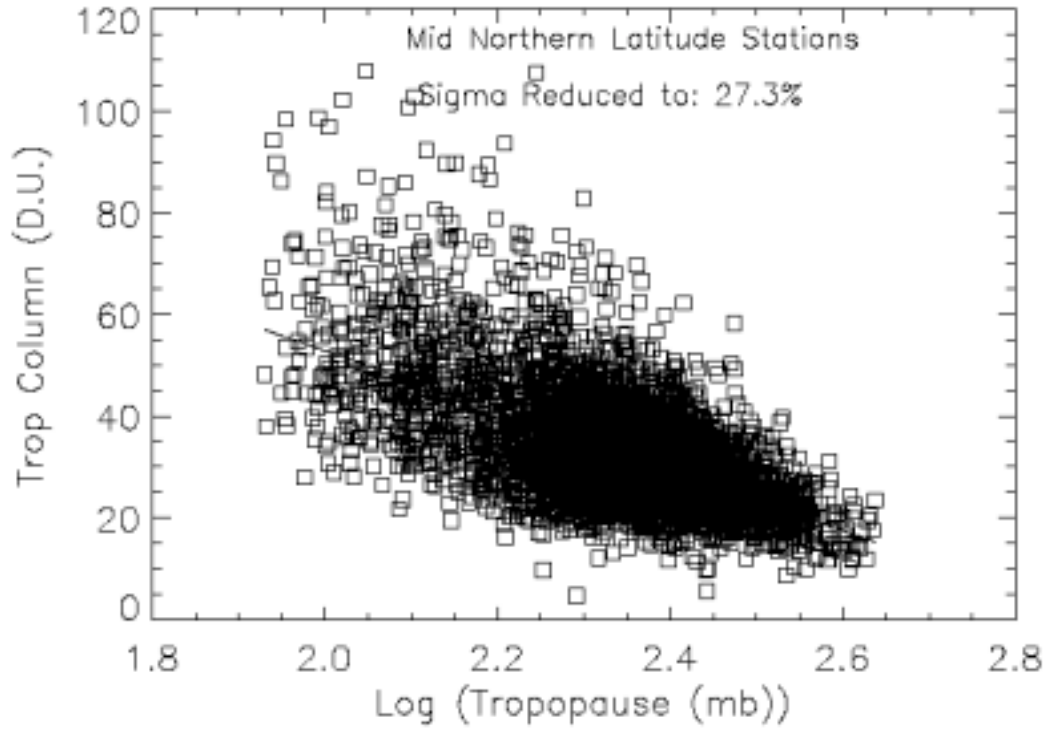

Figure 7.3-7 (b)

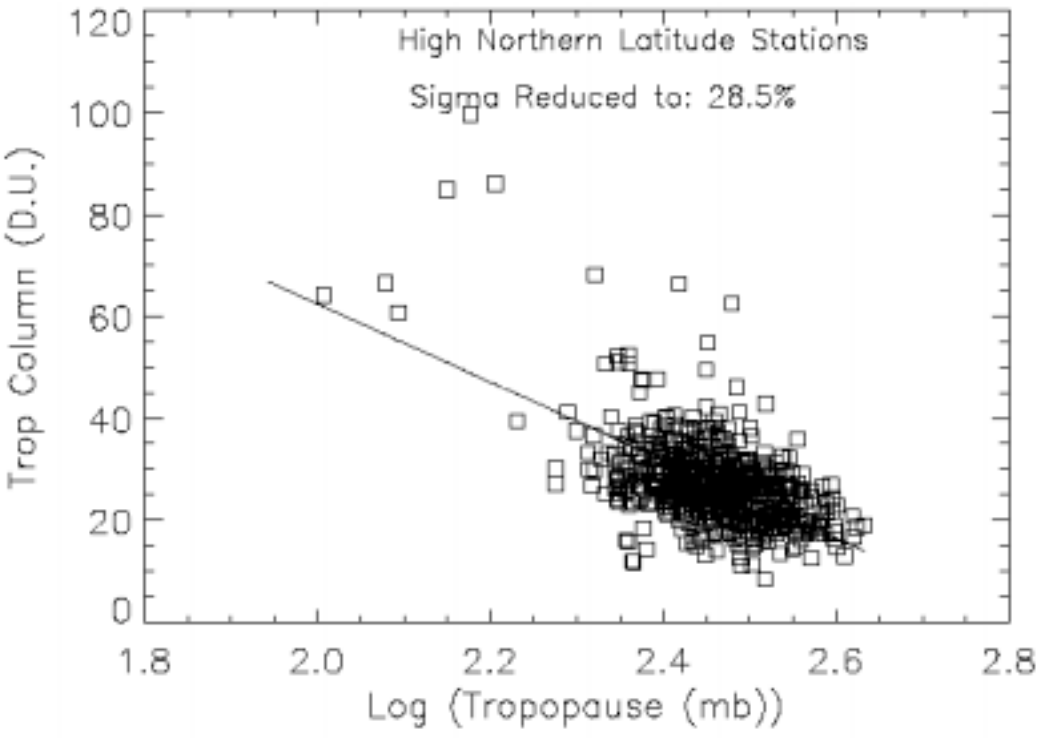

Figure 7.3-7. Tropospheric ozone column vs. tropopause pressure for (a) low, (b) mid, and (c) high latitude ozonesonde stations. At mid and high latitudes, organizing by tropopause pressure greatly reduces the variance in tropospheric ozone.

7.3.3 Global Distribution of Total Column Precision Errors

For allocation purposes, we estimate the precision of a global ensemble of total column retrievals (as a function of total column) based on a distribution of solar zenith angles and of cloud fraction.

The global allocations are calculated as follows. Given two ensembles of M and N elements with standard deviations σ_M and σ_N:

$$\sigma_M^2 = \frac{1}{M-1}\sum_{i=1}^{M}(x_i - \bar{x})^2 \tag{117}$$

$$\sigma_N^2 = \frac{1}{N-1}\sum_{j=1}^{N}(x_j - \bar{x})^2 \tag{118}$$

The variance of the combined ensembles can be estimated as

$$\sigma_{M+N}^2 = \frac{1}{M+N-1}\sum_{k=1}^{M+N}(x_k - \bar{x})^2 = \frac{1}{M+N-1}\sum_{k=1}^{M}(x_k - \bar{x})^2 + \frac{1}{M+N-1}\sum_{k=M+1}^{M+N}(x_k - \bar{x})^2 \tag{119}$$

$$= \frac{1}{M+N-1}\left[(M-1)\sigma_M^2 + (N-1)\sigma_N^2\right] \cong \frac{M}{M+N}\sigma_M^2 + \frac{N}{M+N}\sigma_N^2 \qquad (120)$$

This can be generalized to the combination of more than two ensembles. The individual standard deviations σ_N were derived in sections 7.3.1 and 7.3.2. How they are weighted in a global ensemble (i.e., the derivation of N/(M+N)) is derived as follows.

Global Allocations for Temperature Dependence, Cloud Fraction, and Tropospheric Aerosols. The temperature dependence and cloud fraction error are assumed to be the same under all conditions.

Based on results by Herman et al. (1997), tropospheric aerosols are assumed to cover 10% of the Earth's surface. This corresponds to peak conditions of tropospheric aerosol coverage.

Global Allocations for Sensor Noise and Profile Shape. The distribution of solar zenith angles is based on what would be observed on average along a 0930 orbit. Geographic latitudes are mapped to solar zenith angles based on this local time. The latitude divisions correspond to the profile mixing regimes of the total column algorithm. Ozone amounts are weighted by latitude. This permits an appropriate distribution of ozone column amounts (i.e., 50 and 650 DU total columns are not observed at low latitudes).

	L (lat < 15)	L/M (15 < lat < 45)	M/H (45 < lat < 75)	H (75 < lat)
	SZA < 60		60 < SZA	
125 - 175	0	0	0.75	0.25
225 - 475	0.1875	0.375	0.375	0.0625
525 - 575	0	0	0.75	0.25

This distribution is used to allocate errors based on solar zenith angle (sensor noise and ozone profile). The matrix on the left are the allocations derived in sections 7.3.1 and 7.3.2, and the matrix on the right are the global allocations.

		SZA < 60	60 < SZA < 70	70 < SZA < 80
Sensor	Radiance SNR	0.20%	0.25%	0.33%
	Solar Calibration	0.20%	0.25%	0.33%
	Ozone profile	0.10%	0.10%	0.50%

125 - 175	225 - 475	525 - 575
0.29%	**0.24%**	**0.29%**
0.29%	**0.24%**	**0.29%**
0.36%	**0.25%**	**0.36%**

Global Allocations for Cloud Top / Surface Pressure and Tropospheric Ozone. Based on all Nimbus 7 TOMS data from 1990 data, the distribution of cloud fraction amounts is:

Cloud Fraction	Percent of Measurements
clfrac = 0.0	13
0.0 < clfrac <= 0.2	40
0.2 < clfrac <= 0.4	18
0.4 < clfrac <= 0.6	12
0.6 < clfrac <= 0.8	9
0.8 < clfrac < 1.0	5
clfrac = 1.0	3

A plot of these results is shown in Figure 8.4-4. Similar results were derived from 1988 data.

The global cloud top / surface pressure allocation is calculated based on this distribution of cloud fraction and the errors derived in section 7.3.2 by simulation.

	Cloud Fraction							
	0	0.0 < f <= 0.2	0.2 < f <= 0.4	0.4 < f <= 0.6	0.6 < f <= 0.8	0.8 < f < 1.0	f = 1.0	
CF	0	0.1	0.3	0.5	0.7	0.9	1	**All**
prob.	0.13	0.4	0.18	0.12	0.09	0.05	0.03	**1**
125 - 175	0.05%	0.23%	0.38%	0.49%	0.58%	0.66%	0.70%	**0.38%**
225 - 475	0.05%	0.21%	0.35%	0.45%	0.54%	0.61%	0.64%	**0.35%**
525 - 575	0.05%	0.23%	0.38%	0.49%	0.58%	0.66%	0.70%	**0.38%**

Because the efficiency of the buv technique in detecting tropospheric ozone goes to zero when the ozone is under clouds, the tropospheric ozone allocations are weighted in the same way as the cloud top / surface pressure. The basic allocations in the second and third column are derived as described in section 7.3.2.

Tropospheric Ozone			Cloud Fraction							
	clear	cloudy	0	0.0 < f <= 0.2	0.2 < f <= 0.4	0.4 < f <= 0.6	0.6 < f <= 0.8	0.8 < f < 1.0	f = 1.0	All
125	1.53	2.35	1.53	1.64	1.82	1.99	2.14	2.28	2.35	**1.81**
175	1.66	2.53	1.66	1.77	1.96	2.14	2.30	2.45	2.53	**1.95**
225	1.74	3.27	1.74	1.94	2.31	2.62	2.90	3.15	3.27	**2.29**
275	2.30	4.17	2.30	2.55	2.99	3.37	3.71	4.02	4.17	**2.97**
325	2.33	4.17	2.33	2.57	3.00	3.37	3.71	4.02	4.17	**2.98**
375	2.36	4.17	2.36	2.60	3.02	3.39	3.72	4.03	4.17	**3.01**
425	2.41	4.18	2.41	2.64	3.05	3.41	3.73	4.03	4.18	**3.04**
475	2.50	4.18	2.50	2.72	3.10	3.45	3.76	4.05	4.18	**3.09**
525	3.37	4.22	3.37	3.46	3.64	3.82	3.98	4.14	4.22	**3.64**
575	3.62	4.24	3.62	3.69	3.82	3.94	4.06	4.18	4.24	**3.81**

Based on these weightings, the global sensor and algorithm allocations, in Dobson Units, are:

All Cases	50	125	175	225	275	325	375	425	475	525	575	650
Radiance SNR	0.15	0.37	0.51	0.55	0.67	0.80	0.92	1.04	1.16	1.54	1.68	1.90
Solar Calibration	0.15	0.37	0.51	0.55	0.67	0.80	0.92	1.04	1.16	1.54	1.68	1.90
Temp depend.	0.50	0.50	0.50	0.50	0.50	0.50	0.50	0.50	0.50	0.50	0.50	0.50
Cloud top / surface pressure	0.19	0.47	0.66	0.78	0.96	1.13	1.31	1.48	1.66	1.99	2.18	2.47
Cloud Fraction	0.15	0.38	0.53	0.68	0.83	0.98	1.13	1.28	1.43	1.58	1.73	1.95
Ozone profile	0.18	0.45	0.63	0.56	0.69	0.81	0.94	1.06	1.19	1.89	2.07	2.34
Aerosol Correction	0.08	0.20	0.28	0.36	0.43	0.51	0.59	0.67	0.75	0.83	0.91	1.03
Tropospheric ozone	1.81	1.81	1.95	2.29	2.97	2.98	3.01	3.04	3.09	3.64	3.81	3.81
Total (RSS) precision	**1.92**	**2.10**	**2.40**	**2.76**	**3.50**	**3.68**	**3.90**	**4.13**	**4.39**	**5.38**	**5.77**	**6.20**

These allocations correspond to the curve "Allocation, Sensor and Algorithms" in Figure 7.3-1.

7.4 Mapping Uncertainty

The mapping uncertainty of the nadir total column ozone is derived from sensor and spacecraft specifications and from the geometry of the observation. The allocation of uncertainties is summarized in **Figure 7.4-1**.

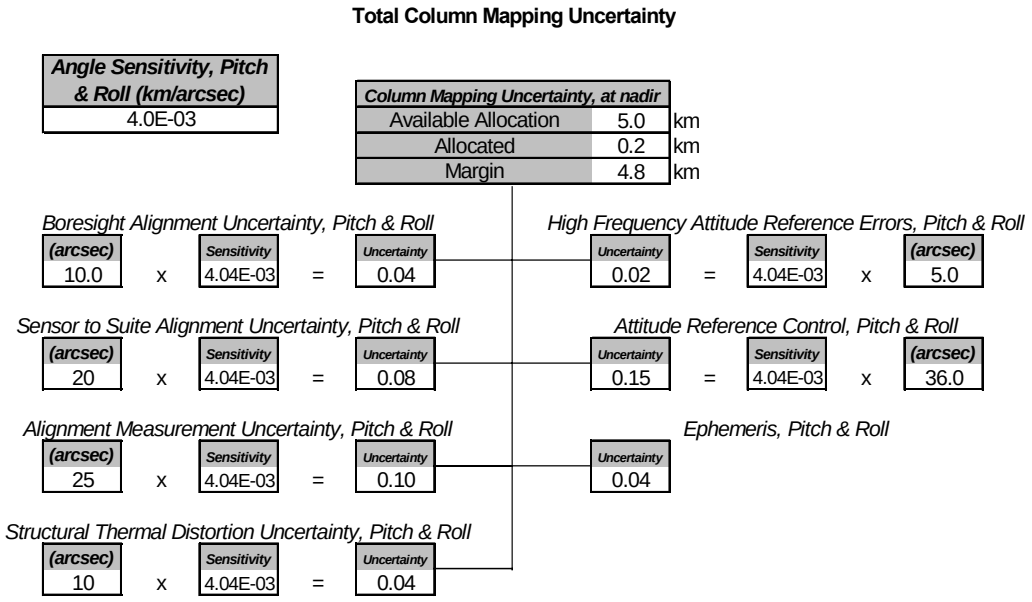

Figure 7.4-1. Error tree addressing the mapping uncertainty of the nadir total column measurements

8 References

Ahmad, Z., and P. K. Bhartia, Effect of molecular anisotropy on backscattered ultraviolet radiance, *Appl. Opt., 34*, 8309-8314, 1995.

Bass, A.M., and R. J. Paur, The ultraviolet cross-sections of ozone: II. The measurements, in *Proceedings of the Quadrennial Ozone Symposium*, ed. C.S. Zerefos and A. Ghazi, D. Reidel Publishing, 661-671, 1984.

Dave, J.V., Meaning of successive iteration of the auxiliary equation in the theory of radiative transfer, *Astrophys. J., 140*, 1292-1303, 1964.

Dave, J. V., Effect of aerosols on the estimation of total ozone in an atmospheric column from the measurement of its ultraviolet radiance, *J. Atmos. Sci., 35*, 899-911,1978.

Fleig, A.J., et al., Nimbus 7 Solar Backscatter Ultraviolet (SBUV) Ozone Products User's Guide, *NASA Reference Publication 1234*, 1990.

Gurevich, G.S. and A.J. Krueger, Optimization of TOMS wavelength channels for ozone and sulfur dioxide retrievals, *Geophys. Res. Lett., 24*, 2187-2190, 1997.

Hall, D. F., Flight measurement of molecular contaminant deposition, *Proc. SPIE, 2261*, 58-71, 1994.

Herman, J.R., P.K. Bhartia, O. Torres, N.C. Hsu, C.J. Seftor, and E. Celarier, Global distribution of absorbing aerosols from Nimbus-7/TOMS data, *J. Geophys. Res., 102*, 16911, 1997.

Herman, J.R. and E.A. Celarier, Earth surface reflectivity climatology at 340-380 nm from TOMS data, *J. Geophys. Res., 102*, 28003, 1997.

Hilsenrath, E., H. Herzig, D. E. Williams, C. J. Brugge, and A. E. Stiegman, Effects of Space Shuttle flight on the reflectance characteristics of diffusers in the near-infrared, visible, and ultraviolet regions, *Opt. Eng., 33*, 3675-3682, 1994.

Jaross, G., et al., Calibration and postlaunch performance of the Meteor 3/TOMS instrument, *J. Geophys. Res., 100*, 2985—2995, 1995.

Jaross, G., A. J. Krueger, and C. G. Wellemeyer, Sensitivity of Total Ozone Mapping Spectrometer products to diffuse reflectance measurements, *Metrologia, 35*, 663-668, 1998a.

Jaross, G., R. Cebula, M. DeLand, R. McPeters, E. Hilsenrath, and A. Krueger, Backscatter ultraviolet instrument solar diffuser degradation, *Proc. SPIE, 3427*, 432-444, 1998b.

Joiner, J., P. K. Bhartia, R. P. Cebula, E. Hilsenrath, and R. D. McPeters, Rotational-Raman Scattering (Ring Effect) in Satellite Backscatter Ultraviolet Measurements, *Appl. Opt., 34*, 4513-4525, 1995.

Klenk, K.F. , P.K. Bhartia, A.J. Fleig, V.G. Kaveeshwar, R.D. McPeters, and P.M. Smith, Total ozone determination from the backscattered ultraviolet (BUV) experiment, *J. Appl. Meteorol. 21*, 1672-1684, 1982.

McPeters, R.D., et al., Earth Probe Total Ozone Mapping Spectrometer (TOMS) Data Product User's Guide, *NASA/TP-1998-206895*, November 1998.

McPeters, R.D., P.K. Bhartia, A.J. Krueger, J.R. Herman, B.M. Schlesinger, C.G. Wellemeyer, C.J. Seftor, G. Jaross, S.L. Taylor, T. Swissler, O. Torres, G. Labow, W. Byerly, and R. P. Cebula, Nimbus-7 TOMS Ozone Mapping Spectrometer (TOMS) Data Products User's Guide, *NASA Reference Publication 1384*, April 1996.

Seftor, C.J., G. Jaross, J.R. Herman, X. Gu, L. Moy, S.L. Taylor, and C.G. Wellemeyer, The Meteor 3/total ozone mapping spectrometer version 7 data set: Calibration and analysis, *J. Geophys. Res., 102*, 19247-19256, 1997.

Torres, O., P.K. Bhartia, J.R. Herman, Z. Ahmad, and J. Gleason, Derivation of aerosol properties from satellite measurements of backscattered ultraviolet radiation: Theoretical Basis, *J. Geophys. Res., 103*, 17099, 1998.

Wellemeyer, C.G., S.L. Taylor, G. Jaross, M.T. Deland, C.J. Seftor, G. Labow, T.J. Swissler, and R.P. Cebula, Final report on Nimbus-7 TOMS Version 7 calibration, *NASA Contractor Report 4717*, March 1996.

Wellemeyer, C. G., S. L. Taylor, C. J. Seftor, R. D. McPeters, and P. K. Bhartia, A correction for total ozone mapping spectrometer profile shape errors at high latitude, *J. Geophys. Res., 102*, 9020, 1997.

Weiser, M., The global digital terrain model TUG87, Internal Report on Set-up, Origin and Characteristics, Institute of Mathematical Geodesy, Technical University of Graz, Austria, 1987.

Woods, T.N., et al., Validation of the UARS Solar Ultraviolet Irradiances: Comparison with the ATLAS 1 and 2 Measurements, *J. Geophys. Res., 101*, 9541-9569, 1996.

Ziemke, J. R., S. Chandra, and P. K. Bhartia, Two new methods for deriving tropospheric column ozone from TOMS measurements: Assimilated UARS MLS/HALOE and convective-cloud differential techniques, *J. Geophys. Res., 103*, 22,115-22,127, 1998.